Biological Growth in the Fractal Space-time with Temporal Fractal Dimension

Marcin Molski

Adam Mickiewicz University of Poznań
Theoretical Chemistry Department
PL 60-780 Poznań, Poland
E-mail: mamolski@amu.edu.pl

Abstract: In the biological systems the fractal structure of space in which cells interact and differentiate is essential for their self-organization and emergence of the hierarchical network of multiple cross-interacting cells, sensitive to external and internal conditions. Hence, the biological phenomena take place in the space whose dimensions are not represented onlyby integer numbers (1,2,3 etc.) of Euclidean space. In particular malignant tumors and neuronal cells grow in a space with noninteger fractal dimension. Since, cellular systems grow not only in space but also in time, an idea has been developed that the growth curves representing neuronal differentiation or malignant tumor progression can be successfully fitted by the temporal fractal function $y(t)$, which describes the time-evolution of the system, characterized by the temporal fractal dimension b_t and scaling factor a_t. One may prove that in the case of biological systems whose growth is described by the Gompertz function, the temporal fractal dimension and scaling factor are time-dependent functions $b_t(t)$ and $a_t(t)$, which permit calculation their values at an arbitrary moment of time or their mean values at an arbitrary time-interval. The model proposed has been applied to determine the temporal fractal dimension of the tumor growth and synapse formation as qualitatively these processes are described by the same Gompertz function. The results obtained permit formulation of two interesting rules:

(i) each system of interacting cells within a growing system possesses its own, local intrasystemic fractal time, which differs from the linear ($b_t=1$) scalar time of the extrasystemic observer;

(ii) fractal structure of space-time in which biological growth occurs, is lost during progression.

It will be proved that the fractal function $y(t)$ is a special case solution of the quantal annihilation operator for the space-like, minimum-uncertainty coherent states of the time-dependent Kratzer-Fues oscillator. Such states propagate along the well defined time trajectory being coherent in space.Hence, the biological growth in the space-time with temporal fractal dimension is predicted to be coherent in space.

Keywords: Fractal space-time, Synapse formation, Tumorigenessis, Biological growth

1. Introduction

The morphometric computer-aided image analysis reveals that growth of biological systems occurs in the space-time with the spatial fractal dimension (also called Haussdorff dimension) defined by

$$b_s = \lim_{\varepsilon \to 0} \frac{\ln n(\varepsilon)}{\ln(1/\varepsilon)}$$

Here, $n(\varepsilon)$ is the minimum number of hypercubes of dimension ε required to completely cover the biological, physical or mathematical object under consideration. The fractal dimension can be defined also by the self-similar power low scaling function

$$y(x) = a_s x^{b_s} \qquad x > 0$$

in which y(x) denotes the number of self-similar objects in the sphere or circle of a radius x; b_s and a_s stand for the spatial fractal dimension and the scaling factor, respectively. In the case of biological systems the fractal structure of space in which cells interact and differentiate is essential for their self-organization and emergence of the hierarchical network of multiple cross-interacting cells, sensitive to external and internal conditions. Hence, the biological phenomena take place in the space whose dimensions are not represented only by integer numbers (1,2,3 etc.) of Euclidean space. In particular tumors and synapses grow in a space with non-integer fractal dimension. Cellular systems grow not only in space but also in time. Recently, an idea has been developed that the curves describing the growth of biological systems can be successfully fitted by the temporal counterpart of the space fractal function [1,2]

$$y(t) = a_t t^{b_t} \qquad t > 0$$

in which y(t) characterizes the time-evolution of the system, b_t is its temporal fractal dimension whereas a_t - a scaling factor. The main idea of the work is mapping the Gompertz function of growth [3]

$$G(t) = G_0 e^{\frac{b}{a}\left(1-e^{-at}\right)}$$

widely applied to fit the demographic, biological and medical data, onto the fractal function y(t). In this way we obtain the the-time dependent expressions $b_t(t)$ and $a_t(t)$, which permit calculation their values at an arbitrary moment of time or their mean values at an arbitrary time-interval. In the Gompertz function G_0 stands for the initial mass, volume, diameter or number of proliferating cells, a is retardation constant whereas b denotes the initial growth or regression rate constant.

2. The model

To find the explicit form of $b_t(t)$ and $a_t(t)$ the relation

$$a_t t^{b_t} = e^{\frac{b}{a}\left(1-e^{-at}\right)} - 1$$

and its first derivative

$$b_t a_t t^{b_t - 1} = be^{-at} e^{\frac{b}{a}\left(1-e^{-at}\right)}$$

are taken into consideration. The first of them satisfies the proper boundary conditions for t→0 for G_0=1 (one cell). Combining the above equations, we arrive at the analytical expressions

$$b_t(t) = bte^{-at} \frac{e^{\frac{b}{a}\left(1-e^{-at}\right)}}{e^{\frac{b}{a}\left(1-e^{-at}\right)} - 1} \qquad a_t(t) = t^{-b_t}\left[e^{\frac{b}{a}\left(1-e^{-at}\right)} - 1 \right]$$

which define the temporal fractal function describing the growth of Gompertzian systems

$$y(t) = a_t(t)t^{b_t(t)}$$

By plotting one may easily prove that function y(t) is indistinguishable from the Gompertz function G(t), hence the mapping procedure is successful.

3. The results

The synapse formation can be characterized by the Gompertz growth curve obtained by the fitting the experimental data obtained by Jones-Villeneuve et al. [4]. The fit provided the following parameters: a=0.0739(89) [day], b=0.3395(378) [day] for constrained G_0=1 evaluated with the nonlinear regression coefficient R=0.9737. In the next step the parameters a and b have been used to calculate the time-dependent fractal dimension $b_t(t)$ and scaling factor $a_t(t)$ using the above specified formulae. Their plots are presented in Fig. 1.
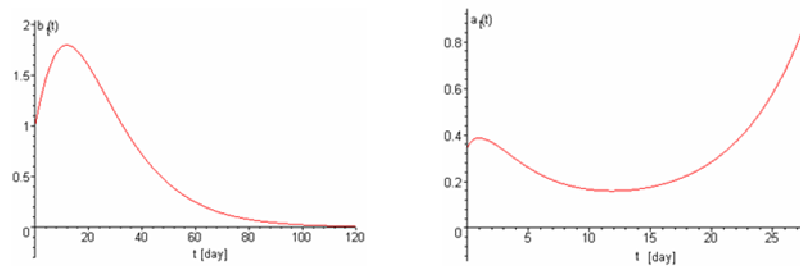

Fig. 1. Plots of the time-dependent temporal fractal dimension $b_t(t)$ and scaling factor $a_t(t)$ for neuronal cells growth characterized by the Gompertz parameters a=0.0739(89) [day] and b=0.3395(378) [day].

In the case of tumorigenessis we consider as an example the Flexner-Jobling rat's tumor whose growth is described by the Gompertz function with

parameters: a=0.0490(63) [day], b=0.394(66) [day] determined by Laird [5].
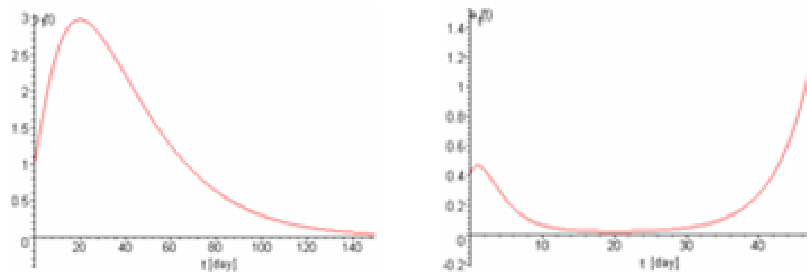They were used to generate plots of $b_t(t)$ and $a_t(t)$ presented in Fig. 2.

Fig. 2. Plots of the temporal fractal dimension $b_t(t)$ and the scaling factor $a_t(t)$
for Flexner-Jobling rat's tumor whose growth is characterized by the parameters
a=0.0490(63) [day], b=0.394(66) [day].

Analysis of the results obtained reveal that during neuronal differentiation and
synapse formation, the temporal fractal dimension $b_t(t)$ increases from 1 for t=0
to a maximal value 1.80 for t=11.97 [day] and then decreases to zero. We find
here an interesting correlation with the spatial fractal dimension calculated *in
vivo* for retinal neurons; it takes value 1.68(15), whereas a diffusion-limitted-
aggregation model predicts 1.70(10) [6]. Those spatial dimensions are equal in
the range specified standard errors to temporal fractal dimension 1.80
determined in this work. In the case of the brain's neurons of two teleost species
Pholidapus dybowskii and *Oncorhynchus keta*, the application of the box-
counting method provided the fractal dimension equal to 1.72 for less
specialized neurons, whereas highly specialized neurons displayed a relatively
low dimension [7]. We conclude that the temporal fractal dimension can be
applied as a numerical measure of the neuronal complexity emerging in the
process of differentiation, which is correlated with the morphofunctional cell
organization. In particular, the change from maximal value of the fractal
dimension $b_t(t=11.97)=1.80$ to dimension attained at plateau $b_t(t=50)=0.43$
reflects the appearance of the highly specialized neurons evolving from the less
specialized ones. The temporal fractal dimension of the Flexner-Jobling's tumor
growth increases from 1 for t=0 to a maximal value 2.98 for t=20[day] and then
decreases to zero. Both $b_t(t)$ and $a_t(t)$ determined for neuronal differentiation and
tumour progression behave in the identical manner. We conclude that
tumorigenesis has a lot in common with the neuronal differentiation and synapse
formation, although the dynamics of these processes are different: the maximal
values of the temporal fractal dimension are equal to 1.8 and 2.98, respectively.

4. The origin of y(t)

One may demonstrate that the fractal function y(t)) is a special case solution of the annihilation operator

$$\hat{A}|\alpha\rangle = \alpha|\alpha\rangle$$

for the space-like, minimum-uncertainty coherent states of the time-dependent counterpart of the Kratzer-Fues oscillator [8]. In the above equation

$$\hat{A} = \frac{1}{\sqrt{2}}\left(\frac{d}{dx} + \beta_0 - \frac{b}{x}\right) \quad |\alpha\rangle = x^b \exp[-\beta_0 x]\exp[\sqrt{2}\alpha x]$$

and $x=t/t_0$ dimensionless temporal variable appearing in the time-dependent version of the Kratzer-Fues potential $V(x)=D(1-1/x)^2$. In the limiting case $\alpha\to0$, $\beta_0 \to0$ the ground coherent state reduces to the fractal function y(t)

$$\lim\nolimits_{\alpha,\beta_0\to0}|\alpha\rangle = y(t) = at^b$$

5. Conclusions

The results obtained permit formulation of two interesting rules governing the biological growth in the fractal space-time:

(i) each system of interacting cells within a growing system possesses its own, local intrasystemic fractal time, which differs from the linear (b_t=1) scalar time of the extrasystemic observer;

(ii) fractal structure of space-time in which biological growth occurs, is lost during progression.

The possibility of mapping the Gompertz function, describing the biological growth, onto the temporal fractal power law scaling function confirms a thesis that biological growth is a self-similar, alometric and coherent process of a holistic nature [9]. It means that all spatially separated subelements (cells) of the whole system, are interrelated via long-range (slowly decaying) interactions, which seem to be an essential ingredient of the self-organized systems. Such interactions can be mediated e.g. through diffusive substances (growth factors), which interact with specific receptors on the surface of the cells, affecting and controlling proliferation. It has been proved [9] that the Gompertz function represents the coherent state of the growth which is a macroscopic analog of the quantal minimum-uncertainty coherent state of the Morse oscillator. Such states are space-like (nonlocal) and propagate along the well-defined time trajectory being coherent in space. The mapping procedure transfers this peculiar property of the Gompertz function onto the fractal function y(t). Hence, the biological growth in the fractal space-time with temporal fractal dimension is predicted to be coherent in space.

References

1. M. Molski, J. Konarski, Tumor growth in the space-time with temporal fractal dimension. Chaos, Solitons & Fractals 36: 811-818 (2008).

2. M. Molski, J. Konarski, Neuronal differentiation and synapse formation in the fractal space-time with temporal fractal dimension. *Synapse* 60: 567 (2006).

3. B. Gompertz, On the nature of the function expressive of the law of human mortality, and on a new mode of determining the value of life contingencies. *Phil Trans Roy Soc London* 115: 513-585 (1825).

4. E.M. Jones-Villeneuve, M.W. McBurney, K.A. Rogers, V.I. Kalnins. Retinoic acid induces embryonal carcinoma cells to differentiate into neurons and glial cells. *J Cell Biol* 94: 253-262 (1982).

5. A.K. Laird, Dynamics of tumor growth. *Brit J Canc* 18: 490-502 (1964); A.K.Laird. Dynamics of tumor growth: comparison of growth rates and extrapolation of growth curves to one cells. *Brit J Canc* 19:278-291 (1965).

6. F. Caserta F, H.E. Stanley, W.D. Eldred, G. Daccord, R.E. Hausman, J. Nittmann. Physical mechanisms underlying neurite outgrowth: a quantitative analysis of neuronal shape. *Phys Rev Lett* 64:95-98 (1990).

7. V.V Isaeva, E.V. Puschina, Y.A. Karetin. The quasi-fractal structure of fish brain neurons. *Russ J Marine Biol* 30: 127-134 (2004).

8. M. Molski. Coherent states of the Kratzer-Fues oscillator. *Phys Rev A* 76: 022107 (2007).

9. M. Molski, J. Konarski. Coherent states of Gompertzian growth. *Phys Rev E* 68: 021916(1-7) (2003).

Adaptive control of the
singularly perturbed chaotic systems
based on the scale time estimation
by keeping chaotic property

Mozhgan Mombeini, Ali Khaki Sedigh, Mohammad Ali Nekoui

Science and Research Branch, Islamic Azad University, Hesarak, Punak, Tehran, Iran
E-mail: M.Mombeini80@gmail.com, Sedigh@kntu.ac.ir, Manekoui@eetd.kntu.ac.ir

Abstract
In this paper, a new approach to the problem of stabilizing a chaotic system is presented. In this regard, stabilization is done by sustaining chaotic properties of the system. Sustaining the chaotic properties has been mentioned to be of importance in some areas such as biological systems.
The problem of stabilizing a chaotic singularly perturbed system will be addressed and a solution will be proposed based on the OGY (Ott, Grebogi and Yorke) methodology. For the OGY control, Poincare section of the system is defined on its slow manifold. The multi-time scale property of the singularly perturbed system is exploited to control the Poincare map with the slow scale time. Slow scale time is adaptively estimated using a parameter estimation technique. Control with slow time scale circumvents the need to observe the states. With this strategy, the system remains chaotic and chaos identification is possible with online calculation of lyapunov exponents.
Using this strategy on ecological system improves their control in three aspects. First that for ecological systems sustaining the dynamical property is important to survival of them. Second it removes the necessity of insertion of control action in each sample time. And third it introduces the sufficient time for census.

Keywords: OGY, lyapunov exponent, slow manifold, adaptive, singular perturbation, scale time

1. Introduction
Nonlinear singularly perturbed models are known by dependence of the system properties on the perturbation parameter [5]. Multi time scale characteristic is an important property of this class of nonlinear systems. For this class of systems a two-stage procedure for design composite controller is presented in [9]. On the other hand, chaotic behavior is an important characteristic of a class of nonlinear systems. Many researchers have shown interest in the analysis and control of the chaotic systems. Among the proposed approaches is the control of the Poincare Map (the OGY-Method) [8].
In this paper, the OGY method is applied to the singularly perturbed chaotic systems. The proposed control strategy exploits the chaotic property of the system and a discrete system model on the Poincare map is defined. This Poincare map lies on the slow manifold of the system. It is shown that by using the two time scale property of the system, an OGY control with slow time scale on the slow manifold of system, could be defined.

This strategy of control results in keeping chaotic property of the system and then online identification of chaos with calculation of lyapunov exponents is possible. An adaptive parameter estimation technique is used to estimate perturbation parameter and the slow time scale of the singularly perturbed system. Population models are examples of systems where sustaining the dynamical property of controlled systems is important for survival of them. Chaotic model of food chains were initially found in [2,4]. Recently, chaotic impulsive differential equations are used in biological control [6,11-13]. Multi time scale approach was first used in [7] for food chain models. Method is implemented on a prey-predator type of population model.

The paper is organized as follows. In section 2 the slow-fast manifold separation based on the slow and fast states for singularly perturbed systems is introduced.
In section 3 an adaptive estimation technique for the estimation of perturbation parameter is proposed.
In section 4 chaotic property of the system is exploited and the OGY control is implemented for the stabilizing problem. Then singularly perturbed property is exploited and slow manifold of the system is selected as the Poincare section. Then a new control based on the slow scale time estimation is introduced.
Section 5 presents the results of employing the proposed method on the ecological prey-predator system.

2. Problem Formulations
In this paper, chaotic singularly perturbed systems of the following form are considered,

$$\varepsilon \dot{x} = f(x, y)$$
$$\dot{y} = g(x, y) \quad \textbf{(1)}$$

Where, $x \in R$, $y \in R^{n-1}$ and ε is a small parameter. $f : R^n \to R$, $g : R^n \to R^{n-1}$ are both smooth functions and the system is chaotic.
The slow manifold of (1) is defined with

$$0 = f(x, y)$$
$$\dot{y} = g(x, y) \,(2)$$

This S manifold $S : \{f = 0\}$ is smooth and results in separation of time scales as x the fast, and y as the slow variable. It is easily seen that,

$$\frac{\dot{y}}{\dot{x}} = \frac{g(x, y)}{\varepsilon f(x, y)} \xrightarrow{\varepsilon \langle \langle 1} \frac{\dot{y}}{\dot{x}} \propto \frac{1}{\varepsilon} \,(3)$$

By taking

$$\tau = \frac{t}{\varepsilon} \,(4)$$

the second scale time of system is $T = \dfrac{1}{\varepsilon}$.

3. Adaptive Estimation of ε

In [10] an estimation method for constant terms using the least-squares approach is proposed. Here the method is used here for ε estimation. The estimated ε is found to minimize the total prediction error as

$$J = \int_0^t e^2(r)\,dr$$

Where the prediction error $e(t)$ is defined as

$$e(t) = \hat{\varepsilon} g(x, y)\dot{x} - f(x, y)\dot{y}$$

This total error minimization can average out the effects of measurement noise. The resulting estimation is [4]

$$\hat{\varepsilon} = \frac{\int_0^t \dot{x} g(x, y) \dot{y} f(x, y)\,dr}{\int_0^t \dot{x}^2 g(x, y)^2\,dr} \,(5)$$

To reduce the size of manipulations we defined w window , then (5) changes to (6)

$$\hat{\varepsilon} = \frac{\int_{t-w}^t \dot{x} g(x, y) \dot{y} f(x, y)\,dr}{\int_{t-w}^t \dot{x}^2 g(x, y)^2\,dr} \,(6)$$

4. OGY Control Based On Second Time Scale Estimation

In this part a new control strategy is proposed such that controlled system remains chaotic. This strategy exploits OGY method to design control and then uses two time scale property of the system to improve the designed control such that system remains chaotic.

4.1 Fast Direction Properties

Consider the chaotic singularly perturbed system (1). As ε is a small parameter, an approximation of the fastest eigenvalue of Jacobian matrix (7) is $\frac{1}{\varepsilon} \times \frac{\partial g}{\partial z}$. Since the chaotic systems are dissipative and the absolute value of the sum of negative exponents is bigger than the sum of the positive Lyapunov exponents, this big value is almost negative. It means that calculation of Lyapanov exponents in fast direction is not necessary in chaos identification. And for system with one perturbation term the fast direction is a stable direction.

$$
J = \begin{bmatrix}
\dfrac{1}{\varepsilon} \times \dfrac{\partial f}{\partial x} & \cdots & \cdots & \dfrac{1}{\varepsilon} \times \dfrac{\partial f}{\partial y_{n-1}} \\
\dfrac{\partial g_1}{\partial x} & \dfrac{\partial g_1}{\partial y_1} & \cdots & \dfrac{\partial g_1}{\partial y_{n-1}} \\
\vdots & \cdots & \cdots & \vdots \\
\dfrac{\partial g_{n-1}}{\partial x} & \dfrac{\partial g_{n-1}}{\partial y_1} & \cdots & \dfrac{\partial g_{n-1}}{\partial y_{n-1}}
\end{bmatrix} \qquad (7)
$$

4.2 OGY Control On The Slow Manifold

In the OGY control design, a manifold is defined such that the discrete model of the system will be obtained by the intersections of this manifold with system trajectories. Then, the control of this discrete model on this manifold will result in the control of the system. It is obvious that the manifold approach will result in a more accurate control of system if it contains all unstable modes of the system. Stable modes lead the system dynamics toward a desired point. One of the modes should be eliminated to have a manifold with unit co-dimension. Eliminating the fastest stable mode and letting it to be free leads to a more accurate control (compared to the elimination of other modes). Considering Jacobian matrix (7) Where x_{eq} is the value on the fixed point of the system while the fixed point is calculated as:

$$
\begin{aligned}
f(x_{eq}, y_{eq}) &= 0 \\
g(x_{eq}, y_{eq}) &= 0
\end{aligned} \qquad (8)
$$

Then, the discrete model will be:

$$
y_{k+1} = p(y_k, u_k), x = x_{eq} \qquad (9)
$$

The OGY control, u_k proposed with the following strategy on slow manifold will be:

$$
u_k = \begin{cases} K(y_k) & if\left(\left|y_k - y_{eq}\right| \le \Delta \right. \\ 0, & otherwise \end{cases} \qquad (10)
$$

Where Δ is the dead zone in traditional OGY method and $K(y_k)$ is a control for slow states of discrete model (9) designed with a suitable method for example, proportional feedback.

4.3 New OGY Control Based On Slow Time Scale Estimation

In the OGY method, control of the Poincare map is equivalent to the control of the chaotic system (1). According to two time scale property of the system, to control this Poincare section on the slow manifold, it is sufficient to control it with the slow scale time, because the states on the slow manifold have slower motions than total dynamical system. Hence, control is designed by following strategy: Control starts with the OGY control and as soon as the first section with the Poincare map is detected, system could be controlled with the slow scale time.

Suppose that T is the estimation of slow scale time of the system. And k_0 is the time of first section or first pulse, the system can be controlled by inserting control action (10) only in the following instants;

$$k = k_0 + nT, n = 0,1,2,\ldots$$

Where, according to (4) T is

$$T = \left[\frac{1}{\varepsilon}\right] (11)$$

and $[\ldots]$ is a bracket symbol.

an approximation of the fastest mode will be $\dfrac{1}{\varepsilon} \times \dfrac{\partial g}{\partial z}$. Then the accurate manifold is defined by the equation;

$0 = f(x, y)$ which is the slow manifold of the system. In other expression with this strategy, the Poincare section in this problem lies on the slow manifold (2). For stabilizing problem in fixed point Poincare section becomes:

$$S = \{y : x = x_{eq}\} \qquad (12)$$

The main idea of this new control method is keeping the system on its chaotic state without resisting to be settled down in the desired rejoin.

The control strategy can be summarized as; when the chaotic system states enter the dead zone, by insertion of the control pulse, the states settle more in the neighborhood of the slow manifold. Afterward system works in open loop and remains by its dynamic in the slow manifold. This slow manifold contains all unstable modes that are also all slow. If unstable modes try to abduct trajectory from the desired point, it needs a time. Since smaller ε result in bigger fast stable modes then the time that system remains on slow manifold increases too, an approximation of this time is slow time scale of the system.

During this time after the application of the control pulse, states of the system remain in the neighborhood of the desired trajectory. Then, after this time before the exit from the desired region, the loop is closed again and insertion of an enough effective control pulse returns the trajectories closer in the slow manifold. Then system becomes open loop again and so on.

Result 1: control of Poincare map and control of system (1) are equivalent. With T period the system is controlled. Then all needed information to control the Poincare map exist at $k = k_0 + nT$. Then T is the sufficient census time (sufficient period of observation) for system (1).

Result 2: By this method between the pulses system is open loop. Then system remains chaotic and online calculation of the Lyapunov exponents result in positive maximum lyapaunov exponent. By defining Γ as

$$\Gamma = u(\lambda_{max}) = \left\{ \begin{array}{l} 0, \lambda_{max} \leq 0 \\ 1, \lambda_{max} \rangle 0 \end{array} \right\} (13)$$

When $\Gamma = 1$ the system identified as chaotic and control rule (10) could be inserted adaptively.

4.4 Algorithm

According to the above discussions a new algorithm to adaptive OGY control for the one term singularly perturbed systems is proposed as follows:

Step 0: By the slow manifold (12) construct the Poincare map (9) and design $K(y_k)$ appropriately to control this discrete model.

Step 1: At the first time t that condition (10) is satisfied, insert the impulse control u_k. $pulses = 1$

Step 2: During t to $t + w$ estimate ε using (5) to estimate the slow scale time (T) with (11).

$$census = census + w$$

Step 3: do no act till $t = t + T$ If condition (10) is satisfied insert control u_k.

$$pulses = pulses + 1$$

Step 4: back to 2.

5. Simulation Results

In this section, the planned algorithm of section 4 is implemented on the Rosenzweig–MacArthur model. The system is model of food chains of prey-predator type. Chaotic property of the system in some range of parameters is proved in [1,3]. This model includes three states: a prey (x), a predator (y) and a top-predator (z), with the following equations:

$$\varepsilon \frac{dx}{dt} = x(1 - x - \frac{y}{\beta_1 + x})$$
$$\frac{dy}{dt} = y(\frac{x}{\beta_2 + x} - \delta_1 - \frac{z}{\beta_2 + y}) \qquad \textbf{(14)}$$
$$\frac{dz}{dt} = \xi z(\frac{y}{\beta_2 + y} - \delta_2)$$

Where

$$\beta_1 = 0.3, \beta_2 = 0.1, \delta_1 = 0.1, \delta_2 = 0.62, \xi = 0.3$$

Problem of stabilizing equilibrium point of saddle type is addressed. The Poincare section is on the following slow manifold

$$S = \{(y,z) : x = x_{eq}\}$$

Extinction of species is not desired. While, the equilibrium point with positive and nonzero terms are desired (of biological significance). Desired fixed point is $(0.8593, 0.1632, 0.1678)$.

To design OGY and new method of control, Poincare section is linearized, and proportional feedback is used to control it. For efficiency of the method, close loop poles selected enough faster than the fastest stable pole.

Figures (1) shows the result of stabilizing with OGY control and new method. It indicates that the stabilizing with new method converges to results of OGY method. New method has lower accuracy only in the early times. But the

numbers of inserted pulses decreased considerably in comparison to OGY method of control (approximately proportional to $\left[\dfrac{1}{\varepsilon}\right]$).

Figures (2) shows the lyapunov exponents under new method. It indicate that maximum lyapunov exponent is positive and the condition $\Gamma = 1$ for insertion the control rule (10) is satisfied and positive lyapunov exponent are in slow directions.

Figure (3) shows slow variations of states in neighbourhoud of slow manifold and effect of control pulses on the staes under new method. It indicates that in interval between the pulses, the states have slow variations.
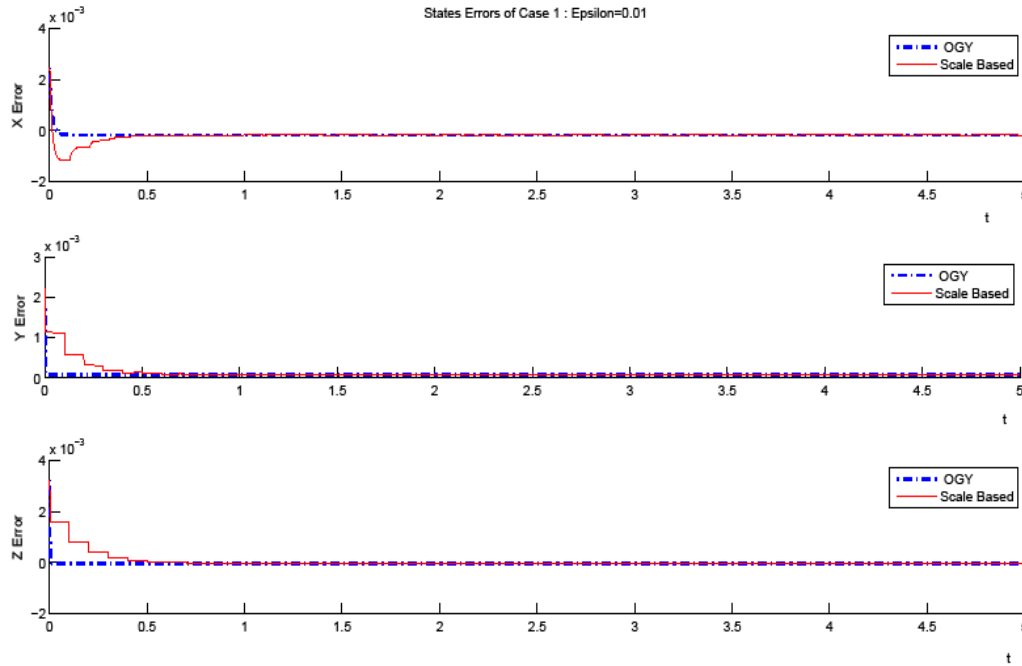

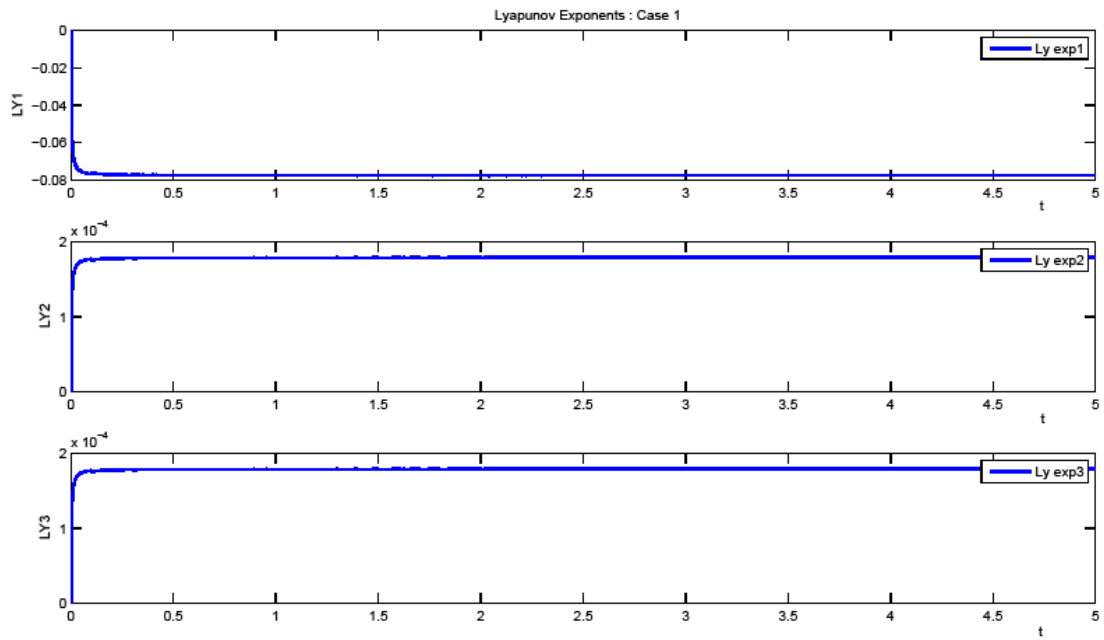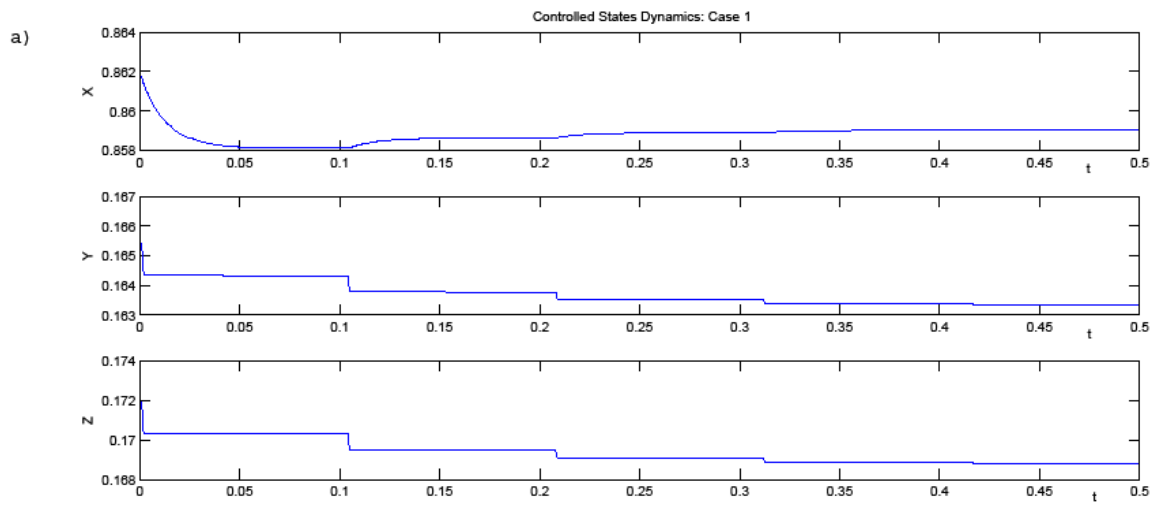Figure (1) Comparison of the states errors by OGY control and new method (for $\varepsilon = 0.01$).

Figure (2) Lyapunov exponents of the controlled system by new method (for $\varepsilon = 0.01$).
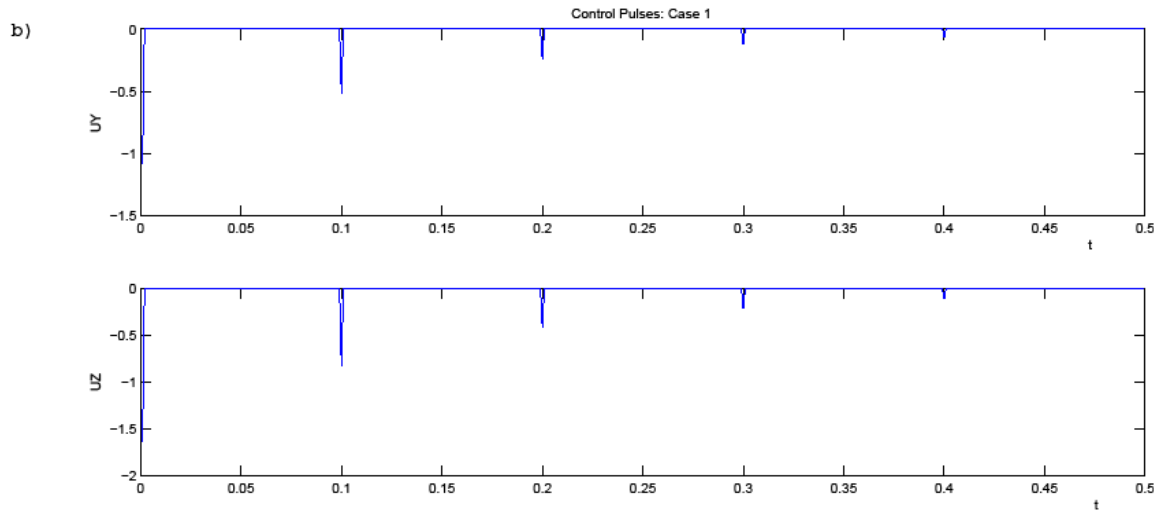
Figure (3)   a) variation of controlled states by new method in neighbourhood of slow manifold, b) inserted control pulses (for $\varepsilon = 0.01$).

This variations are such slow that dynamic of this open loop situation remains in the neighborhood of the desired trajectory. Each time insertion of the control pulses approaches systems more to the desired trajectory.

6. Conclusions

The simulation results on ecological model satisfying the efficiency of the new method. In proposed OGY control on slow manifold, instead of trying to drive the system trajectory to a stable rejoin, system is guided to a dynamical unstable slow manifold. Since that instability is slow, by applying the control pulses in proper times, states of system remains in neighborhood of the desired point. One of the advantages of this control strategy is that it removes necessity of observation of states for all samples. This is very important for situations that census has high expenditure (for example in biological populations) or for situation that dispatch of control action has higher expenditure (for example in pesticide). Also, maximum Lyapunov exponents remain positive and then it is useful for online adaptive identification of chaotic property of the system.

Refrences

[1] B. Deng. Food chain chaos due to junction fold point. Am. Inst. Phys 11:514–525, 2001.
[2] ME. Gilpin. Spiral chaos in a predator-prey model. Am Nat 113: 306–308, 1979.

[3] JM. Ginoux, B. Rossetto and JL. Jamet. Chaos in a three-dimensional Volterra-Gause model of predator-prey type. International Journal of Bifurcation and Chaos Vol. 15, No. 5: 1689-1708, 2005.

[4] P. Hogeweg and B. Hesper. Interactive instruction on population interactions. Comput. Biol. Med 8:319–327, 1978.

[5] H. Khalil. Nonlinear systems. Michihan state University [2nd ed.], 1996.

[6] X. Liu and L. Chen. Complex dynamics of Holling type II Lotka-Volterra predator-prey system with impulsive perturbations on the predator. Chaos Solitons & Fractals 16:311-320, 2003.

[7] S. Muratori and S. Rinaldi. Low-and high-frequency oscillations in three-dimensional food chain systems. SIAM J Appl Math 52:1688–706, 1992.

[8] E. Ott, C. Grebogi and JA. Yorke. Controlling chaos. Phys Rev Lett 64:1196–9, 1990.

[9] A. Saberi and H. Khalil. Stabilization and regulation of nonlinear singularly perturbed system composite control, IEEE Transactions Automatic Control 30: 739-747, 1985.

[10] JJE. Slotin and W. Li. Applied nonlinear control. Library of Congress Catalogigng-in-Publication Data 321.

[11] S. Zhang, L. Chen. A Holling II functional response food chain model with impulsive perturbations. Chaos Solitons & Fractals 24:1269-1278,2005.

[12] S.Zhang, D.Tan and L.Chen. Dynamic complexities of a food chain model with impulsive perturbations and Beddington-DeAngelis functional response. Chaos Solitons & Fractals 27:768-777, 2006.

[13] S. Zhang,F. Wang and L. Chen . A food chain model with impulsive perturbations and Holling IV functional response .Chaos Solitons and Fractals 26: 855–866, 2005.

**Analysis of Two Time Scale Property of
Singularly Perturbed System on
Chaotic Attractor**

Mozhgan Mombeini, Ali Khaki Sedigh, Mohammad Ali Nekoui

Science and Research Branch, Islamic Azad University, Hesarak, Punak, Tehran, Iran
E-mail: M.Mombeini80@gmail.com, Sedigh@kntu.ac.ir, Manekoui@eetd.kntu.ac.ir

Abstract
The idea that chaos could be a useful tool for analyze nonlinear systems considered in this paper and for the first time the two time scale property of singularly perturbed systems is analyzed on chaotic attractor. The general idea introduced here is that the chaotic systems have orderly strange attractors in phase space and this orderly of the chaotic systems in subscription with other classes of systems can be used in analyses. Here the singularly perturbed systems are subscripted with chaotic systems.
Two time scale property of system is addressed. Orderly of the chaotic attractor is used to analyze two time scale behavior in phase plane.
Keywords: chaos, singular perturbation, strange attractor, phase space

1. Introduction
Phase space analysis is common method in analysis of nonlinear systems [3]. Chaotic systems are class of nonlinear systems that are known by dependance of system dynamics on initial values. Since for first time in 1963 chaotic property introduced by Lornz , many researchers have shown interest in the analysis of them. On other hand nonlinear Singular perturbation models are known by dependence of the system properties on the perturbation parameter [3]. Multiple time scale characteristic is an important property of this class of systems. In this paper for the first time the two time scale property of singularly perturbed systems is analyzed on chaotic attractor. The general idea introduced here is that the chaotic systems have orderly strange attractors in phase space and this orderly of the chaotic systems in subscription with other classes of systems can be used in analyses. Here the singularly perturbed systems are subscripted with chaotic systems.
Two time scale property of system is addressed. Orderly of the chaotic attractor is used to analyze two time scale behavior in phase plane. Linearization method only gives the information around the point that system is linearized but phase space analysis gives all information about all points of the system. Mathematical models of ecological systems are examples of chaotic sinularly perturbed systems that analysis done on them here.
The paper is organized as follows. In section 2 the two time scale property of the singularly perturbed systems is introduced. In section 3 linearization method introduced to analyze the time scale.
Section 4 presents the results of employing the linearization method on the three ecological prey-predator systems.
In section 5 the two time scale behavior of singularly perturbed system on the chaotic attractor is analyzed. Section 6 contains the conclusion of this paper.

2. Two Time Scale Singularly Perturbed Systems
In this paper, chaotic singularly perturbed systems of the following form are considered,
$$\varepsilon \dot{x} = f(x, y)$$
$$\dot{y} = g(x, y) \quad \textbf{(1)}$$

Where, $x \in R$, $y \in R^{n-1}$ and ε is a small parameter. $f : R^n \rightarrow R$, $g : R^n \rightarrow R^{n-1}$ are both smooth functions and the system is chaotic.
The slow manifold of (1) is defined with

$$0 = f(x, y)$$
$$\dot{y} = g(x, y) \quad (2)$$

This S manifold $S : \{ f = 0 \}$ is smooth and results in separation of time scales as x the fast, and y as the slow variable. It is easily seen that,

$$\frac{\dot{y}}{\dot{x}} = \frac{g(x, y)}{\varepsilon f(x, y)} \xrightarrow{\varepsilon \langle \langle 1} \frac{\dot{y}}{\dot{x}} \propto \frac{1}{\varepsilon} \quad (3)$$

By taking

$$\tau = \frac{t}{\varepsilon} \quad (4)$$

as the slow time and t as the fast time, rescaling gives

$$\frac{dx}{d\tau} = x' = f(x, y)$$

$$\frac{dy}{d\tau} = y' = \varepsilon g(x, y)$$

The fast manifold yields:

$$x' = f(x, y)$$

$$y' = 0$$

3. Analysis of Two Time Scale Behavior with Linearization around Slow Manifold

In this section system (1) is linearized around its fixed point. Then slow manifold produced with (2). Then eigenvalues of jacobian matrix for full system and reduced system (slow manifold) used to analyze the speed of states. The equations

$$\dot{x} = 0$$
$$\dot{y} = 0 \tag{5}$$

or equivalently the equations

$$0 = f(x, y)$$

$$0 = g(x, y) \tag{6}$$

give the fixed points (x_{eq}, y_{eq}) of the system (1). And according to (2) the slow manifold yields with

$$S = \{(y) : x = x_{eq}\} \tag{7}$$

Linearization of full system around the fixed point result in fallowing jacobian matrix

$$J = \begin{bmatrix} \dfrac{1}{\varepsilon} \times \dfrac{\partial f}{\partial x} & \cdots & \cdots & \dfrac{1}{\varepsilon} \times \dfrac{\partial f}{\partial y_{n-1}} \\ \dfrac{\partial g_1}{\partial x} & \dfrac{\partial g_1}{\partial y_1} & \cdots & \dfrac{\partial g_1}{\partial y_{n-1}} \\ \vdots & \cdots & \cdots & \vdots \\ \dfrac{\partial g_{n-1}}{\partial x} & \dfrac{\partial g_{n-1}}{\partial y_1} & \cdots & \dfrac{\partial g_{n-1}}{\partial y_{n-1}} \end{bmatrix} \tag{8}$$

and linearization of reduced system result in following jacobian matrix

$$J = \begin{bmatrix} \dfrac{\partial g_1}{\partial y_1} & \cdots & \dfrac{\partial g_1}{\partial y_{n-1}} \\ \vdots & \cdots & \vdots \\ \dfrac{\partial g_{n-1}}{\partial y_1} & \cdots & \dfrac{\partial g_{n-1}}{\partial y_{n-1}} \end{bmatrix} \tag{9}$$

It is obvious that eigenvalues with nonzero real parts of this matrixes (8),(9) show the speeds of states around the fixed pointes.

4. The Linearization Method on Three Ecological Models

Here the linearization method is implemented on three models of food chains of prey-predator type. The Rosenzweig–MacArthur, the Hastings–Powell, and the Volterra–Gause model are investigated here. All are singularly perturbed and the chaotic property of them in some range of parameters is proved in [1-2].The models include three states: a prey (x), a predator (y) and a top-predator (z).

4.1. The Rosenzweig–Mac Arthur Model

$$\varepsilon \frac{dx}{dt} = x(1 - x - \frac{y}{\beta_1 + x})$$

$$\frac{dy}{dt} = y(\frac{x}{\beta_2 + x} - \delta_1 - \frac{z}{\beta_2 + y}) \quad (10)$$

$$\frac{dz}{dt} = \xi z(\frac{y}{\beta_2 + y} - \delta_2)$$

Where

$$\beta_1 = 0.3, \beta_2 = 0.1, \delta_1 = 0.1, \delta_2 = 0.62, \xi = 0.3$$

Fixed point $(0.8593, 0.1632, 0.1678)$ is on the slow manifold. Eigenvalues of Jacobian matrix around this point for full system and reduced system for $\varepsilon = 0.1$ are

$$\lambda(\varepsilon = 0.1) = \begin{bmatrix} -7.516 \\ 0.182 + 0.112i \\ 0.182 - 0.112i \end{bmatrix}$$

$$\lambda_{reduced}(\varepsilon = 0.1) = \begin{bmatrix} 0.199 + 0.0759i \\ 0.199 - 0.0759i \end{bmatrix}$$

For $\varepsilon = 0.01$ eigenvalues change to

$$\lambda(\varepsilon = 0.01) = \begin{bmatrix} -75.467 \\ 0.181 + 0.112i \\ 0.181 - 0.112i \end{bmatrix}$$

$$\lambda_{reduced}(\varepsilon = 0.01) = \begin{bmatrix} 0.199 + 0.076i \\ 0.199 - 0.076i \end{bmatrix}$$

4.2. The Volterra–Gause Model

$$\varepsilon \frac{dx}{dt} = x(1-x) - \sqrt{x}\, y$$

$$\frac{dy}{dt} = -\delta_1 y + \sqrt{x}\, y - \sqrt{y}\, z \quad \textbf{(11)}$$

$$\frac{dz}{dt} = \xi z (\sqrt{y} - \delta_2) z$$

Where

$$\delta_1 = 0.577, \delta_2 = 0.376, \xi = 1.428$$

Fixed point $(0.8463235, 0.141376, 0.1289524)$ is on the slow manifold. Eigenvalues of jacobian matrix around this point for full system and reduced system for $\varepsilon = 0.1$ are

$$\lambda(\varepsilon = 0.1) = \begin{bmatrix} -7.604 \\ 0.040 + 0.302i \\ 0.040 - 0.302i \end{bmatrix}$$

$$\lambda_{reduced}(\varepsilon = 0.1) = \begin{bmatrix} 0.086 + 0.291i \\ 0.086 - 0.291i \end{bmatrix}$$

For $\varepsilon = 0.01$ eigenvalues change to

$$\lambda(\varepsilon = 0.01) = \begin{bmatrix} -76.857 \\ 0.040 + 0.301i \\ 0.040 - 0.301i \end{bmatrix}$$

$$\lambda_{reduced}(\varepsilon = 0.01) = \begin{bmatrix} 0.086 + 0.291i \\ 0.086 - 0.291i \end{bmatrix}$$

4.3. The Hastings–Powell Model

$$\varepsilon \frac{dx}{dt} = x(1-x) - \frac{a_1 xy}{1 + \beta_1 x})$$

$$\frac{dy}{dt} = y(\frac{a_1 x}{1 + \beta_1 x} - \delta_1) - \frac{a_2 yz}{1 + \beta_2 y}) \quad (12)$$

$$\frac{dz}{dt} = \xi z (\frac{a_2 y}{1 + \beta_2 y} - \delta_2)$$

Where

$$a_1 = 5, a_2 = 0.1, \delta_1 = 0.4, \delta_2 = 0.01, \beta_1 = 3, \beta_2 = 2, \xi = 0.2$$

Fixed point $(0.8192, 0.125, 9.808)$ is on the slow manifold. Eigenvalues of Jacobian matrix around this point for full system and reduced system for $\varepsilon = 0.1$ are

$$\lambda(\varepsilon = 0.1) = \begin{bmatrix} -6.818 \\ 0.034 + 0.011i \\ 0.034 - 0.101i \end{bmatrix}$$

$$\lambda_{reduced}(\varepsilon = 0.1) = \begin{bmatrix} 0.148 \\ 0.008 \end{bmatrix}$$

For $\varepsilon = 0.01$ eigenvalues change to

$$\lambda(\varepsilon = 0.01) = \begin{bmatrix} -68.978 \\ 0.034 + 0.011i \\ 0.034 - 0.101i \end{bmatrix}$$

$$\lambda_{reduced}(\varepsilon = 0.01) = \begin{bmatrix} 0.148 \\ 0.008 \end{bmatrix}$$

It is obvious that for three systems fast mode is in perturbed direction. Fast modes are stable and very big in comparison to other poles. With decrement of ε stable fast mode becomes faster and slow modes approximately remain unchanged. Then two time scale behavior in such systems means that with decrement of ε value fast states become faster and slow sates speed is approximately unchanged. The eigenvalues of the reduced system (slow manifold) also remain unchanged with ε value changes.

5. Phase Space Analysis on Chaotic Attractor

Phase space analysis is common method in analysis of nonlinear systems. For nonlinear systems the phase portrait of a solution is a plot in phase space of the orbit evolution [4]. One of the most important properties of chaotic systems is that they have strange attractors; that has an apparent qualitative and bounded shape for each systems in range of parameters that system is chaotic and initial conditions that arisen from basin of attraction. We named here this property as orderly of the chaotic systems.

Strange attractor can be shown with plot of trajectories in phase portrait. Here the property of chaotic systems that "qualitative shape of system attractor is unchanged and bounded", or in other expression the orderly of the strange attractor of chaotic systems in phase portrait, is used to analyze the two time scale behavior of singularly perturbed chaotic systems in phase space.

According to (3) by ε variation, speeds of systems states meet different scale times proportional to $1/\varepsilon$, theoretically. Figures (1) shows the strange attractor of three above ecological systems for two different ε values in phase space. According to figure (1) by changing the ε value the qualitative shape of attractor is approximately unchanged.
Figure (2) shows the two dimensional plot of attractors for fast states (y,z). According to figure (2) the qualitative shape and quantitative domain of variation of attractor for slow states is approximately independent on variation of ε value and there is no sensible variation in slow states.

Figure (3) shows the two dimensional plot of the same attractors for the fast state (x) and one of the slow states(y). It shows that the speed of states increase in fast direction.
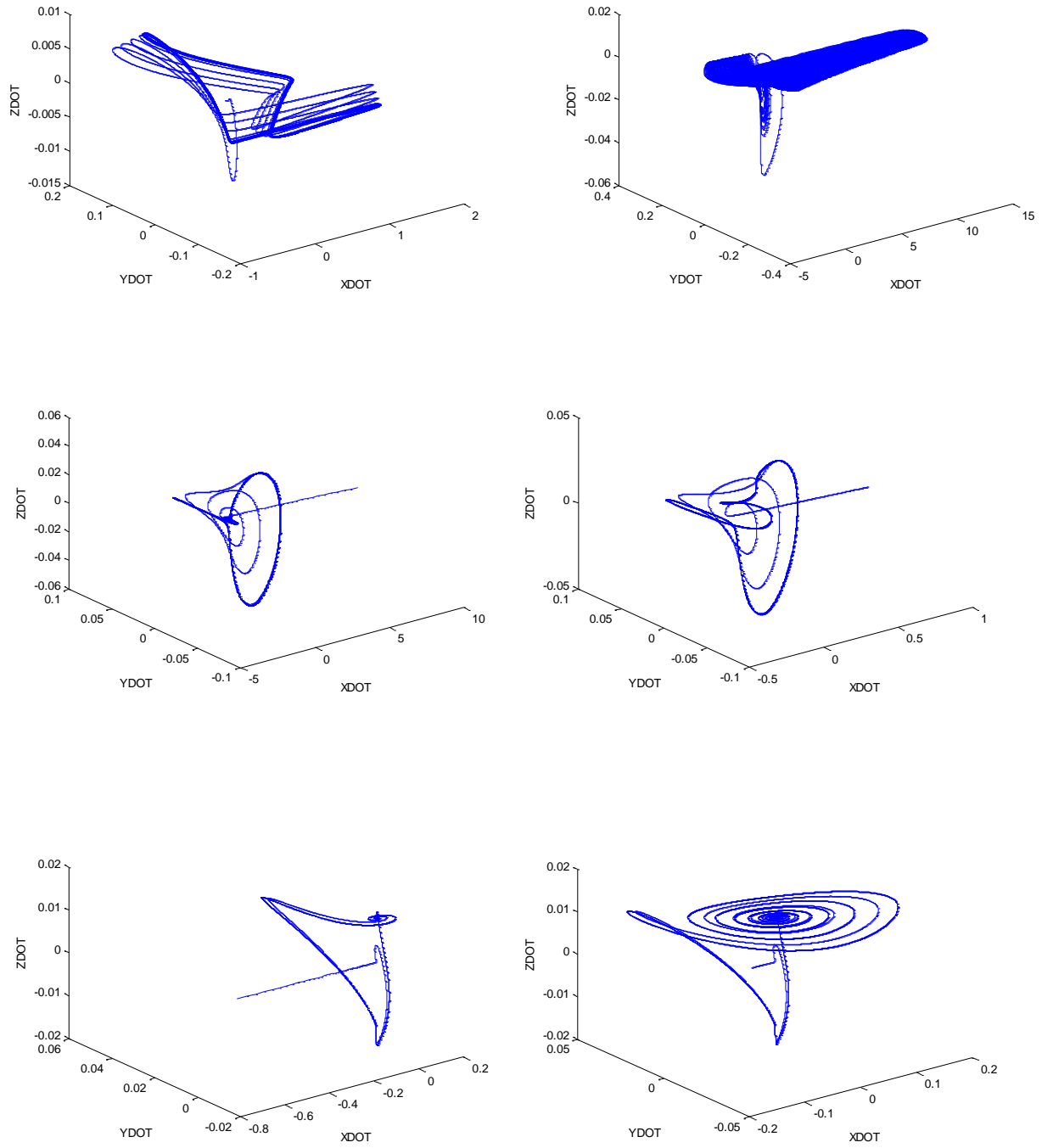
Figure (1) chaotic strange attractor of three food chain models (for $\varepsilon = 0.1$ in left and for $\varepsilon = 0.01$ in right).
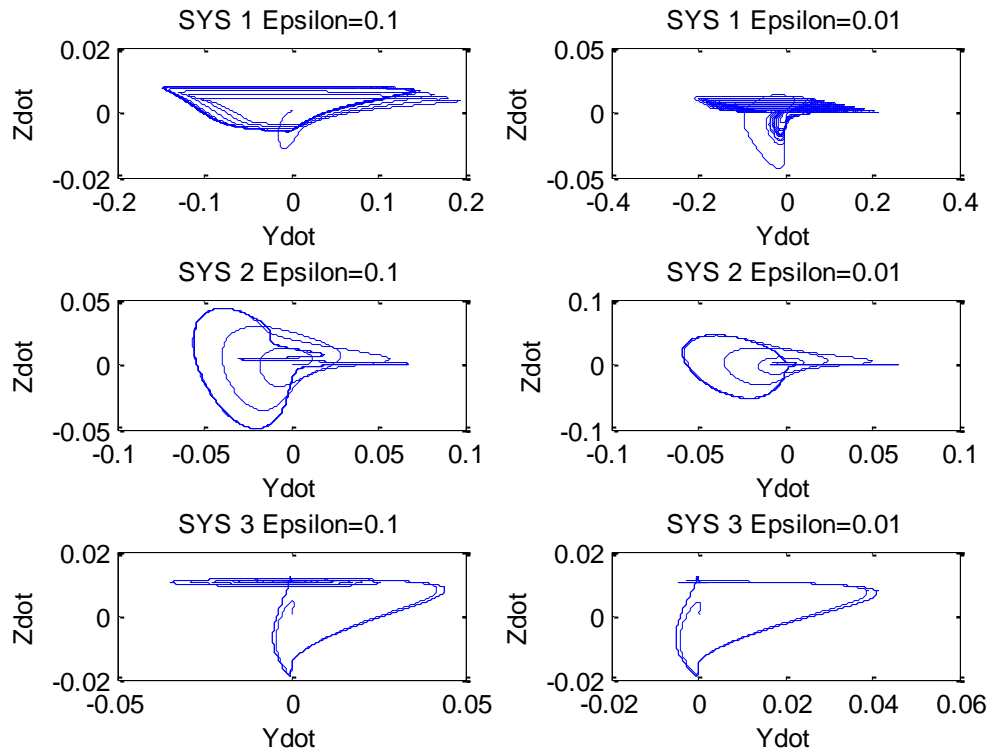
Figure (2) 2-Dimensional perspective of chaotic attractor of three food chains models for slow states (for $\varepsilon = 0.1$ in left and for $\varepsilon = 0.01$ in right).
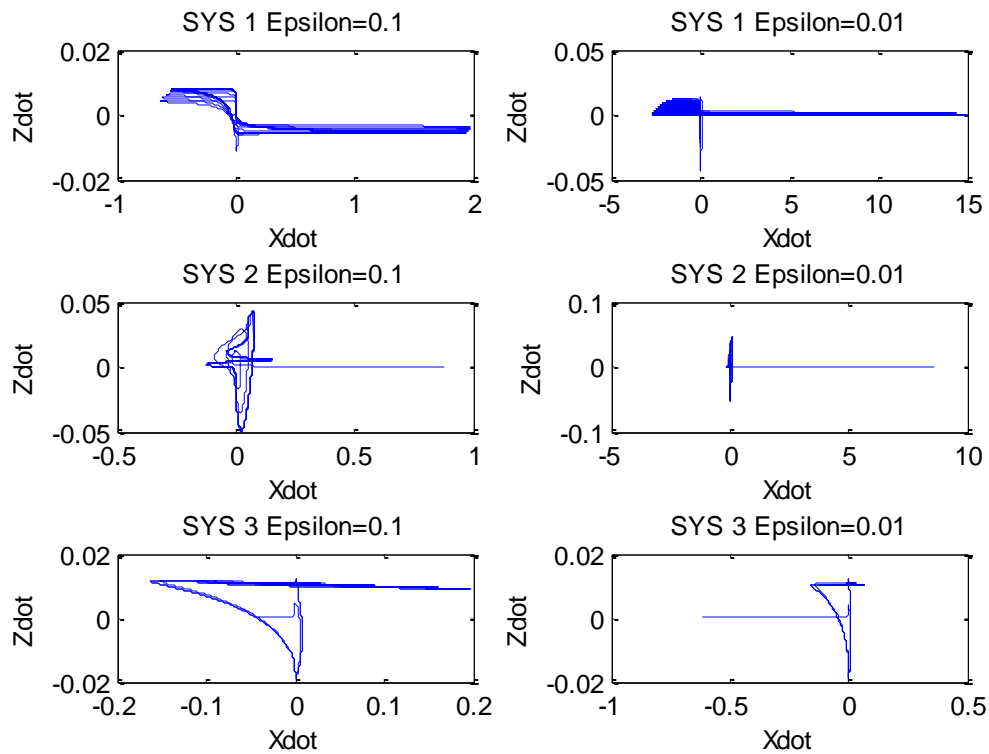
Figure (3) 2-Dimensional perspective of chaotic attractor of three food chains models for fast state x (respect to one of the slow states z (for $\varepsilon = 0.1$ in left and for $\varepsilon = 0.01$ in right).

According to these figures, the quantitative domain of variation of attractor in the direction of fast state increased by the decrement of ε value, and for slow states is approximately is no sensible variation.

Then, analyze of the two scale time behavior of singularly perturbed systems on chaotic attractor shows that be ε decrement the slow states speed is approximately unchanged but the speed of fast states increase. This result is for all trajectories of the system not only about the around the fixed point on slow manifold.

6. Conclusions

In linearization method the eigenvalues with nonzero real parts introduced to analyze the multi time scale property of system around the point that system linearized. Results of implementation of this method on three ecological models show that the eigenvalues of jacobian matrix in fast direction are very bigger than slow directions. To analyze the system behavior on all points the phase portrait method is used. Because the system is chaotic its strange attractor in phase portrait is bounded and has a regular qualitative shape. Using phase portrait method satisfied the results of linearization method but applicable for all points of the system on the strange attractor. Both method show that by decrement of ε value the speed of fast state increases but the speed of slow states are approximately unchanged. The orderly of the chaotic system on strange attractor used to analyze the two scale time property of the singularly perturbed class of nonlinear systems. Using chaotic property in subscription with other classes of nonlinear systems may be extendable to analyze them.

Refrences

[1] B. Deng. Food chain chaos due to junction fold point. Am. Inst. Phys 11:514–525, 2001.

[2] JM. Ginoux, B. Rossetto and JL. Jamet. Chaos in a three-dimensional Volterra-Gause model of predator-prey type. International Journal of Bifurcation and Chaos Vol. 15, No. 5: 1689-1708, 2005.

[3] H. Khalil. Nonlinear systems. Michihan state University [2nd ed.], 1996.

[4] K. Tomasz and S. R. Bishop. The illustrated dictionary of nonlinear dynamics and chaos. John wiley & sons,1999.

Nonlinear oscillations and chaotic response of Shape Memory Alloys

Mohamed Ould Moussa[1], Ziad Moumni[1], Olivier Doaré[1], Cyril Touzé[1], and Wael Zaki[2]

[1]Unité de Mécanique (UME), ENSTA-ParisTech, Chemin de la Hunière, 91761 Palaiseau Cedex, France
[2]Khalifa University of Science, Technology and Research (KUSTAR), PO.Box 127788, Abu Dhabi, UAE
(E-mail: mohamed.ould-moussa@polytechnique.edu)

Abstract. Shape Memory Alloys (SMAs) present unusual behaviour compared to more standard linear elastic materials. Indeed, they can accomodate large reversibe strain (pseudo-elasticity) or recover their shape, after being strained, by simple heating (shape memory effect). These behaviours are due to a displacive first order phase transformation called martensitic transformation. These features promote their use in many applications ranging from biomedical field to spatial domain. In the current work, we focus on the pseudoelastic behaviour. To this end, the thermomechanical constitituve law developped by Moumni and Zaki [1] is used. Firstly, the behaviour is reduced to a single degree of freedom. Secondly, inertial effect is considered and the forced oscillations of a device witnessing a pseudoelastic behaviour are studied. The analysis of the results through frequency-response curves and Poincaré maps reveals softening behaviour, jump phenomena, symmetry-breaking bifurcations and occurence of chaos. Results are in good agreement with those found in the literature [2] and using a different modelisation of the shape-memory effect.
Keywords: hysteresis loop, damping capacity, softening behaviour, chaotic solutions, symmetry breaking, Poincaré map.

1 Introduction

The interesting behaviour of shape memory alloys (SMA) is usually attributed to their ability to undergo a reversible solid‑solid phase change between a parent phase called austenite and a product phase called martensite. The transition from austenite to martensite is accompanied by a loss of crystallographic symmetry, which produces entropy and heat. Austenite can usually transform into martensite when the SMA is mechanically stressed, the resulting transformation strain can then be recovered by unloading. This seemingly elastic yet dissipative behaviour is called *pseudoelasticity*. During a pseudoelastic transformation, a considerable amount of heat can be generated due to phase change, which can result in temperature variations that readily impact the behaviour of the SMA resulting in a strong thermomechanical coupling. This paper is devoted to the computation of the dynamic

response of a pseudoelastic device in isothermal condition. The behaviour of the device is derived from a full 3D model that has been exhaustively presented in [1]. It is recalled in section 2. The reduction to a one-dimensional system is exhibited in section 3 by assuming axial loading of a slender beam, resulting in a non-linear pseudoelastic spring characteristic. An added mass ensures inertia effect, and the oscillator model is completed with a dashpot and external harmonic forcing. Comparing with the model used in [2], [3] and [4], the originality of the current work is the use of a thermodynamic admissible 3-D law which allows studying vibrations of either continuous or discrete systems. The frequency-response of the pseudoelastic device is computed in the vicinity of its eigenfrequency corresponding to purely austenitic (small amplitude) motions. In the lines of the results presented in [2], a softening behaviour, characterized by a shift of the resonance frequency to lower frequencies, is found, resulting in jump phenomena. Moreover, symmetry-breaking bifurcations and onset of chaotic responses are detected for selected parameters values.

2   ZM model-3D version

The Zaki-Moumni (ZM) model for shape memory alloys is based on the of solid-solid phase change modelisation developed by Moumni [5] and was first introduced by Zaki and Moumni [1]. It was later extended to take into account cyclic SMA behaviour and training [6], tension-compression asymmetry [7] and irrecoverable plastic deformation of martensite [8]. The model is developed within the framework of Generalized Standard Materials with internal constraints ([9], [5]) in order to guarantee thermodynamic consistency. For the original ZM model, the thermodynamic potential is chosen as the Helmholtz free energy density taken as:

$$
\begin{aligned}
\mathcal{W} = {} & (1-z)\left[\frac{1}{2}\left(\boldsymbol{\epsilon}_{\mathrm{A}}\right):\boldsymbol{S_{\mathrm{A}}}^{-1}:\left(\boldsymbol{\epsilon}_{\mathrm{A}}\right)\right] \\
& + z\left[\frac{1}{2}\left(\boldsymbol{\epsilon}_{\mathrm{M}}-\boldsymbol{\epsilon}_{\mathrm{ori}}\right):\boldsymbol{S_{\mathrm{M}}}^{-1}:\left(\boldsymbol{\epsilon}_{\mathrm{M}}-\boldsymbol{\epsilon}_{\mathrm{ori}}\right)+C(T)\right] \\
& + G\frac{z^2}{2}+\frac{z}{2}\left[\alpha z+\beta\left(1-z\right)\right]\left(\frac{2}{3}\boldsymbol{\epsilon}_{\mathrm{ori}}:\boldsymbol{\epsilon}_{\mathrm{ori}}\right)
\end{aligned}
\tag{1}
$$

In the above equation, $\boldsymbol{\epsilon}_{\mathrm{A}}$ and $\boldsymbol{\epsilon}_{\mathrm{M}}$ are the local strain tensors of austenite and martensite respectively, T is temperature, z is the volume fraction of martensite, and $\boldsymbol{\epsilon}_{\mathrm{ori}}$ is the orientation strain tensor. $\boldsymbol{S}_{\mathrm{A}}$ and $\boldsymbol{S}_{\mathrm{M}}$ are the compliance tensors of austenite and martensite respectively. ρ is the mass density, G, α, and β are material parameters that influences the shape of the superelastic hysteresis loop and the slopes of the stress-strain curve during phase change and martensite orientation. The parameter $C(T)$ is an energy density that depends on temperature as follows:

$$
C(T) = \xi(T-T^0) + \kappa,
\tag{2}
$$

where ξ and κ are material parameters. The state variables obey the following physical constraints :

- The macroscopic strain tensor $\boldsymbol{\epsilon}$ is an average over the REV (Representative Elementary Volume) of the strain within austenite and martensite phases. By construction, $\boldsymbol{\epsilon}$ is given by

$$(1 - z)\,\boldsymbol{\epsilon}_{\mathrm{A}} + z\boldsymbol{\epsilon}_{\mathrm{M}} - \boldsymbol{\epsilon} = 0, \tag{3}$$

- z is the volume fraction of martensite, restricted to the [0,1] interval,
- The equivalent orientation strain cannot exceed a maximum γ:

$$\gamma - \sqrt{\frac{2}{3}\boldsymbol{\epsilon}_{\mathrm{ori}} : \boldsymbol{\epsilon}_{\mathrm{ori}}} \geq 0. \tag{4}$$

The above constraints derive from the following potential:

$$W_{\mathrm{l}} = -\boldsymbol{\lambda} : [(1 - z)\,\boldsymbol{\epsilon}_{\mathrm{A}} + z\boldsymbol{\epsilon}_{\mathrm{M}} - \boldsymbol{\epsilon}] - \mu\left(\gamma - \sqrt{\frac{2}{3}\boldsymbol{\epsilon}_{\mathrm{ori}} : \boldsymbol{\epsilon}_{\mathrm{ori}}}\right) - \nu_1 z - \nu_2\,(1 - z)\,, \tag{5}$$

where the Lagrange multipliers ν_1, ν_2, and μ are such that

$$\begin{aligned} &\nu_1 \geq 0, \nu_1 z = 0, \\ &\nu_2 \geq 0, \nu_2\,(1 - z) = 0, \\ &\text{and } \mu \geq 0, \mu\left(\gamma - \sqrt{\frac{2}{3}\boldsymbol{\epsilon}_{\mathrm{ori}} : \boldsymbol{\epsilon}_{\mathrm{ori}}}\right) = 0. \end{aligned} \tag{6}$$

The sum of the Helmholtz energy density (1) and the potential W_{l} (5) gives the Lagrangian $\mathcal{L}$, which is then used to derive the state equations. With some algebra, the following stress-strain relation is obtained:

$$\boldsymbol{\sigma} = \boldsymbol{S}^{-1} : (\boldsymbol{\epsilon} - z\boldsymbol{\epsilon}_{\mathrm{ori}})\,, \tag{7}$$

where $\boldsymbol{S}$ is the equivalent compliance tensor of the material, given by

$$\boldsymbol{S} = (1 - z)\,\boldsymbol{S}_{\mathrm{A}} + z\boldsymbol{S}_{\mathrm{M}}. \tag{8}$$

The thermodynamic forces associated with z and $\boldsymbol{\epsilon}_{\mathrm{ori}}$ are taken as subgradients of a pseudo-potential of dissipation D defined as

$$D = [a\,(1 - z) + bz]\,|\dot{z}| + z^2 Y\sqrt{\frac{2}{3}\dot{\boldsymbol{\epsilon}}_{\mathrm{ori}} : \dot{\boldsymbol{\epsilon}}_{\mathrm{ori}}}, \tag{9}$$

where a, b are positive material parameters, and Y is a parameter linked to the orientation yield stress. This allows the definition of yield functions for phase change ($\mathcal{F}_{\mathrm{z}}^1$ and $\mathcal{F}_{\mathrm{z}}^2$) and for martensite orientation ($\mathcal{F}_{\mathrm{ori}}$). The evolutions of the state variables z and $\boldsymbol{\epsilon}_{\mathrm{ori}}$ are governed by the consistency

conditions associated with yield functions. If the orientation-finish stress is lower than the critical stress for forward phase change (*i.e.* if $\sigma_{\text{rf}} < \sigma_{\text{ms}}$), the model is such that the stress-induced martensite is completely oriented as soon as forward phase change begins.

In the next section, the ZM model will be reduced to 1D dimension in order to derive the dynamic response of a SMA device.

3 SMAs device-1D version

A single degree of freedom device can be considered by using a SMA beam with length l and cross-section area S. The SMA beam can be assimilated to a spring with nonlinear stiffness by studying relative displacement of its extremities. Figure 1 represents a sketch of the device, where a viscous structural damping $(\mathcal{C})$ is added to model internal losses that are not contained into the hysteresis loop. The mass $\mathcal{M}$ is subjected to external harmonic excitation of amplitude E_{max} and frequency ω as: $\mathcal{E}_e(t) = E_{max} \cos(\omega t)$. Assuming that in the direction $(\overrightarrow{x})$, $\sigma_{xx} = \left(\frac{F}{S}\right)$, $\varepsilon_{xx} = \left(\frac{X}{l}\right)$ and $\varepsilon_{ori,xx} = \left(\frac{X_{ori}}{l}\right)$, dimensioned model equations are summarized in table 1, where $\mathcal{K}(z)$ represents the nonlinear stiffnes. It is defined by: $\mathcal{K}(z) = \left(\frac{1-z}{\mathcal{K}_a} + \frac{z}{\mathcal{K}_m}\right)^{-1}$, where $\mathcal{K}_a = \left(\frac{E_a S}{l}\right)$ (respectively $\mathcal{K}_m = \left(\frac{E_m S}{l}\right)$) is the the stiffness in austenitic phase (resp. martensitic phase), related to their respective Young's modulus E_a and E_m. In the remainder, forward transformation means phase change from *austenitic* phase to *martensitic* one and reverse transformation in the inverse direction. Finally, X_{ori} is an internal displacement of the device due to detwinning process and is defined by $X_{ori} = X_{max} sgn(F)$, where $sgn(F)$ stands for the sign of F; a, b, G, α, β, ε_0, ξ, κ, θ_0 and Y are material parameters [1].

Motion equation :
$$\mathcal{M}\ddot{X} + \mathcal{C}\dot{X} + F(X, z, X_{ori}) = \mathcal{E}_e(t)$$
Behaviour equation :
$$F(X, z, X_{ori}) = \mathcal{K}(z)(X - z.X_{ori})$$
Thermodynamic force :
$$\mathcal{A}_z = \frac{-1}{2E_a}\left(\frac{F}{S}\right)^2 + \frac{1}{2E_m}\left(\frac{F}{S}\right)^2 + \frac{1}{Sl}F.X_{ori} - C(T) - Gz - \left((\alpha - \beta)z + \frac{\beta}{2}\right)\left(\frac{X_{ori}}{l}\right)^2,$$
Forward transformation criterion :
$$\mathcal{F}_1^{cri} = \mathcal{A}_z - a(1-z) - bz$$
Reverse transformation criterion :
$$\mathcal{F}_2^{cri} = -\mathcal{A}_z - a(1-z) - bz$$

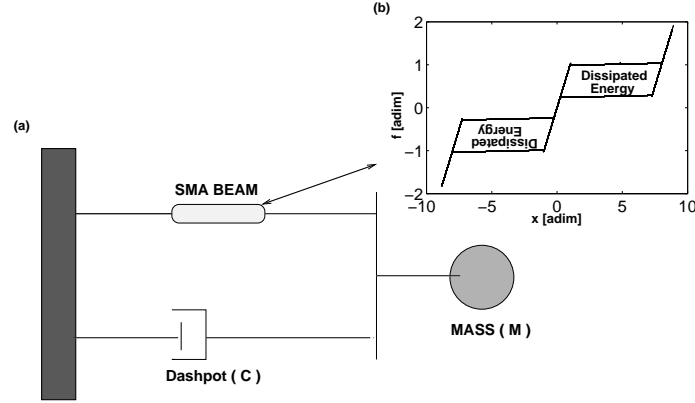**Table 1.** Dimensionalized equations

Fig. 1. (a) The pseudo-elastic device (b) Pseudo-elastic behaviour of the SMA beam

For calculations convenience, the following dimensionless equations are introduced : $\Omega = \frac{\omega}{\omega_n}$, $\tau = \omega_n t$, $x = \frac{X}{X_{ms}}$, $\gamma = \frac{E_{max}}{F_{ms}}$, $\zeta = \frac{C}{2\omega_n \mathcal{M}}$ and $f = \frac{F}{F_{ms}}$ where ω_n is the natural frequency of the device in its *austenitic* phase and is given by $\omega_n = \sqrt{\frac{\mathcal{K}_a}{\mathcal{M}}}$, X_{ms} and F_{ms} are respectively displacement and force tresholds of forward transformation. Assuming $\mathcal{K}_a = \mathcal{K}_m$, the dynamics of the systems is finally given by:

$$\begin{cases} \ddot{x} + 2\zeta\dot{x} + (x - z.x_{ori}) = \gamma \cos \Omega\tau & (10) \\ f(x, z, x_{ori}) = (x - z.x_{ori}) & (11) \end{cases}$$

A Newmark scheme for time integration of motion equation with parameters $\gamma_1 = \frac{1}{2}$ and $\beta_1 = \frac{1}{4}$ is used, where the internal Newton-Raphson iterations allows incremental fulfillement of the conditions provided by the criteria functions.

4   Results and discussion

In the remainder of the paper, the material parameters and the damping coefficient have been set to: $a=17.920Mpa$, $b=17.920Mpa$, $\varepsilon_0 = 0.112$, $\alpha = 1.4732Gpa$, $\beta = 1.4732Gpa$, $G = 26.88Mpa$, $\kappa = 8.68Mpa$, $\xi = 0.53114Mpa/^oC$, $T_0 = 233.3498K$, $A_f = 238.5945K$, $Y = 164Mpa$, $E_a = 50Gpa$, $E_m = 50Gpa$ and $\zeta = 0.05$. These values have been identified from the simulations shown in [2] in order to compare results. Frequency-response curves are obtained, for a given excitation frequency Ω, by numerical integration. The transient is removed and the maximal value of the displacement is recorded. Ω is then increased and decreased so as to obtain all stables branches of solutions. Figure 2 (a) shows the results obtained for increasing values of γ. For $\gamma = 0.1$, the response is linear, as no phase change is involved for that amplitude of response. For $\gamma = 0.2$ and $\gamma = 0.5$, the amplitude of the response exceeds 1: phase transformation occurs and the non-linear behaviour is characterized by a softening-type nonlinearity, as the resonance

frequency is seen to shift to lower values. Indeed, the equivalent stiffness of the pseudoelastic oscillator decreases. Saddle-node bifurcation points are then noted at points **A**, **B**,**C** and **D**, where jump phenomena are observed: when continuously varying the excitation frequency, the solution jumps to a stable solution to another one. For highest amplitude $\gamma = 0.8$, an additional branch of solutions is found between points **F** and **G**, it corresponds to cases where the phase transformation is completed ; the material becomes fully martensitic. The solution branch is bent to high frequencies as the stiffness increases from the transition plateaus to the purely martensitic case, with a volumic fraction z equal to 1. These results agree well with those in [2]. To go beyond, the amplitude $\gamma = 1.2$ is computed, results are shown in Fig. 2 (b). Before the resonance, for $\Omega \in [0, 0.5]$, a succession of erratic points are found, corresponding to the occurrence of superharmonic resonances of different orders. In order to get insight into the observed regimes for $\Omega \in [0, 0.5]$,
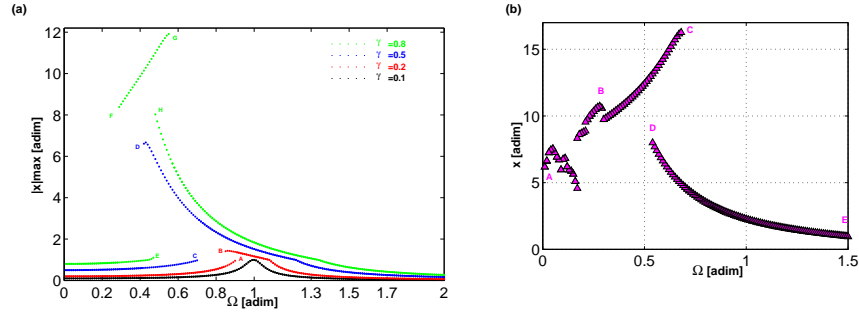
Fig. 2. (a)x_{max} vs. Ω at different γ, (b) x_{max} vs. Ω at $\gamma = 1.2$

Poincaré maps are computed by making a stroboscopy of the response at the excitation frequencies. Results are presented in Fig.3, they clearly show the presence of chaos for a narrow frequency band [0.22, 0.28]. By decreasing the excitation frequency, a period-doubling route to chaos is observed from point **D**. On the other hand, for $\Omega \in [0, 0.22]$, periodic solutions persist. The chaotic solutions at the beginning of their existence window, namely for $\Omega = 0.23$, are shown in Fig.4(a). The temporal solution shows that chaos is driven by the erratic behaviour of the enveloppe. Phase portrait reveals a fractal attractor. Interestingly, Fig.4(b) shows the emergence of even harmonics in the FFT of the displacement signal although the behaviour is symmetric. This shows that the bifurcation scenario when entering the chaotic window from low-frequencies is that of a symmetry-breaking bifurcation, as already observed in the Duffing oscillator [10].
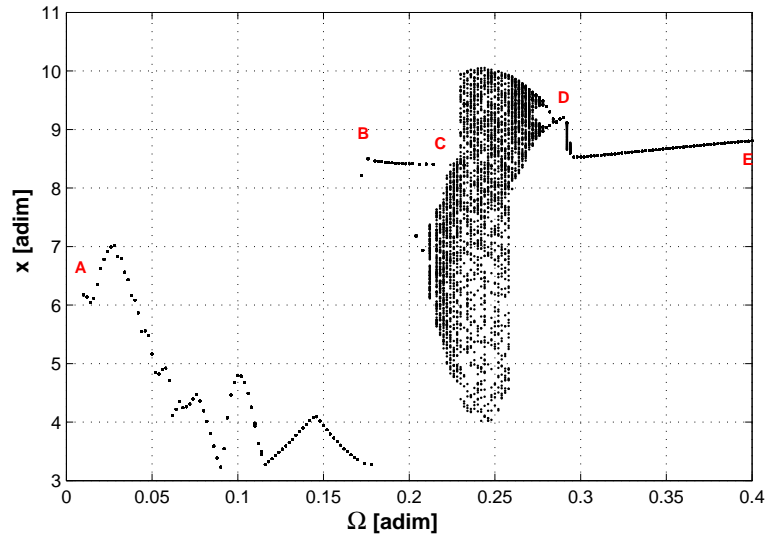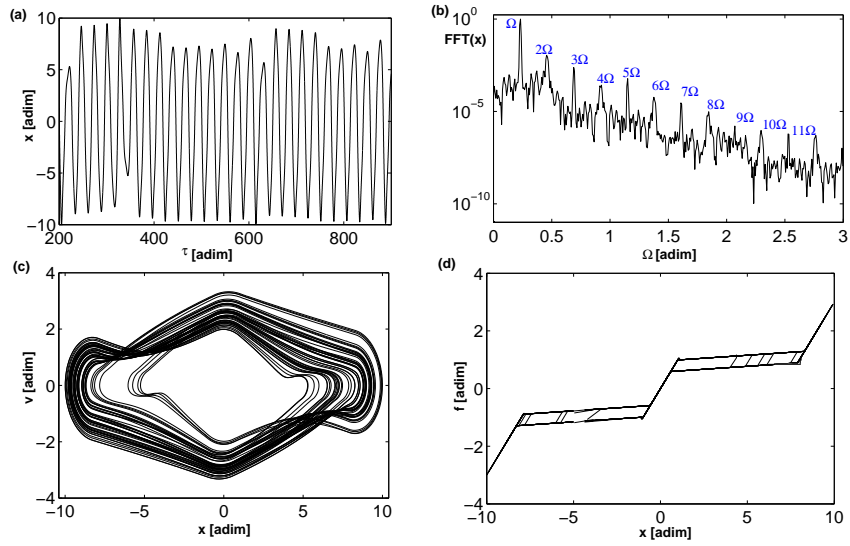
Fig. 3. Poincaré map at $\gamma = 1.2$

Fig. 4. (a) x vs. τ, (b) FFT(x) vs. Ω, (c) v vs. x and (d) f vs. x at $\gamma = 1.2$ and $\Omega = 0.23$:

5 Conclusion

The non-linear dynamic responses of pseudoelastic SMAs have been studied through reduction of a complete 3D model to a single degree-of-freedom oscillator. Results shows the emergence of chaotic solutions in the computed responses, for high values of the forcing amplitude. The chaotic region is delimited by a symmetry-breaking bifurcation and a period-doubling scenario.

Acknowledgments

References

1. Zaki W. and Moumni Z. A three-dimensional model of the thermomechanical behavior of shape memory alloys. *Journal of the Mechanics and Physics of Solids*, 55(11):2455–2490, 2007.
2. Lacarbonara W., Bernardini D., and Vestroni F. Nonlinear thermomechanical oscillations of shape-memory devices. *International Journal of Solids and Structures*, 41:1209–1234, 2004.
3. Bernardini D. and Vestroni F. Non-isothermal oscillations of pseudoelastic devices. *International Journal of Non-Linear Mechanics*, 38:1297–1313, 2003.
4. Bernardini D. and Rega G. The influence of model parameters and of the thermomechanical coupling on the behavior of shape memory devices. *International Journal of Non-Linear Mechanics*, 2009.
5. Moumni Z., Zaki W., and NGuyen Q.S. Theoretical and numerical modeling of solid-solid phase change : Application to the description of the thermomechanical behavior of shape memory alloys. *International Journal of Plasticity*, 24:614–645, 2008.
6. Zaki W. and Moumni Z. A 3d model of the cyclic thermomechanical behavior of shape memory alloys. *Journal of the Mechanics and Physics of Solids*, 55(11):2427–2454, 2007.
7. Zaki W. An approach to modeling tensile-compressive asymmetry for martensitic shape memory alloys. *Smart Materials and Structures*, 19 (2010) 025009 (7pp), 2010.
8. Zaki W., Zamfir S., and Moumni Z. An extension of the zm model for shape memory alloys accounting for plastic deformation. *Mechanics of Materials*, 42:266–274, 2010.
9. Moumni Z. Sur la modélisation du changement de phase solide : application aux maté- riaux à mémoire de forme et à endommagement fragile partiel. *Thèse de doctorat, Ecole Nationale des Ponts et Chaussées*, 1995.
10. Parlitz U. and Lauterborn W. Superstructure in the bifurcation set of the duffing equation. *Physics Letters A*, 107(8):351–355, 1985.

Influence of activator-inhibitor transport ratio on Turing patterns in three coupled CSTRs with glycolytic oscillatory reaction

F. Muzika, I. Schreiber

Institute of Chemical Technology, Prague, Department of Chemical Engineering, Center for Nonlinear Dynamics of Chemical and Biological Systems, Technická 5, 166 28, Praha 6, Czech Republic.: tel. +420-220445118, fax: +420-220444320, e-mail: Frantisek.Muzika@vscht.cz

Abstract: This work study three CSTRs in parallel, coupled by two membranes, in order to find and analyse Turing instability. Our goal is to extend the theory of compositional complementarity in the origin of life and propose usage of Turing patterns as memory arrays and cellular logical units. Every CSTR have glycolytic oscillatory reaction, which is realized by model proposed by Moran and Goldbeter (1984). Turing instability reacts sensitively to ratio of transport of activator and inhibitor through every membrane it the system. Solution diagrams and Turing patterns as schematic concentration profiles are shown for three different ratios of transport coefficients of inhibitor and activator $q=100$, $q=1$ and $q=0.8$.
Keywords: Turing instability, Turing pattern, glycolysis, memory array, logical unit

1. Introduction

There are many types of organisms, which differ in shape and metabolism. Common property is asymmetric shape and asymmetric location of their sensing arrays and propulsion system. That should not be possible, if diffusion had homogenizing effect for every two subsystems of such organism. A possible explanation was given by Alan Turing in 1952, when he proposed a mechanism, where diffusion dehomogenizes the system of coupled cells [1]. Turing instability mechanism was also proposed for many problems concerning pigmentation and agglomeration of organism, which was summarized in [2] and this field of research is extended for example by [3]. Turing instability was found in neural networks and brain tissue models [4, 5]. There are also other mechanisms, that have probably major occurrence inside neural network. It is the bistability based network of reactors, which can be compared to a Hopfield network and which can create logic gates by setting the right coupling strength between reactors [6]. Similar network can be used to store any pattern according to Hebbian rule and it is also resistent to small errors or undesirable perturbation [7, 8, 9]. Turing patterns are able to store memory as well [10].

As a general example of biochemical processes, two steps of glycolysis are taken. It can generate many cases of interesting dynamical behavior [11]. Membrane proper for ATP/ADP transport can be found in mitochondria, where outer membrane is permeable for both species and inner membrane posses

ability of active transport of ATP with very small permeability for ADP [12]. This transport unequality gives opportunity for occurrence of Turing patterns from primary branch point bifurcation of homogeneous stationary state. Inner membrane of mitochondria currently does not contain phosphofructokinase, but it can be found in outer membrane of mitochondria of *Tetrahymena thermophilia* [13]. It is possible, that phosphofructokinase was present in inner membrane of mitochondria or similar organism like *Rickettsia prowazekii* [14] in the past and with aid of Turing instability, it could have important role during evolution, like in theories of compositional complementarity [15]. There is also ATP/ADP permeable membrane inside nervous system, where ATP acts as neurotransmitter. Its permeability is given by the presence of purin based receptors, which are partially described in [16, 17]. There are still many purin based receptors undiscovered in brain tissue and they are expected in slime molds, because genetic coding for such receptors is in their DNA. There is also a possibility of artificial urea based membrane [18], which is capable of ATP transport, when calcium ion is added.

In the first part of this paper, we describe the glycolysis model for three coupled continuous stirred tank reactors and its Turing instability region schematic location in parametric and extended parametric space. Then solution diagrams with changing ratio of transport coefficients of inhibitor over activator are shown. Ratio parameter is set to q=100, q=1 and q=0.8.

The second part of this paper is dedicated to dynamic simulations of static Turing patterns and oscillatory behavior with proposed technical usage as memory array and three input XOR+AND logic gate.

2. Model of Glycolysis

For purpose of simplicity we took model of glycolysis inside yeast [19]. Intercellular diffusion element was added as product of transport coefficient of ADP (k_{ADP}) and concentration difference of one specie between two specified reactors. Diffusion rate coefficient of ATP and ADP based on its molecular structure and permeability through membrane is $\sim 10^{-6}$ cm^2/sec according to [20]. It is element of overall transport rate coefficient of ADP, which is defined as = *(diffusion rate coefficient / membrane thickness) x (cell surface / cell volume)*. For purpose of future usage as three-input logic gate or three to one-input memory array, we chose three coupled continuous stirred tank reactors and the model equations are

$$\frac{d[ATP]_1}{d[t]} = f_1([ATP]_{1,}[ADP]_1) + k_{ADP}q([ATP]_2 - [ATP]_1)$$

$$\frac{d[ADP]_1}{d[t]} = f_2([ATP]_{1,}[ADP]_1) + k_{ADP}([ADP]_2 - [ADP]_1)$$

$$\frac{d[ATP]_2}{d[t]} = f_1([ATP]_{2,}[ADP]_2) + k_{ADP}q([ATP]_1 - [ATP]_2)$$

$$\frac{d[ADP]_2}{d[t]} = f_2([ATP]_{2,}[ADP]_2) + k_{ADP}([ADP]_1 - [ADP]_2)$$

$$\frac{d[ATP]_3}{d[t]} = f_1([ATP]_{3,}[ADP]_3) + k_{ADP}q([ATP]_3-[ATP]_3)$$

$$\frac{d[ADP]_3}{d[t]} = f_2([ATP]_{3,}[ADP]_3) + k_{ADP}([ADP]_3-[ADP]_3)$$

$$f_1 = \square + \square_i \frac{[ADP]_1^n}{K^n+[ADP]_1^n} - \square_M \frac{[ATP]_1(1+[ATP]_1)(1+[ADP]_1)^2}{L+(1+[ATP]_1)^2(1+[ADP]_1)^2}$$

1)
$$f_2 = \square_M \frac{[ATP]_1(1+[ATP]_1)(1+[ADP]_1)^2}{L+(1+[ATP]_1)^2(1+[ADP]_1)^2} - k_S[ADP]_1 - \square_i \frac{[ADP]_1^n}{K^n+[ADP]_1^n}$$
2)

where $[ATP]$ is dimensionless concentration of ATP, $[ADP]$ is dimensionless concentration of ADP, $\square = 1.84$ is uptake rate, $\square_i$ is inhibition rate coefficient, $\square_M$ is autocatalytic rate coefficient, $k_S = 0.06$ is removal of product, $L = 5 \times 10^6$ is allosteric constant, $K = 10$ is Michaelis constant divided by ADP dissociation constant, $n = 4$ is degree of cooperativity (Hill coefficient), k_{ADP} is ADP transport coefficient. Ratio between transport coefficients of ATP and ADP is q .

3. Parametric an Extended Parametric Space

Schematic region of Turing instability can be shown in space of three changeable parameters (Fig. 1). We can also see, that vertical and horizontal cross-sections of such three parametric space would lead to bifurcation diagrams (Fig. 1 d,e,f). Horizontal bifurcation diagram is extended by one stationary concentration parameter and vertical cross-section through extended parametric
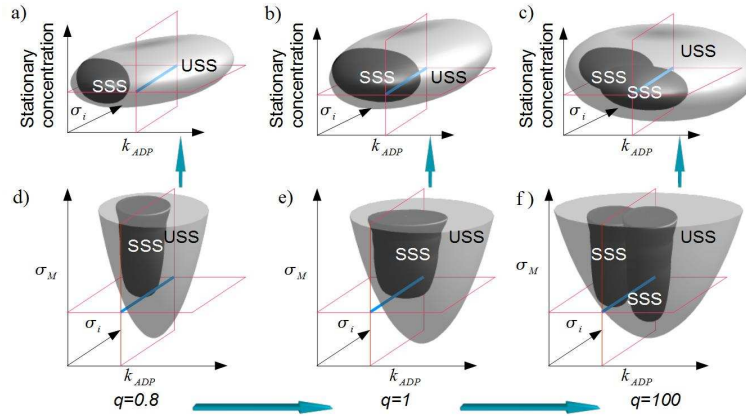
space creates solution diagrams (Fig. 1 a,b,c).

Figure 1.: Schematic Turing instability region inside parametric and extended parametric space. SSS represents stable stationary state, while USS represents
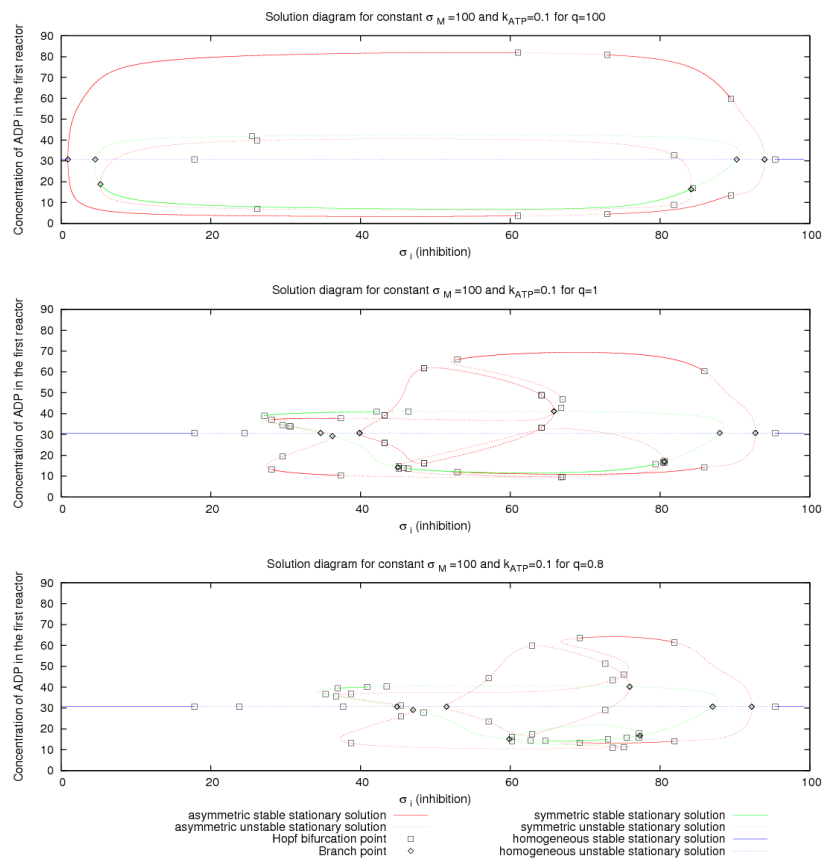
unstable stationary state. Other parameters can be found in "Model" section.

Schematic pictures in (Fig. 1) correspond to the real location and shape of Turing instability region of our model in parametric space. We can generally assume, that the lower the value of ratio of transport coefficient of inhibitor over activator, the smaller is Turing instability region.

4. Solution Diagrams

Solution diagram are calculated by Fortran based program CONT [21]. Continuation parameter is transport coefficient of ADP (k_{ADP}), printed stationary

Solution diagram for constant $\sigma_M = 100$ and $k_{ATP} = 0.1$ for q=100

Solution diagram for constant $\sigma_M = 100$ and $k_{ATP} = 0.1$ for q=1

Solution diagram for constant $\sigma_M = 100$ and $k_{ATP} = 0.1$ for q=0.8

asymmetric stable stationary solution — symmetric stable stationary solution
asymmetric unstable stationary solution — symmetric unstable stationary solution
Hopf bifurcation point □ homogeneous stable stationary solution
Branch point ◇ homogeneous unstable stationary solution

variable is stationary concentration of ADP (Fig. 2).

2.: Solution diagrams with assigned Turing patterns. Constants can be found in "Model" section. Turing patterns have two concentration levels: 1) low (bottom line inside reactor), 2) ... er line inside reactor)

Stable stationary state is marked by full line and if it is inhomogeneous,

370
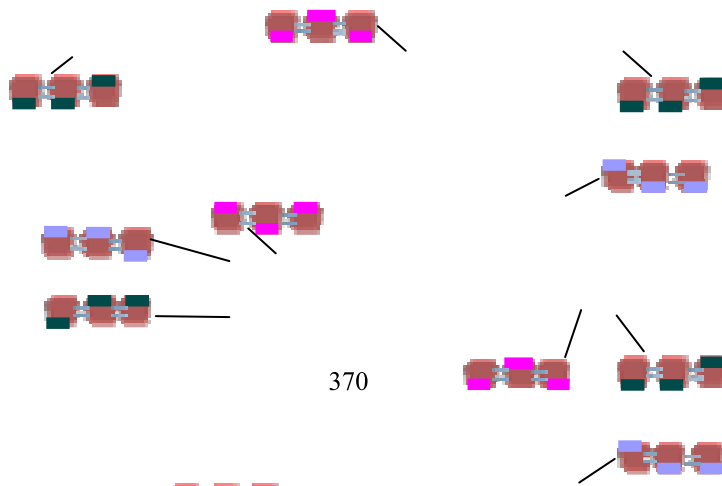
resulting Turing pattern is assigned. Dashed line represents unstable stationary state. Three type of points are present. Branch points represent division or union of multiple stationary states, it is also point of occurrence of Turing instability. Limit points represent parametric border of stationary state, the point, where inhomogeneous stationary curve turns its direction inside parametric space. Hopf bifurcation points represent point of occurrence or disappearance of oscillations, which are not drawn here. Their stability depends on stability of previous curve, so it transfers stability from oscillations into stationary states. We divide curves in solution diagram into symmetric, asymmetric and homogeneous, because it is more transparent (Fig. 2).

5. Dynamic Behavior of Static Turing Patterns

There are generally two types of Turing patterns, first are static Turing patterns, which are found in solution diagrams (Fig. 2) and the second one are dynamic Turing patterns. Their behavior and mathematical basis is descibed in [4]. The apparent multiplicity of stationary states (Fig. 2) and change of dynamic Turing patterns lead us to idea of switching between static Turing patterns by perturbations. Perturbations are chosen to have similar values, in order to gain modularity of the system. Dynamic simulations are made by fortran based program CONT [21]. System is set for equal transport rates of activator and inhibitor due to focus on using most simple coupling membrane possible, thus $q=1$. System prefers stable oscillations, when it is not externally influenced. We confirmed it by many calculations.

Our simulation is designed for simultaneous perturbation of all reactors. There are many possibilities leading to Turing patterns, but there are only three perturbation combinations, which can change stable oscillations into Turing patterns and after applying the same or other perturbation combination of this type, Turing pattern will change to other Turing pattern or stay the same. To gain such perturbation combination, we need to perturb reactors simultaneously with perturbations of ATP with values 1.2 for two reactors and -0.5 for remaining reactor. We thus obtain three possibilities of perturbation combination with three resulting Turing patterns. Such patterns can be used for storing one digital information in first an third reactor. Other perturbation combinations lead to stable oscillations. We can declare, that perturbation of ATP with value of 1.2 will be taken as digital 1 signal and perturbation of ATP with value of -0.5 will be taken as digital 0 signal. Turing pattern can be understand as stationary stable concentration level of each reactor. There are purin based receptors [17], capable of reading ADP concentration level and than open itself to transport ATP. If there will be receptor, which will read high concentration level from third reactor and than transport ATP from that reactor with value of 1.2, than result of three input reactor array will be digital 1 signal and it can be used for other reactor array as input signal. If there will be receptor, which will read low concentration level of third reactor and than transport ATP from extracellular space or other reactor array into that reactor with value of 0.5, than result of

three input reactor array will be digital 0 signal and it can be used for other reactor array as input signal. Many inputs result in stable oscillations. These oscillations can be changed into Turing patterns by the mentioned receptor mechanism, but the receptor would react to higher concentration than in case of Turing instability. Such regulatory receptors need to be in every cell. In (Fig. 3) we use oscillation regulation based on digital 1 for first and second reactors and digital 0 for third rector. Signals from receptors from third reactor will give the same output as XOR+AND logic gate.
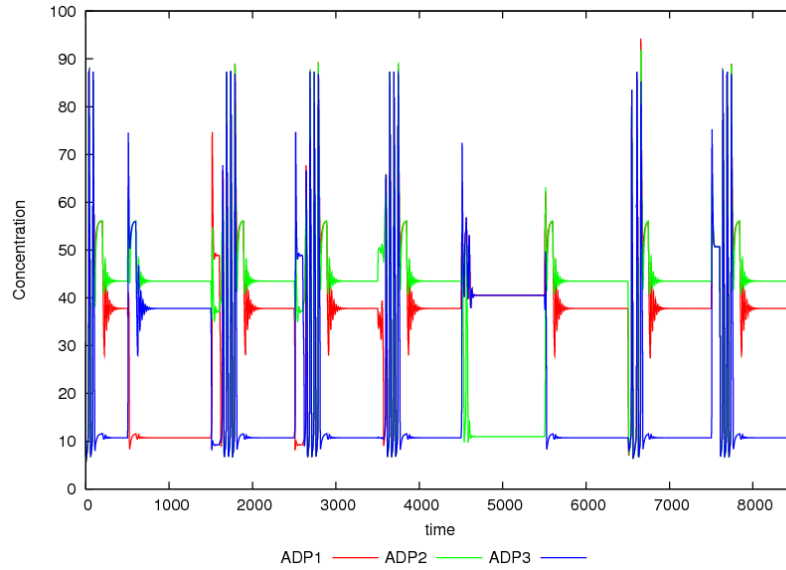
Figure 6.: System with three perturbation inputs regulated by controlling perturbation into Turing patterns. Third reactor output correspond to XOR+AND logic gate. Input perturbations are written in order first, second, third reactor. Values of perturbations are taken for 1.2 as digital 1 and for -0.5 as digital 0. Input perturbations are: (0 1 1) t=500, (1 0 0) t=1500, (0 0 1) t=2500, (0 1 0) t=3500, (1 0 1) t=4500, (1 1 0) t=5500, (0 0 0) t=6500, (1 1 1) t=7500. Every perturbation have time length 100, controlling perturbations are applied with time difference 200 from start of oscillations with values (1 1 0). Constants are set to: $\nu = 1.84$ *,* $\kappa_i = 35$ *,* $\kappa_M = 100$ *,* $k_S = 0.06$ *,* $L = 5 \times 10^6$ *,* $K = 10$ *,* $n = 4$ *,* $k_{ADP} = 0.1$ *,* $q = 1$ *. ADP1 represents ADP in first reactor, ADP2 represents ADP in second reactor and ADP3 represents ADP in third reactor.*

6. Results and discussion
Turing instability was found in three coupled reactors with glycolytic oscillatory reaction for parameters, where inhibitor is transported 100 times faster then

activator. Then it was found in system with equal transport rates and for 1.25 times faster activator transport rate. It occurs due to secondary stabilization of unstable branches, bifurcated from Turing instability. Secondary stabilization was realized by Hopf bifurcations. System with faster activator transport rate can be found in fuel cells and system with equal transport rates is very common. We suggest, that for such common transport parameters, we can propose procedure of memory storage and logic gate based on diffusion mechanism as dehomogenizing factor. Our procedure is in contrast with experiments, based on diffusion as homogenizing factor, made by Hjelmfelt, Schneider and Ross, where memory storage and logic functions are possible because of bistability.

Three coupled reactors with glycolysis model, with parameters leading to supecritical Turing instability, can create memory array and with oscillation control can create XOR+AND gate. We will focus on finding other logic gates and other technical usage of Turing patterns in our future work.

7. Aknowledgements

References

1. A. M. Turing. The chemical basis of morphogenesis, *Phil. Trans. R. Soc. Lond. B* 237:37-72, 1952.

2. J. D. Murray. Matematical biology II: Spatial Models and Biomedical 112 Applications (Third edition); *Springer Science+Business Media*, LLC; USA 2003.

3. M. Banerjee , S. Petrovskii. *Self-organised spatial patterns and chaos in a ratio-dependent predator-prey system,Theor Ecol 4:37–53, DOI 10.1007/s12080-010-0073-1*, 2011.

4. N. A. Venkov, S. Coombes, P.C. Mathews. Dynamic instabilities in scalar neural field equations with space-dependent delays, *Physica D 232*,1–15, 2007.

5. M. L. Steyn-Ross, D. A. Steyn-Ross, M. T. Wilson, J. W. Sleigh. Modeling brain activation patterns for the default and cognitive states, *NeuroImage*, Vol. 45, Iss. 2, Pages 298-311, New Zeland., 2009.

6. A. Hjelmfelt, J. Ross. Implementation of logic functions and computations by chemical kinetics, *Physica D 84*, 180-193, 1995.

7. A. Hjelmfelt, F. W. Schneider, J. Ross. Pattern Recognition in Coupled Chemical Kinetic Systems*, Science*, New Series, Vol. 260, No. 5106, pp. 335-337, 1993.

8. A. Hjelmfelt, J. Ross. Mass-Coupled Chemical Systems with Computational   Properties, *J. Phys. Chem.*, 97, 1988-1992, 1993.

9. A. Hjelmfelt, J. Ross. *Pattern recognition, chaos, and multiplicity in neural   networks of excitable systems*, *Proc.Natl. Acad.Sci. USA Vol. 91*, pp. 63-67, Biophysics, 1994.

10. P. Arena, S. De Fiore, L. Patané. Cellular Nonlinear Networks for the emergence of perceptual states: Application to robot navigation control, *Neural Netw.*, 22(5-6):801-11, Italy, 2009.

11. A. Goldbeter. Biochemical oscillations and cellular rhythms: The molecular bases of periodic and chaotic behavior. Cambridge University Press, 1996.

12. M. Klingenberg. The ADP and ATP transport in mitochondria and its carrier. *Biochimica et Biophysica Acta.*1778 1978–2021, Institut Physiologische Chemie der Universität München, Germany, 2008.

13. M. Eldan, J.J. Blum. Localization of Phosphofructokinase on the Mitochondria of Tetrahymena pyriformis*, *The Journal of Biological Chemistry*, Vol. 248, No. 21, Issue of November 10, pp. 7445-7448, USA, 1973.

14. H. H. Winkler and H. E. Neuhaus. Non-mitochondrial ATP transport. *Reviews.*TIBS 24 –FEBRUARY 1999.

15. A. Hunding, F. Kepes, D. Lance , A. Minsky, V. Norris, D. Raine, K. Sriram, R. Root-Bernstein. Compositional complementarity and prebiotic ecology in the origin of life, *BioEssays 28:399-412*, 2006.

16. B. S. Khakh, R. A. North. P2X receptors as cell-surface ATP sensors in health and disease, *Nature Vol 442*, doi:10.1038/nature04886, 2006.

17. C. Verderio, M. Matteoli. ATP in neuron–glia bidirectional signalling, *BRAIN RESEARCH REVIEWS 66*, 106 – 114, 2011.

18. M. Barboiu, S. Cerneaux, Arie van der Lee, G. Vaughan. *Ion-Driven ATP Pump by Self-Organized Hybrid Membrane Materials,* JACS Articles, France, 2004.

19. A. Goldbeter, F. Moran. Onset of birhytmicity in a regulated biochemical system*, Biophys. Chem. 20*: 149-56, 1984.

20. A. D. Nazarea. Critical length of the Transport-Dominated region for oscillating Non-linear Reactive Processes, *Proc. Nat. Acad. Sci. USA.* Vol. 71, No 9, pp.3751-3753, 1974.

21. I. Schreiber. Program CONT, 1999.

Improvement Performance of TH-UWB System Using Spatiotemporal Chaotic Sequences

Anis Naanaa and Safya Belghith

Sys'com laboratory, Ecole Nationale d'Ingénieurs de Tunis (ENIT), Tunisia
(E-mail: anis_naanaa@yahoo.com, safya.belghith@enit.rnu.tn)

Abstract. The residential environments are an important scenario for Ultra Wide Band (UWB) communication systems. In this paper, the performance of correlating receivers operating in a Line-Of-Sight (LOS) scenario in these environments is evaluated. In such channel the interference between users is an additional source of noise, that may deteriorate the performance of the system. In this research axis; it aims to exploit the richness of chaotic and spatiotemporal sequences with respect to topologic properties. We check through simulations, that chaotic sequences are shown to have improved performance compared to the Gold sequences in terms of Bit Error Rate (BER).
Keywords: Time hopping Utra wide band, Chaotic sequences, Multi-path channel, Spatiotemporal..

1 Introduction

Ultra-wideband (UWB) systems [1] use ultrashort impulses to transmit information which spreads the signal energy over a very wide frequency spectrum of several GHz. The sucess of UWB systems for short-range wireless communications [1,4] is due to the fact that they potentially combine reduced complexity with low power consumption, low probability-of-intercept (LPI) and immunity to multipath fading. In 2004, the IEEE 802.15.4a group presented a comprehensive study of the UWB channel over the frequency range 2-10 GHz for indoor residential, indoor office, industrial, outdoor and open outdoor environments [5]. In this work we are concerned with the indoor residential environment channel.

In time-hopping format (TH-UWB) TH codes are used as multiple user diversity and pulse position modulation (PPM) as data transmission [1,4]. As any wireless communication system, the interference between users is an additional source of noise, that may degrade the performance of the system. Thus the choice of the modulation type, the multiple access techniques, the codes allowing multiple access is important in the determination of the system performance. Different works have tackled the statistical characteristics of the Multi-User Interference (MUI). Many of them have modeled the MUI as a random Gaussian process [1,4,6]. Due to this assumption, no code optimization has been considered.

Other works have dealt with the optimization of the performance by code selection [2,3]. In [3], the authors considered the asynchronous case, multi channel propagation such IEEE 802.15.3a channel model and rake receiver; they derived a criterion to find optimal codes that minimizes the variance of the MUI of a reference user. The proposed criterion appears as a significant measure to design TH-codes that optimize the performance of a reference user.

In [7] a criterion named Average Collision Number (ACN) that minimize the MUI variance has been defined then the average BER of active users was computed to confirm the relevance of this criterion, it has been shown that sequences having smaller ACN allow better BER. As we show later this criterion is unsuitable in some cases for selecting codes. In this contribution, instead of the ACN criterion we will use the new criterion called Average of Squared Collision Number

(ASCN). Based on this criterion we will analyse how much chaoticity of the chaotic codes affects the performance of the considered TH-UWB system. To validate our criterion, the performance in terms of BER is computed by simulating the TH-UWB system with line-of-sight (LOS) multi-path and AWGN channel in a residential environment IEEE 802.15.4a.

This paper is organized as follows. Section 2 gives a detailed description of the TH-UWB system; after introducing the TH-UWB-PPM system model, we give the format of the channel model IEEE 802.15.4a and the statistics of correlation receiver. In Section 3 the ASCN criterion is defined and compared to ACN [7]. In section 4 we define the different considered sequences; for chaotic sequences, the ASCN is computed versus bifurcation parameter and compared to Lyapunov exponent. In section 5, we validate our method by reporting simulation results showing the advantage of using ASCN. Finally we conclude in section 6.

2 System description

In this section, we begin by reminding the TH-UWB system model and the expression of the received signal in a synchronous TH-UWB system using the PPM modulation. Then we compute the variance of the MUI versus TH-codes when a correlation receiver is used.

2.1 System model

A typical expression of the TH-UWB transmitted signal for a user j is given by equation 1.

$$s^{(j)}(t) = \sum_{k=-\infty}^{\infty} \sum_{l=0}^{N_f-1} w(t - kT_s - lT_f - \widetilde{c}_l^{(j)} T_c - d_k^{(j)} \delta) \tag{1}$$

Where $w(t)$ is the transmitted UWB pulse shape, T_s is the period of one bit. Every bit is conveyed by N_f frames. Each frame has a duration of T_f and is divided into N_c time slots. Each time slot has a duration of T_c. $\widetilde{c}_l^{(j)}$ is the TH code sequence assigned to the user j, where $\widetilde{c}_l^{(j)} \in \{0, 1, \ldots, N_c-1\}$. The location of each pulse in each frame is defined by the code $\widetilde{c}_l^{(j)}$. $d_k^{(j)} \in \{0, 1\}$ is the binary transmitted symbol at time k by user j, δ is the time shift associated with binary PPM, the pulses corresponding to bit 1 are sent δ seconds later than the pulses corresponding to bit 0. $N = N_c N_f$ presents the total processing gain of the system.

2.2 IEEE 802.15.4a Channel Model (CM1)

The IEEE 802.15.4a has recently proposed a channel model [5] propagation in residential area [5]. According to this model the impulse response is [5,8],

$$h^{(j)}(t) = \sum_{m=0}^{M-1} \sum_{r=0}^{R-1} \alpha_{r,m}^{(j)} \delta(t - T_m^{(j)} - \tau_{r,m}^{(j)}) \tag{2}$$

where $\alpha_{r,m}$ is the tap weight of the r-th ray (path) in the m-th cluster, T_m is the arrival time of the m-th cluster and $\tau_{r,m}$ is the arrival time of the r-th ray in the m-th cluster. The distribution of the cluster arrival times is given by a Poisson process and the distribution of the ray arrival times is given by a mixed Poisson process [5]. The small scale fading statistics are modeled as Nakagami-m

distributed with different m-factors for different multipath components. The probability density function of Nakagami-m distribution is given in [5]. The ray amplitudes are lognormal distributed. The channel model which is used in the paper is for LOS scenarios in residential environments, referred to as CM1 [5]. The parameters of the channel are modeled as a function of the transmitter-receiver distance and the line-of-sight (LOS) availability. If N_u is the number of active users transmitting asynchronously; the received signal is

$$r(t) = \sum_{j=1}^{N_u} \sum_{m=0}^{M-1} \sum_{r=0}^{R-1} \alpha_{r,m}^{(j)} s^{(j)}(t - T_m^{(j)} - \tau_{r,m}^{(j)}) + n(t) \tag{3}$$

2.3   Statistics of the correlation receiver

The output of the correlation receiver of the ith user at time h is given by:

$$s_h^{(i)} = \sum_{p=0}^{N_f-1} \int_{hT_s+pT_f+\widetilde{c}_p^{(i)}T_c+\tau_{0,0}^{(i)}+T_0^{(i)}}^{hT_s+pT_f+\widetilde{c}_p^{(i)}T_c+T_c+\tau_{0,0}^{(i)}+T_0^{(i)}} r(t)v(t - hT_s - pT_f - \widetilde{c}_p^{(i)}T_c - \tau_{0,0}^{(i)} - T_0^{(i)})dt \tag{4}$$

where $v(t)$ is the receiver's template signal defined by $v(t) = w(t + \delta) - w(t)$.
An accurate value of $\tau_{0,0}^{(i)}$ can be obtained by UWB acquisition techniques such as [13]. From the previous equations and after variable changes, we obtain

$$s_h^{(i)} = T_U(i) + T_{ISI}(i) + T_I(i) + T_N(i) \tag{5}$$

with

   T_U is the useful signal, T_{ISI} is inter-symbol interference signal, T_I is the MUI and T_N is the term corresponding to the noise.
In [7], we defined a criterion named ACN for selecting codes in synchronous and single-path TH-UWB system. Also we have shown numerically, that this criterion is adequate even in the multi path channel.
Indeed in the synchronous case, it has been shown that

$$T_I(i) = E_w \sum_{j=1, j\neq i}^{N_u} \alpha^{(j)}(2d_h^{(j)} - 1)cn(i,j) \tag{6}$$

where E_w is the amplitude which controls the transmitted power, $\alpha^{(j)}$ is the tap weight of the user j, $d_h^{(j)}$ is the binary sequence, $cn(i,j)$ is the number of collision between codes $\widetilde{c}^{(i)}$ and $\widetilde{c}^{(j)}$. $\widetilde{c}^{(j)}$ can be computed by taking into account the developed Time-Hopping Codes (DTHC) [9] corresponding to TH codes as follows, for a given code $\widetilde{c}^{(j)}$, the DTHC is a binary code of length $N_c N_f$ and is defined by

$$c_r^{(j)} = \begin{cases} 1 \; if \; r = \widetilde{c}_l^{(j)} + lN_c, r = 0 \ldots, N_c N_f - 1. \\ 0 \; otherwise. \end{cases} \tag{7}$$

$$cn(i,j) = \sum_{l=0}^{N_f N_c - 1} c_l^{(i)} c_l^{(j)} \tag{8}$$

The Average Collision Number ACN of the sequence set $(\widetilde{c}^{(j)})$, $j = 1, \ldots N_u$ is therefore defined by [7]:

$$ACN = \frac{1}{N_u(N_u - 1)} \sum_{i=1}^{N_u} \sum_{j=1, j \neq i}^{N_u} cn(i,j) \tag{9}$$

3 ASCN criterion

In [7] we have defined the ACN criterion, and we have showed that the experimental results validate the relevance of the ACN as an 'off-line' performance evaluation criterion for codes sequences. These results motivated us to use the ACN as a tool to predict the performance of code sequences. However, we found intuitively that this criterion may in some cases be unsuitable for code selection. For example we take three users ($N_u = 3$). For scenario A, the THC are respectively $\widetilde{c}_l^{(1)} = [\,0\,0\,1\,1\,]$, $\widetilde{c}_l^{(2)} = [\,1\,1\,1\,1\,]$ and $\widetilde{c}_l^{(3)} = [\,0\,0\,2\,2\,]$. We find that the total number of collisions is equal to 4. For scenario B, the THC are respectively $\widetilde{c}_l^{(1)} = [\,0\,0\,1\,1\,]$, $\widetilde{c}_l^{(2)} = [\,0\,0\,1\,1\,]$ and $\widetilde{c}_l^{(3)} = [\,2\,2\,2\,2\,]$. Also the total number of collisions is equal to 4. In both scenarios, $ACN = \frac{4}{6}$.

To remedy to this drawback, we defined a new criterion called Average of Squared Collision Number ASCN which is defined as:

$$ASCN = \frac{1}{N_u(N_u - 1)} \sum_{i=1}^{N_u} \sum_{j=1, j \neq i}^{N_u} cn^2(i,j) \tag{10}$$

This is motivated by the observation that when the collisions are regrouped on few positions the performance are significantly degraded.

Now if we consider this new criterion; for scenario A, $ASCN = \frac{8}{6}$. For scenario B, $ASCN = \frac{16}{6}$. In this work, we propose to use the ASCN criterion to examine the performance of the TH-UWB system.

This is confirmed by Table 1 where we represented the BER for the two scenarios with $N_u = 3$ and $N_c = 4$. We can see that the BER of scenario A is almost the half of the BER of scenario B.

Table 1. ACN vs ASCN with BER simulation.

	ACN	ASCN	BER
Scenario A	4/6	8/6	0.0728
Scenario B	4/6	16/6	0.1662

4 ASCN optimization using chaotic sequences

Chaotic sequences have some properties that motivate researchers to use them in various applications: determinism, long term unpredictability and high sensitivity to initial conditions. Especially chaotic sequences generated by one dimensional non linear transformation have been used in cryptography, watermarking, spectrum spreading systems [10].

We begin by defining Gold and chaotic sequences that will be considered in this work; then we define the ASCN for chaotic sequences versus their bifurcation parameter, and analyse how chaoticity measured by Lyapunov exponent is correlated with the ASCN.

Gold sequences

The Gold sequence based TH codes are generated as shown in [11], where we illustrate how is generated a sequence taking values in $\{0, 1, \cdots, N_c - 1 = 7\}$ and with a length $N_f \leq 29$.

Sequences generated by Skew tent map

Chaotic sequences are generated by the Skew tent map defined by:

$$x_{n+1} = \begin{cases} \frac{x_n}{r}, & 0 \leq x_n \leq r \\ \frac{1-x_n}{1-r}, & r < x_n \leq 1 \end{cases} \tag{11}$$

The skew tent map exhibits chaotic behavior for every value of the bifurcation parameter $r \in [0\ 1]$.

Sequences generated by Logistic map

The logistic map is given by the following equation:

$$x_{n+1} = rx_n(1 - x_n) \tag{12}$$

The logistic map exhibit alternatively regular and chaotic behavior when r belongs to $[3\ 4]$.

Figures 1 and 2 show the Lyapunov exponent and ASCN versus the bifurcation parameter r for different chaotic sequences. We can see that the curves of the ASCN follow the one of Lyapunov exponent and that the greater the exponent is the smaller the ASCN. For logistic map $r = 4$ gives the best value of Lyapunov exponent and ASCN. For skew tent map $r = 0.5$, have the best ASCN and Lyapuonv exponent. According to these two examples, we showed numerically that the ASCN
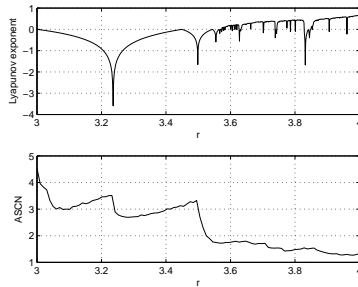

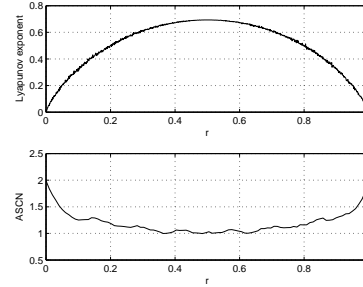**Fig. 1.** Lyapunov exponent and ASCN for logistic.

Fig. 2. Lyapunov exponent and ASCN for skew tent map.

of a quantized chaotic sequence depends on the chaoticity of these sequences measured by their

Lyapunov exponent.

In Figure 3, we represent the ASCN versus user number for $N_c = 8$; for Gold sequences considered here as a reference and the two quantized chaotic sequences defined above; the ASCN of chaotic sequences are averaged over 100 realizations. For both logistic and skew tent maps we considered the bifurcation parameter that gives the best ASCN, i.e. $r = 4$ for logistic map and $r = 0.5$ for skew tent.
The results show that skew tent map chaotic sequences, have a better ASCN than Gold sequences. We can notice likewise that Gold sequences show better performance compared to the chaotic sequence when $N_u < 6$, this is because of the orthogonality of this sequences.
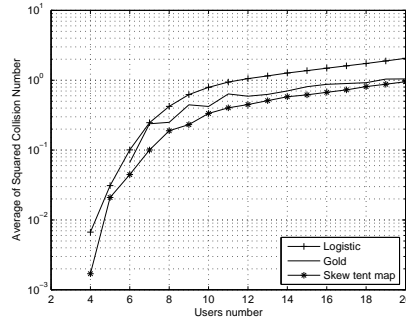
Fig. 3. ASCN versus user number for different types of codes. $N_c = 8$.

Sequences generated by spatiotemporal chaotic systems

Spatiotemporal chaotic systems have been the subject of intensive research in physics in the 80's to model and study some physical phenomena exhibiting chaotic behavior in time and space at once, such as turbulence, convection in chemical reactions and engineering. They have generally been modeled by networks of coupled lattice or CML (Coupled Map Lattices). Different models of CML have been proposed in the literature [12]. In our work we are interested only to the family of CML given by:

$$x_{i+1}(k + 1) = (1 - \epsilon)f[x_{i+1}(k)] + \epsilon f[x_i(k)] \tag{13}$$

Where:

- i is the space index, $i = 1, \cdots, M$, M the system dimension
- k is the time index, $k = 1, \cdots, N$
- f is a one dimensional chaotic map defined in the interval [0 1].
- ϵ is the coupling coefficient.

Spatiotemporal systems exhibit greater complexity compared to classical chaotic systems. They also provide more chaotic sequences, this increases the chaoticity of the system is a property of great importance in the use of CML to generate code sequences.

5   Performance comparaison of classical and chaotic codes sequences

In this section, we present the performance of MA-TH-UWB system in a residential environment CM1 channel by simulating the system and computing the BER; we consider the correlation receiver and the Gaussian pulse defined by:

$$w(t) = (1 - 4\pi(\frac{t}{\tau})^2)\exp(-2\pi(\frac{t}{\tau})^2) \tag{14}$$

The simulation parameters are listed in table 2. For simplicity, we assume that the number of paths

Table 2. Simulations parameters of TH-UWB system

Simulation parameters	Acronym	Value
Pulse duration	τ	0.2ns
Sampling frequency	F_s	8GHz
Chip duration	T_c	1ns
Number of sampling	N_e	50
Number of chip	N_c	8
Number of frame	N_f	4
Number of bits for each user	Nb	10^5
Factor for spread spectrum Gold	N	31
Number of path	L	10
Signal to Noise Ratio	SNR	10dB

L is the same for all users.

For chaos based TH-codes we used logistic and skew tent maps with parameters $r = 4$ and $r = 0.5$ respectively. These values correspond to the minimal of ASCN (the maximal of Lyapunov exponent) in the two cases. The simulation results are shown in Fig. 4 where we presented the BER of the system versus user number for Gold and the two chaos based sequences. We can see that skew tent map based sequences allow the best performance however logistic map based ones allow the worst performance. These results compared to the results shown in Fig. 3 prove that the ASCN is a suitable criterion to select TH-codes.

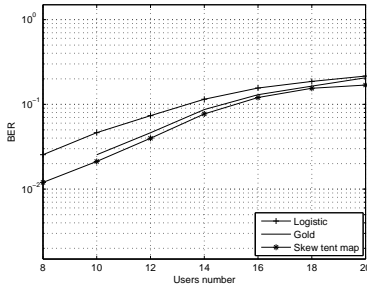The ASCN of the used skew tent map is equal to 1 however it is equal to almost 1.3 for the used

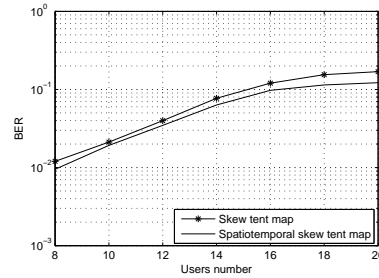**Fig. 4.** BER performance of asynchronous TH-UWB system for different TH codes.

Fig. 5. BER performance of asynchronous TH-UWB system: Skew tent map vs. spatiotemporal.

logistic map. This explains the superiority of skew tent map based sequences with respect to the

logistic map based ones. In Fig. 5 we represent the BER versus user number for the skew tent map and the spatiotemporal system (13) based on skew tent map, for a coupling coefficient $\epsilon = 0.97$, the spatiotemporal are averaged over 100 realizations and the bifurcation parameter is set to the value that gives the best ASCN, i.e. $r = 0.5$. We can see clearly that the THC generated by the CML can get better performance than THC generated by the skew tent map. Thus, the proposed spatiotemporal chaotic system considered is not only advantageous in terms of synchronization, but can also generate THC outperform the conventional chaotic system.

6 Conclusion

In this contribution we considered code selection problem for MA-TH-UWB systems. We defined the ASCN criterion to choose codes and we showed that the lower the ASCN the better the performance. Based on this result, we chose to look for codes with low ASCN by using the features of chaotic transformation; we found that the ASCN of chaotic map based sequences depends on the chaoticity of the map measured by Lyapunov exponent; we showed specifically that the higher the Lyapunov exponent the lower the ASCN; and subsequently the better the performance.

On the other hand, the use of THC generated by spatiotemporal chaotic system has shown better performance in term of BER that other sequences used in this article. This improves the quality and the security of the transmission, and shows the significance of using chaos specifically spatiotemporal chaotic system in communication.

References

1. R. A. Scholtz, "Multiple Access with Time-Hopping Impulse Modulation," in *Proc. MILCOM 1993*, Bedford, MA, October 1993, pp. 447–450.
2. I. Guvenc, and H. Arslan, "Design and performance analysis of TH-sequences for UWB-IR systems," in *Proc. IEEE Wireless Comm. and Networking Conf*, Atlanta, Georgia, USA, Mar. 2004, pp. 914–919.
3. C. J. Le Martret, A. L. Deleuze and P. Ciblat, Optimal TH Codes for Multi-User Interference Mitigation in UWB Impulse Radio, *IEEE Trans On Comm*, vol. 5, No. 6, Jun. 2006.
4. M. Z. Win and R. A. Scholtz, Ultra-Wide Bandwidth Time Hopping Spread-Spectrum Impulse Radio for Wireless Multiple Access Comm, *IEEE Trans. On Comm.*, vol. 48, pp. 679–691, Apr. 2000.
5. A. F. Molisch, and al. *IEEE 802.15.4a channel modelfinal report*,, November 2004.
6. F. Ramirez Mireles, "Error probability of ultra wideband ssma in a dense multipath environment," in *Proc. Milcom Conf*, Anaheim, CA, USA, Oct. 2002, vol. 2, pp. 1081–1084.
7. A. Naanaa, Z. B. Jemaa and S. Belghith, "Average Collision Number Criterion for TH-UWB Code Selection," in *Fifth ICWMC 2009*, Cannes, France, August 2009, pp. 122–127.
8. A. Saleh and R. Valenzuela, *A statistical model for indoor multipath propagation*,. IEEE Journal on Select. Areas Commun., vol. SAC-5, no. 2, pp. 128-137, Feb. 1987.
9. C. J. Le Martret and G. B. Giannakis, "All-Digital impulse radio for wireless cellular systems," *IEEE Trans On Comm*, vol. 50, No. 9, pp. 1440–1450, Sep. 2002.
10. G.M. Maggio, N. RulLov and L. Rggiani, Pseudo chaotic time hopping for UWB impulse radio, *IEEE Trans. Circuits and Systems-I*, vol. 48, No. 12, pp. 1424–1435, Dec. 2001.
11. D. J. E. Clabaugh, *Characterization of Ultra Wide Band Multiple Access Performance Using Time Hopped-Biorthogonal Pulse Position Modulation*. Ph.D. March 2004.
12. P. Almers, J. Karedal, S. Wyne, and al. *Uwb channel measurements in an industrial environment*. In IEEE Global Telecommunications Conference, volume 6, Nov. 2004.
13. W. Suwansantisuk, M. Z. Win, "Multipath Aided Rapid Acquisition: Optimal Search Strategies," *IEEE Trans On Information Theory*, vol. 53, No. 1, Jan. 2007.

Factor Analysis (FA) as ranking and an Efficient Data Reducing approach for decision making units: SAFA Rolling & Pipe Mills Company case study

Reza Nadimi[1], Hamed Shakouri G. [2], Jamshid S. Aram[3]

[1,2]Department of Industrial Engineering, Faculty of Engineering, University of Tehran, Tehran, Iran.
[1,3]Department of System and Methods Engineering, SAFA Rolling & Pipe Mills Company, Saveh, Iran.
Corresponding author: r.nadimi@yahoo.com

Abstract. This article compares two techniques: Data Envelopment Analysis (DEA) and Factor Analysis (FA) to aggregate multiple inputs and outputs in the evaluation of decision making units (DMU). Data envelopment analysis (DEA), a popular linear programming technique, is useful to rate comparatively operational efficiency of DMUs based on their deterministic or stochastic input–output data. Factor analysis techniques, such as Principal Components Analysis, have been proposed as data reduction and classification technique, which can be applied to evaluate of decision making units (DMUs). FA, as a multivariate statistical method, combines new multiple measures defined by inputs/outputs. Nonparametric statistical tests are employed to validate the consistency between the ranking obtained from DEA and FA. Also, the results have been compared with PCA approach. SAFA Rolling & Pipe Mills Company's data is used as a case study to consider the proposed approach in practical. Results of numerical reveal that new approach has a consistency in ranking with DEA.

Keywords: Data Envelopment Analysis; Factor Analysis, Principal Component Analysis; Decision Making; Data Reduction

1 Introduction

Data envelopment analysis (DEA) initially proposed by Charnes *et al.* [1] is a non-parametric technique for measuring and evaluating the relative efficiencies of a set of entities, called decision-making units (DMUs), with the common inputs and outputs. DEA is a linear programming-based technique that converts multiple input and output measures into a single comprehensive measure of productivity efficiency. DEA provides a measure by which one firm or department can compare its performance, in relative terms, to other homogeneous firms or departments. DEA is mainly utilized under two different circumstances. First, it can be used when a department from one firm wants to compare its level of efficiency performance against that of a corresponding department in other firms. Second, DEA can be used in a longitudinal nature by comparing the efficiency of a department or firm over time [2]. There are other ranking methods in the DEA context. Joe Zhu [3] proposed a procedure for ranking of DMUs, based on the principal component analysis (PCA) and showed that the ranking is consistent with the DEA ranking for the data set considered in his article. Sinuany_Stern and Freidman [4] proposed a new method for ranking of DMUs which is a combination of DEA and discriminant analysis of ratios (DR/DEA approach). This article proposes a Factor Analysis approach to evaluate of decision making units (DMUs). In this method, data reduction is comparable to that achieve in PCA. Moreover, correlation between rankings obtained by FA and DEA techniques is much higher than what is gained from the PCA&DEA method, which is introduce by Zhu [3]. The rest of this article is organized as follows. In Section 2, a brief description of the DEA models used for ranking of DMUs is presented. Section 3 gives the fundamental of FA technique. The FA approach is developed in Section 4. Numerical comparison of the proposed FA method versus DEA and PCA procedures is presented in Section 5, using several benchmark data along with a case study of SAFA Rolling & Pipe Mills Company to evaluate consistency of each method. Finally, Section 6 concludes this research.

2 Data Envelopment Analysis

Various models, used for ranking of DMUs, such as CCR [1], BCC [5] and ADD [6] are applied. The BCC model relaxes the constant returns to scale (CRS) assumption in the CCR model and the additive model ADD is an equivalent formulation of the CCR model. The original fractional CCR model proposed by

Charnes *et al.* [1] evaluates the relative efficiency of n DMUs ($j=1,..,n$), each with m input and s outputs denoted by $x_{1j},x_{2j},...,x_{mj}$ and $y_{1j},y_{2j},...,y_{sj}$, respectively, maximizing the ratio of weighted sum of outputs to weighted sum of inputs, as given by (1).
(CCR ratio model)

$$Max \ e_{j0} = \frac{\alpha_1 y_{1j0} + \alpha_2 y_{2j0} + ... + \alpha_s y_{sjo}}{\beta_1 x_{1j0} + \beta_2 x_{2j0} + ... + \beta_m x_{mjo}}$$

subject to

$$\frac{\alpha_1 y_{1j} + ... + \alpha_s y_{sj}}{\beta_1 x_{1j} + ... + \beta_m x_{mj}} \le 1 \quad (j = 1,...,n)$$

$$\alpha_1,\alpha_2,...,\alpha_s \ge 0$$

$$\beta_1,\beta_2,...,\beta_m \ge 0$$

(1).

In model (1), the efficiency of DMUj_0 is determined by e_{j0} while α_i and β_i are the *Factor weights*.

3 Factor Analysis (FA)

Factor Analysis is a statistical method that is based on the correlation analysis of multi-variables. The main applications of factor analytic techniques are: (1) to reduce the number of variables and (2) to detect structure in the relationships between variables, in order to classify variables. Nadimi and Jolai [10] applied factor analysis method to data reduction in decision making units[10], and then they illustrated their proposed method is a good consistency in ranking with DEA. Therefore, factor analysis can be used as a data reduction or structure detection method. There are two major types of FA: *exploratory* and *confirmatory*. Confirmatory FA is a much more sophisticated technique used in the advanced stages of the research process to test a theory about latent processes. Variables are carefully and specifically chosen to reveal underlying processes. To explain the method, a few terms are defined for more details about the following definition look at [8] or [10]. Let $q_{(n\times1)}$ be a random vector with a mean of μ and a covariance matrix named $\Sigma_{(p\times p)}$, where q_i specifies efficiency or an overall performance index of the ith DMU. Then a k-factor model holds for q, if it can be written in the following form:

$$q = Hf + u + \mu \tag{2},$$

where $H_{(n\times k)}$ is a matrix of constants and $f_{(k\times1)}$ and $u_{(n\times1)}$ are random vectors. The elements of f are called common factors and the elements of u are *specific* or *unique* factors. In this study we shall suppose that:

$$E(f) = 0, \ Cov(f) = I$$

$$E(u) = 0, \ Cov(u_i,u_j) = 0; \ i\neq j \tag{3}.$$

$$Cov(f, u) = 0$$

Thus, if (2) holds, the covariance matrix of d can be split into two parts, as follows:

$$\Sigma = H H^T + \Phi \tag{4},$$

where $H H^T$ is called the *communality* and represents the variance of q_i which is shared with the other variables via the common factors and $\Phi=Cov(u)$ is called the *specific* or *unique variance* and is due to the unique factors u. This matrix explains the variability in each q_i that is not shared with the other variables. The main goal of FA is to apply f instead of q for assessing DMUs.

To do this, mainly there are three main stages in a typical FA technique [9]:

1. Initial solution: Variables, as indexes of DMU performance measures, are selected and an inter-correlation matrix is generated. An inter-correlation matrix is a $p\times p$ array of the correlation coefficients of p variables with each other. Usually, each variable is standardized by a certain formula, e.g. to have a mean of 0.0 and a standard deviation of 1.0. When the degree of correlation between the variables is weak, it is not feasible for these variables to have a common factor, and a correlation between these variables is not studied. Kaiser–Meyer–Olkin (KMO) and Bartlett's tests of sphericity (BTS) are then applied to the studied variables in order to validate if the remaining variables are factorable.

2. Extracting the factors: An appropriate number of components (Factors) are extracted from the inter-correlation matrix based on the initial solution. Due to the standardization method, there should be a certain rule to extract the selected effective factors.

3. Rotating the factors: Sometimes one or more variables may load about the same on more than one factor, making the interpretation of the factors ambiguous. Thus, factors are rotated in order to clarify the relationship between the variables and the factors. While various methods can be used for factor rotation, the Varimax method is the most commonly used one.

Let's summarize and formulize the above steps as follows. In this study, we skip the rotation step. First, the correlation matrix, namely R, is computed on the basis of data due to the standardized variables, d_{ij}:

$$R = Corr(D) = D^T D \tag{5},$$

where D is an $n \times p$ matrix of p variables for n DMU's. This matrix can be decomposed to a product of three matrices:

$$R = VLV^T \tag{6},$$

where, V is the $p \times p$ matrix of eigenvectors and $L = Diag([\lambda_1, \ldots, \lambda_p])$ is a diagonal matrix of the eigenvalues, assorted descendingly. At the second step, different criteria may be applied to extract the most important factors. Since sum of the first r eigenvalues divided by the sum of all the eigenvalues, $(\lambda_1 + \lambda_2 + \ldots + \lambda_r) / (\lambda_1 + \lambda_2 + \ldots + \lambda_p)$, represents the "*proportion of total variation*" explained by the first r factor components, we select r principal components as the factors, if $(\lambda_1 + \lambda_2 + \ldots + \lambda_r)/(\lambda_1 + \lambda_2 + \ldots + \lambda_p) > 90\%$. Another criterion is to cut the matrix L from a point that the ratio of $\lambda_i / \lambda_{i+1}$ is maximized. However, r eigenvalues are defined as dominant eigenvalues. The dominant eigenvalues are saved and the other are skipped. To explain more, suppose L and V are decomposed as follows:

$$L = \begin{bmatrix} L_1 & 0 \\ 0 & L_2 \end{bmatrix} \tag{7},$$

where L_1 ($r \times r$) and L_2 are diagonal matrixes. Consequently, the eigenvectors V will be separated into two parts too:

$$V = [V_1, V_2] \tag{8},$$

Similarly, V_1 and V_2 are $p \times r$ and $p \times (p-r)$ matrices, respectively. Suppose (6) is rewritten as follows:

$$R = \left(V\sqrt{L}\right)\left(\sqrt{L}V^T\right) \tag{9}.$$

Then, replacing L with the form given by (7), the first part $V_1\sqrt{L_1}$ is called the *Factor Loading* matrix and denoted by $A_{(p \times r)}$. Equation (9) is frequently called the fundamental equation for FA. It represents the assertion that the correlation matrix is a product of the factor loading matrix, A, and its transpose [8]. It can be shown that an estimate of the unique or specific variance matrix, Φ, in (4) is:

$$B = I - AA^T \tag{10},$$

where $I_{(p \times p)}$ is the identity matrix. So far our study of the factor model has been concerned with the way in which the observed variables are functions of the (unknown) factors, f. Instead, factor scores can be estimated by the following pseudo-inverse method:

$$S^T = (A^T B^{-1} A)^{-1} A^T B^{-1} \tag{11},$$

$$F = DS \tag{12},$$

where F is a $n \times r$ matrix, each row of which corresponds to a DMU. The estimate in (12) is known as Bartlett's factor score, and S is called the *factor score* coefficient matrix. In this paper, we use the FA technique to evaluate DMUs by reducing inputs and outputs whilst minimizing the loss of information. This will be introduced in the next section.

4 New approach: FA method

It can be seen that DEA uses $e^*_{j0} = max\, e_{j0}$ to evaluate and rank DMUs according to their performances. It is still possible to look at ratios of individual output to individual input:

$$d_{ir}^j = y_{rj}/x_{ij} \quad ; i = 1, \ldots, m; r = 1, \ldots, s; j = 1, \ldots, n \tag{13},$$

for each DMU$_j$. Unlike the e_{j0}, d_{ir}^j gives the ratio between every output and every input. Obviously, the bigger the d_{ir}^j, the better the performance of DMU$_j$ in terms of the rth output and the ith input [11].

Now let $d_k^j = d_{ir}^j$, with, e.g. $k=1$ corresponds to $i=1$, $r=1$ and $k=2$ corresponds to $i=1$, $r=2$, etc., where $k=1, \ldots, p'$; $p' = m \times s$; for example: $d_1 = y_1/x_1$, $d_2 = y_1/x_2$, ... We need to find some weights that combine those p' individual ratios of d_k^j for DMU$_j$. Consider the following $n \times p'$ data matrix, composed by d_k^j's: $D^T = [d_1, \ldots, d_{p'}]_{n \times p'}$, where each row represents p' individual ratios of d_k^j for each DMU and

each column represents a specific output/input ratio, i.e. $\boldsymbol{d}_k = \left[d_k^1, ..., d_k^n \right]^T$. In a modified approach, proposed by Premachandra [12], $\boldsymbol{D}^T$ is re-defined as an augmented matrix, the ending column of which is equivalent to the sum of the elements in the first p' columns of the original matrix:

$$d_{p+1}^j = \sum_{k=1}^{p'} d_k^j \quad j = 1, ... n \tag{14}.$$

The new added variable, is supposed to take into account the overall performance of each DMU with respect to all the variables d_{ir}^j. As a normalizing skill, each column is then divided by its least element, thus a new matrix, $\boldsymbol{D}_{p \times n}$; $p = p' + 1$, is generated which will be processed from now on.

In this paper, the factor analysis is employed to find out new independent measures which are respectively different linear combinations of $\boldsymbol{d}_1, ..., \boldsymbol{d}_p$. In fact, we apply the estimation given by (12) to obtain factor scores, thus, the FA process of $\boldsymbol{D}$ is carried out as follows:

Step 1: Calculate the sample correlation matrix, given by (5), to obtain eigenvalues and eigenvectors (solutions to $|\boldsymbol{R} - \lambda \, \boldsymbol{1}_p| = 0$ where $\boldsymbol{1}_p$ is a $p \times p$ identity matrix), as introduced in (6).

Step 2: Considering $\lambda_1 \geq \lambda_2 \geq \dots \geq \lambda_p$ as the sorted eigenvalues, compute the following weightings, which determine share of each factor in the model:

$$w_i = \frac{\lambda_i}{\sum_{k=1}^{p} \lambda_k} ; \ i = 1, ..., \ p \tag{15}.$$

Each weighting actually determines the share of each eigenvalue out of a whole. This approach uses the same method of Zhu [3] to obtain sign of the weightings w_i, i.e. if sum of the corresponding eigenvector elements is positive, then w_i is considered positive, otherwise it is negative.

Step 3: Apply FA technique on $\boldsymbol{D}$ to obtain $\boldsymbol{S}^T$ and then $\boldsymbol{F}$, as defined by (11) and (14).

Step 4: Select the factor components by determination of the dominant eigenvalues according to one of the criteria proposed in Section 3.

Step 5: Compute:

$$z = \sum_{i=1}^{r} w_i \, \boldsymbol{f}_i \tag{16},$$

where $\boldsymbol{f}_i$ is the ith column of the matrix $\boldsymbol{F}$ in (14) and r is the number of the dominant eigenvalues. The value of z gives a combined measure to evaluate and rank performance of DMUs.

5 Numerical results

The proposed method is applied to several sets of sample data, the numerical results of which are illustrated and compared to other methods in this section.

Example1: In order to compare new approach with both the Zhu method, denoted by PCA(Zhu), and the modified PCA method used by Permachandra [12], abbreviated by PCA(PM), we hereby apply data used by Zhu [3]. This data sets describe economic performance of 18 china cites. (x_1: Investment in fixed assets by state owned enterprises, x_2: Foreign funds actually used, y_1: Total industrial output, y_2: Total value of retail sales, y_3: Handling capacity of coastal ports)

Table 1: The data set used by Zhu [3]

DMU	x_1	x_2	y_1	y_2	y_3	DMU	x_1	x_2	y_1	y_2	y_3
dmu1	2874.8	16738	160.89	80800	5092	dmu10	428.4	574	53.69	47504	430
dmu2	946.3	691	21.14	18172	6563	dmu11	6228.1	29842	258.09	151356	4649
dmu3	6854	43024	375.25	144530	2437	dmu12	697.7	3394	38.02	45336	1555
dmu4	2305.1	10815	176.68	70318	3145	dmu13	106.4	367	7.07	8236	121
dmu5	1010.3	2099	102.12	55419	1225	dmu14	5439.3	45809	116.46	56135	956
dmu6	282.3	757	59.17	27422	246	dmu15	957.8	16947	29.2	17554	231
dmu7	17478.6	116900	1029.09	351390	14604	dmu16	1209.2	15741	65.36	62341	618
dmu8	661.8	2024	30.07	23550	1126	dmu17	972.4	23822	54.52	25203	513
dmu9	1544.2	3218	160.58	59406	2230	dmu18	2192	10943	25.24	40267	895

Obviously, x_1 and x_2 can be assumed as two inputs and y_1, y_2, and y_3 as three outputs, data of which are presented in Table 1. First, variables are generated by (13) based on data set given in Table 1, and an additional variable is calculated by (14) to form matrix $D_{7\times7}$.

Table 2: FA&PCA result with PM and FA approaches.

Dominant Eigenvalues	4.31	2.06
Shares of Eigenvalues (w_i)	0.62	0.29
Dominant Eigenvectors	v_1	v_2
v_{i1}	0.40	-0.20
v_{i2}	0.46	0.04
v_{i3}	0.45	-0.13
v_{i4}	0.45	0.10
v_{i5}	0.05	0.68
v_{i6}	0.04	0.69
v_{i7}	0.47	0.01

Table 3: Component score coefficients

	Components	
	1	2
Output1	0.19	-0.14
Output2	0.22	0.03
Output3	0.21	-0.09
Output4	0.22	0.07
Output5	0.03	0.47
Output6	0.02	0.48
Output7	0.23	0.01

Then we used MATLAB 7, to test the proposed approach fulfilling the steps introduced in Section 4. Table 2 and Table 3 represent the Eigen-analysis of the correlation matrix calculated by (5). Here, we have two components which account for 90.502% of the total sample variance; i.e. V_1 in (8) contains two vectors, columns of which are named v_i. Note that the sum of all eigenvalues is 7, equal to the number of total variables. Since there are two dominant eigenvalues, regarding Table 2 and Table 3, data can be summarized to two factors. Therefore, F and z can be obtained with the following specifications, while the results due to each DMU are given in Table 4:

$$z = 0.616*f_1 + 0.293*f_2$$

The CCR model in (1) is applied to measure efficiencies. Besides that ranking and efficiency resulted of the new approach is compared to that of the original DEA and PCA in Table 5.

Table 4: Elements of matrix F and vector z

DMU	f_1	f_2	z	DMU	f_1	f_2	z
dmu1	5.152027	15.05106	7.598766	dmu10	38.77745	34.08271	33.91536
dmu2	26.30816	354.0689	120.2769	dmu11	4.296202	7.290633	4.790482
dmu3	3.795629	2.50461	3.075336	dmu12	9.06524	22.04124	12.06491
dmu4	6.753832	13.45095	8.115659	dmu13	12.50429	15.1375	12.15531
dmu5	17.25288	24.79452	17.92009	dmu14	1.439878	0.995586	1.179994
dmu6	26.36602	14.3498	20.46666	dmu15	1.76438	0.716694	1.298013
dmu7	3.936839	6.127137	4.22705	dmu16	4.555125	2.040313	3.406946
dmu8	7.868007	24.35411	12.00684	dmu17	2.634921	1.407985	2.037696
dmu9	15.18935	28.80653	17.82752	dmu18	2.25695	3.98423	2.561933

To compare significance of the methods, correlation between rankings obtained for each method, i.e. PCA (Zhu), PCA (PM) and FA (New Method), with the rankings of the DEA method is computed.

Table 5: Efficiency and ranking with three methods

DMU	DEA		PCA(Zhu)		PCA(PM)		FA(New Method)	
	Efficiency	Rank	Score	Rank	Score	Rank	Score(z)	Rank
dmu1	0.469066	13	-0.44767	10	12.93987	10	7.598766	10
dmu10	1.000000	3	2.669271	1	64.00527	2	33.91536	2
dmu11	0.277912	15	-0.74310	13	8.572844	11	4.790482	11
dmu12	0.502220	5	0.098945	7	20.89581	7	12.06491	7
dmu13	0.631077	4	0.286791	6	22.3876	6	12.15531	6
dmu14	1.000000	16	-1.19004	18	2.262825	18	1.179994	18
dmu15	0.358036	11	-1.08807	17	2.560632	17	1.298013	17
dmu16	0.495945	9	-0.59194	11	6.690926	13	3.406946	13
dmu17	0.657663	10	-0.85912	15	3.966397	16	2.037696	16
dmu18	1.000000	14	-1.08282	16	4.568629	15	2.561933	15
dmu2	0.300970	1	1.904927	3	182.9389	1	120.2769	1
dmu3	0.786606	17	-0.81823	14	5.914462	14	3.075336	14
dmu4	0.751444	12	-0.30670	9	14.31571	9	8.115659	9
dmu5	0.115331	6	0.698640	4	32.53710	4	17.92009	4
dmu6	0.186711	2	1.917903	2	39.79927	3	20.46666	3
dmu7	0.470368	18	-0.72208	12	7.622350	12	4.227050	12
dmu8	0.305945	8	-0.24401	8	20.33831	8	12.00684	8
dmu9	0.195259	7	0.517300	5	31.58701	5	17.82752	5

It is easy to find that correlations between ranking of DEA&PCA (Zhu), DEA&PCA (P.M.) and DEA&FA are 0.83, 0.80 and 0.80 respectively. Obviously, all of the methods result in significant correlations (at level 1%), and approximately are equal.

Example 2: In this example, we apply data set used by Wong et al. [14], to compare efficiencies of seven university departments. Three inputs and three outputs are defined as follows, data of which is listed in Table 6.

x_1: Number of academic staff

x_2: Academic staff salaries

x_3: Support of undergraduate students

y_1: Number of undergraduate students

y_2: Number of postgraduate students

y_3: Number of research papers published

Table 6: Data set used by Wong et al.[14]

DMU	x_1	x_2	x_3	y_1	y_2	y_3
dmu1	12	400	20	60	35	17
dmu2	19	750	70	139	41	40
dmu3	42	1500	70	225	68	75
dmu4	15	600	100	90	12	17
dmu5	45	2000	250	253	145	130
dmu6	19	730	50	132	45	45
dmu7	41	2350	600	305	159	97

The same procedure of section 4 is followed. The matrix D is generated by 10 variables extracted out of data in Table 6, and four dominant eigenvectors are selected and Table 7 includes the results of ranking.

Table 7: Efficiencies and rankings obtained by the three methods

DMU	DEA		PCA(Zhu)		PCA(PM)		FA(New method)	
	Efficiency	Rank	Score	Rank	Score	Rank	Score	Rank
dmu1	1.829615	1	0.51261	2	4.13838	1	2.011187	1
dmu2	1.048895	6	0.288772	4	3.315666	5	1.712316	5
dmu3	1.198308	4	0.011661	5	3.25405	6	1.559566	6
dmu4	0.819737	7	-1.9633	7	1.616393	7	0.895427	7
dmu5	1.219992	3	0.456634	3	3.801057	3	1.943119	2
dmu6	1.190642	5	0.918423	1	3.846452	2	1.917534	3
dmu7	1.266094	2	-0.2248	6	3.47953	4	1.883721	4

In this example the correlation between results obtained by PCA(Zhu) and DEA is 0.321, while correlation between DEA&PCA(PM) is 0.678. However, the new approach of FA has a higher correlation with the DEA, that is, 0.75, due to the scores given to the dmu5 and dmu6. This example shows that the FA approach can lead to better results, in the sense of DEA ranking, compared to the both PCA approaches proposed by Zhu and Premachandra.

Case Study: SAFA Rolling & Pipe Milling Company, Saveh, Iran.

SAFA Rolling & Pipe Mills Company by possessing 297.877 sqm of covered area has the annual capacity of producing 1.6 million tons of pipes for oil, gas, petrochemical, water, and industrial and construction industries application [15]. It is one the biggest company in producing of oil, gas and water pipe in Middle East. Electrical Resistance Welding (ERW) and Submerged-Arc Welding (SAW) are two welding processes in this company. In fact, this company is divided into four factories which are called "SPIRAL", "ROLL BENDING (RB)", "ERW" and "COATING" factories. The latter has been established to cover up the required pipe with the Epoxy, Polyethylene and Paste. However, manufacturing efficiency determines how well a factory operates in production. To avoid wasting money, all processes in manufacturing must be as efficient as possible. Calculating a numerical value to the efficiency helps to identify if improvements to the production process need to be made. In follow, we will illustrate how the proposed approach can be used to measure the efficiency of RB factory given the existence of multiple inputs and outputs.

Table 8: SAFA Company data

Year	Season	DMU	Electricity Consumption (KW) x1	Man-hours (Man-hours) x2	Total produced pipe weight (Ton) y1	Total produced pipe length (KM) y2
2010	3	d1	1642087.1	117768	18904.47	60880
2010	2	d2	1571303.8	133829	12940.54	51981
2010	1	d3	1840209.6	142704	23191.82	54248.99
2009	4	d4	1701038	145971	16724.54	20815.6
2009	3	d5	1113093	119571	18504.58	24750.13
2009	2	d6	582130	73057	7092.62	8766.8
2009	1	d7	1577788	121611	25510.27	35524.17
2008	4	d8	1748892	132331	9444.83	55652.56
2008	3	d9	1681965	117292	11593.18	71118.11
2008	2	d10	919053	83136	6493.39	42605.97

The proposed approach is applied on mentioned data and its results are compared to show the capability of the proposed approach with other methods. In Table 9 bellow, the scores and ranking of DMUs by four methods are given to evaluate the efficiency of different methods.

Table 9: Efficiencies and rankings obtained by the three methods

DMU	DEA Efficiency	DEA Rank	PCA(Zhu) Score	PCA(Zhu) Rank	PCA(PM) Score	PCA(PM) Rank	FA(New method) Score	FA(New method) Rank
dmu1	1.0000	3	0.6774	4	4.2177	3	2.8049	3
dmu2	0.8227	7	0.4689	5	3.2996	5	2.1772	6
dmu3	0.9409	6	-0.1295	6	3.2252	6	2.2209	4
dmu4	0.5857	10	-1.2947	9	1.3048	9	0.992	9
dmu5	1.0000	4	-1.2036	8	1.9863	8	1.5357	8
dmu6	0.7154	9	-1.3613	10	1.2067	10	0.9702	10
dmu7	1.0000	5	-1.0185	7	2.5829	7	1.902	7
dmu8	0.7398	8	0.7474	3	3.4045	4	2.1842	5
dmu9	1.0000	1	1.5931	1	4.7861	1	3.056	1
dmu10	1.0000	2	1.5206	2	4.3851	2	2.8165	2

Correlation between results obtained by PCA (Zhu) and DEA, DEA&PCA(PM) and DEA&FA (New method) here, are respectively 0.685, 0.745 and 0.782. It illustrates that the proposed approach is in high consistency with DEA methods.

6 Conclusion

The current article presents alternative approach to evaluate and rank DMUs which have multiple outputs and multiple inputs. The DEA –non-statistical method– uses linear programming technique to obtain a ratio between weighted outputs and weighted inputs. The new approach proposed in this paper is the Factor Analysis to evaluate efficiencies and rank DMUs. Results obtained by numerical experiments employed as well as the case study in manufacturing area, show that there is a high correlation between DEA and FA methods, even higher than what obtained by the PCA methods. Thus, we can use FA to evaluate efficiency and ranking DMUs instead of DEA with enough significance and minimum lose of information.

References

[1] Charnes, W.W. Cooper, E. Rhodes, Measuring the efficiency of decision making units, European Journal of Operations Research 2 (1978) 429 -444.

[2] L. Easton, D.J. Murphy, J.N. Pearson , Purchasing performance evaluation: with data envelopment analysis , European Journal of Purchasing & Supply Management 8 (2002) 123–134

[3] J. Zhu, Data envelopment analysis vs principal component analysis: An illustrative study of economic performance of Chinese cities, European Journal of Operation Research 111,(1998) 50-61.

[4] L. Friedman & Z. Sinuany-Stern, Scaling units via the canonical correlation analysis in the DEA context, European Journal of Operations Research 100(3),(1997) 629-637.

[5] R.D. Banker , A. Charnes, W.W. Cooper, Some models for estimating technical and scale inefficiencies in data envelopment analysis, Management Science 30(9)(1984)1079-1092

[6] A. Charnes, W.W. Cooper,B. Golany,L. Seiford, Foundations of data envelopment analysis for Pareto-Koop-mans efficient empirical production functions, Journals of Econometrics 30 (1985) 91-107.

[7] P. Andersen, N.C. Petersen, Aprodedure for ranking efficient units in data envelopment analysis, Management science 39(10), (1993) 1261-1294.

[8] B.G. Tabachnick L.S. Fidell, using multivariate statistics, fourth edition, allyn& bacon person education company (1996) 582-627.

[9] How to perform and interpret Factor analysis using SPSS, www.ncl.ac.Uk/iss/statistics/docs/Factoranalysis.html, 2002.

[10] R. Nadimi, F. Jolai, Joint Use of Factor Analysis (FA) and Data Envelopment Analysis (DEA) for Ranking of Data Envelopment Analysis, International Journal of Engineering and Natural Sciences 2:4 2008

[11] N. Adler, B. Golany, Evaluation of deregulated airline networks using data envelopment analysis combined with principal component analysis with an application to Western Europe, European Journal of Operations Research 132, (2001) 260-273.

[12] I.M. Premachandra, A note on DEA vs principal component analysis: An improvement to Joe Zhu's approach, Journal of Operational Research Society 132(2001) 553-560.

[13] S.H. Kim, C.G. Park, K.S. Park, An application of Data Envelopment Analysis in telephone offices evaluation with partial data. Computers & Operation Research 26(1999), 59-72.

[14] Y.H.B. Wong, J.E. Beasley, Restricting weight flexibility in data envelopment analysis, Journal of Operational Research Society 41(9), (1990) 829-835.

[15] http://www.safarolling.com

Some Problems of Convergence and Approximation in Random Systems Analysis

Gabriel V. Orman and Irinel Radomir

"Transilvania" University of Braşov, 500091 Braşov, Romania
(E-mail: `ogabriel@unitbv.ro`)

Abstract. In some previous papers we have introduced numerical functions able to characterize classes of derivations according to a given generative system up to an equivalence. They are referred to as "derivational functions". In this paper we establish some new properties by considering a new type of generation of the words. Also, we shall refer, in short, to new aspects concerning the Brownian motion as one of the most important stochastic processes. Finally the Markov property is discussed shortly.
Keywords: generative systems, Brownian motion, Markov process, transition probabilities, Markov property.

1 A problem of approximation in generative systems

To find new possibilities to characterize the process of generation of the words by sequences of intermediate words we have adopted a stochastic point of view involving Markov chains. Because such sequences of intermediate words (called *derivations*) by which the words are generated are finite, it results that finite Markov chains will be connected to the process. Such derivations are considered according to the most general class of formal grammars from the so-called *Chomsky hierarchy*, namely those that are free of any restrictions and are called *phrase-structure grammars*.

The process of generation of the words is organized by considering the set of all the derivations according to such a grammar split into equivalence classes, each of them containing derivations of the same length (here we are not interested in the internal structure of the intermediate words of a derivation but only in its length).

We remind some basic definitions and notations. A finite nonempty set is called an *alphabet* and is denoted by Σ. A *word* over Σ is a finite sequence $u = u_1 \cdots u_k$ of elements in Σ. The integer $k \geq 0$ is *the length* of u and is denoted by $|u|$. The word of length zero is called *the empty word* and is denoted by ε. If Σ is an alphabet, let us denote by Σ^* *the free semigroup*, with identity, generated by Σ (Σ^* is considered in relation to the usual operation of concatenation).

For y and z in V^* it is said that y *directly generates* z, and one writes $y \Rightarrow z$ if there exist the words t_1, t_2, u and v such that $y = t_1 u t_2$, $z = t_1 v t_2$ and $(u, v) \in P$. Then, y is said *to generate* z and one writes $y \overset{*}{\Rightarrow} z$ if

either $y = z$ or there exists a sequence $(w_0, w_1, \cdots, w_j)$ of words in V^* such that $y = w_0, z = w_j$ and $w_i \Rightarrow w_{i+1}$ for each i (we write $\overset{*}{\Rightarrow}$ for the reflexive-transitive closure of $\Rightarrow$). The sequence $(w_0, w_1, \cdots, w_j)$ is called a *derivation* of *length j* and from now on will be denoted by $D(j)$. Because a derivation of length 1 is just a production we shall suppose that the length of any derivation is ≥ 2.

Now we consider that a word is in a random process of generation, the equivalence classes of derivations being connected into a simple Markov chain. Obviously, it can or cannot be generated into the equivalence class D_x. Thus, if it is, then the probability that it should be also generated into the class D_{x-1} is denoted by γ; but given that it is not generated into D_x, the probability that it should be generated into D_{x+1} is denoted by β. Now we take into consideration only the case when a word cannot be generated by an equivalence class of derivations. Thus, if it is not generated by the class D_x, $x \geq 2$, then it will be generated by the class D_{x-1} with probability q and by the class D_{x+1} with probability $p = 1 - q$. Relating to the first and the last classes we suppose that it can or cannot be generated by them.

Let us remain in the case when a word is generated by more derivations according to a given generative system. This is a specific propriety of the so-called *ambiguous languages*, that is interesting to be characterized.

To this end let ν_x be the number of derivations into the equivalence class D_x, $x \geq 2$, by which the word w is generated. Obviously ν_x is a random variable that takes the values 1 and 0 with the probabilities p_x and $q_x = 1 - p_x$ respectively. Then, the number of derivations in $n - 1$ equivalence classes by which w is generated is the following

$$\nu = \sum_{x=2}^{n} \nu_x.$$

Now, because the equivalence classes of the derivations are connected into a homogeneous Markov chain, the expectation and the variance of ν are as follows

$$E\nu = \sum_{x=2}^{n} E\nu_x = (n-1)p + \sum_{x=2}^{n}(p_1 - p)\delta^{x-1} = (n-1)p + (p_1 - p)\frac{\delta - \delta^n}{1 - \delta} \quad (1)$$

and

$$D\nu = E\left[\sum_{x=2}^{n}(\nu_x - p_x)\right]^2 = \sum_{x=2}^{n} E(\nu_x - p_x)^2 + 2\sum_{i<j, i\geq 2} E(\nu_i - p_i)(\nu_j - p_j) \quad (2)$$

Now regarding the expectation of ν, excepting $(n-1)p$ the other term is bounded as n increases, such that it results $E\nu = (n - 1)p + u_n$, while regarding its variance excepting $(n-1)pq$ and $npq\frac{\delta}{1-\delta}$, the other all terms are bounded as n increases, so that we get $D\nu = (n-1)pq + 2npq\frac{\delta}{1-\delta} + v_n$,

where u_n and v_n are certain quantities that remain bounded as n increases. Thus, the following main result is obtained

Theorem 1 *If among the equivalence classes of the derivations according to a generative system G, a Markov dependence exists then, $L(G)$ tends to become an ambiguous language of order n if there exists a word $w \in L(G)$ such that the expectation and the variance of the random variable giving the number of derivations by which w is generated verify the following relations*

$$E\nu = (n-1)p + u_n, \qquad D\nu = pq\left[n\frac{1+\delta}{1-\delta} - 1\right] + v_n.$$

1.1 The alternating generation procedure

Now we consider the special case when a word can be generated into the equivalence class of a derivation on the following conditions:

1 It can be generated into the class $D_x, x \geq 2$, by more of its elements.
2 If it is not generated into the class $D_x, x \geq 2$, then it is generated into the preceding and the next class.

We refer to such a way for generating words as being *an alternating generation procedure*. We shall use the notation w for the case when this word is generated into an equivalence class and the notation $\overline{w}$ otherwise.

We propose to determine the probability $P_n(k)$ that a word w should be generated by $m\,(m < n)$ derivations in the following ways:

(i) It will be generated by the first class and the last and there is a direct rule (σ, w);
(ii) It will be generated by the first class but it will be not generated by the last and there is a direct rule (σ, w);
(iii) It will be not generated by the first class but it will be generated by the last and there is not a direct rule (σ, w);
(iv) It will be not generated both by the first class and the last and there is not a direct rule (σ, w).

Then $P_n(k)$ is given by the following equality

$$P_n(k) = P_n(k, ww) + P_n(k, w\overline{w}) + P_n(k, \overline{w}w) + P_n(k, \overline{w}\overline{w}) \qquad (3)$$

where $P_n(k, ww)$ is the notation for (i), and so on.

Now, computing the terms in (3), it results:

$$P_n(k, ww) \approx \frac{p_1\beta}{\sqrt{2\pi[k\gamma(1-\gamma) + (n-k)\beta(1-\beta)]}}\, e^{-\frac{z^2}{2}},$$

$$P_n(k, w\overline{w}) \approx \frac{p_1(1-\gamma)}{\sqrt{2\pi[k\gamma(1-\gamma) + (n-k)\beta(1-\beta)]}}\, e^{-\frac{z^2}{2}},$$

$$P_n(k, \overline{w}w) \approx \frac{q_1 \beta}{\sqrt{2\pi[k\gamma(1-\gamma)+(n-k)\beta(1-\beta)]}} \, e^{-\frac{z^2}{2}},$$

$$P_n(k, \overline{ww}) \approx \frac{q_1(1-\gamma)}{\sqrt{2\pi[k\gamma(1-\gamma)+(n-k)\beta(1-\beta)]}} \, e^{-\frac{z^2}{2}}.$$

$P_n(k)$ will be obtained by adding these probabilities, and we get

$$P_n(k) \approx \frac{p_1\beta + p_1(1-\gamma) + q_1\beta + q_1(1-\gamma)}{\sqrt{2\pi[k\gamma(1-\gamma)+(n-k)\beta(1-\beta)]}} \, e^{-\frac{z^2}{2}}.$$

or, after some transformations

$$P_n(k) \approx \frac{1-\gamma+\beta}{\sqrt{2\pi npq(1+\gamma-\beta)(1-\gamma+\beta)}} \, e^{-\frac{z^2}{2}}.$$

Thus, the following main result is obtained

Theorem 2 *If a word is generated by an alternating generation procedure, according to a generative system just considered, the derivations of which belonging to n equivalence classes then, the probability that it should be generated by k classes out of n is given by the following relation*

$$P_n(k) \approx \frac{1}{\sqrt{2\pi npq}} \sqrt{\frac{1-\gamma+\beta}{1+\gamma-\beta}} \, e^{-\frac{z^2}{2}} \ .$$

[Details and connected problems can be seen in Orman[11], Orman[9]].

2   Brownian motion

Brownian motion, used especially in Physics, is of ever increasing importance not only in Probability theory but also in classical Analysis. Its fascinating properties and its far-reaching extension of the simplest normal limit theorems to functional limit distributions acted, and continue to act, as a catalyst in random Analysis. It is probable the most important stochastic process. As some authors remarks too, the Brownian motion reflects a perfection that seems closer to a law of nature than to a human invention.

In 1828 the English botanist Robert Brown observed that pollen grauns suspended in water perform a continual swarming motion. The chaotic motion of such a particle is called ***Brownian motion*** and a particle performing such a motion is called a ***Brownian particle***.

The first important applications of Brownian motion were made by L. Bachélier and A. Einstein. L. Bachélier derived (1900) the law governing the position of a single grain performing a 1-dimensional Brownian motion starting at $a \in R^1$ at time $t = 0$

$$P_a[x(t) \in db] = g(t, a, b)db \tag{4}$$

where $(t, a, b) \in (0, +\infty) \times R^2$ and g is the Green (or the *source*) function

$$g(t, a, b) = \frac{1}{t\sqrt{2\pi}} e^{-\frac{(b-a)^2}{2t^2}}$$

of the problem of heat flow

$$\frac{\partial u}{\partial t} = \frac{1}{2} \frac{\partial^2 u}{\partial^2 a}, \qquad (t > 0).$$

Bachélier also pointed out the Markovian nature of the Brownian path but he was unable to obtain a clear picture of the Brownian motion and his ideas were unappreciated at that time. This because a precise definition of the Brownian motion involves a measure on the path space, and it was not until 1908-1909 when the works of É. Borel and H. Lebesgue have been appeared. Beginning with this moment was possible to put the Brownian motion on a firm mathematical foundation and this was achived by N. Wiener in 1923.

It is very interesting that A. Einstein also derived (4) in 1905 from statistical mechanical considerations and applied it to the determination of molecular diameters. He wanted also to model the movement of a particle suspended in a liquid. Einstein's aim was to provide a means of measuring Avogadro's number, the number of molecules in a mole of gas, and experiments suggested by Einstein proved to be consistent with his predictions.

We remind, for example, the following aspect. Let us consider that $\mathbf{x}(t)$ is the notation for the displacement of the Brownian particle. Then, the probability density of this displacement, for sufficiently large values of t, is as follows

$$p(\mathbf{x}, t, \mathbf{x}_0, \mathbf{v}_0) \approx \frac{1}{(4\pi D t)^{\frac{3}{2}}} e^{-\frac{|\mathbf{x}-\mathbf{x}_0|^2}{4Dt}} \tag{5}$$

where D is

$$D = \frac{kT}{m\beta} = \frac{kT}{6\pi a\eta} \tag{6}$$

and is referred to as the *diffusion coefficient*.

Furthermore it results that $p(\mathbf{x}, t, \mathbf{x}_0, \mathbf{v}_0)$ satisfies the diffusion equation given below

$$\frac{\partial p(\mathbf{x}, t, \mathbf{x}_0, \mathbf{v}_0)}{\partial t} = D\Delta p(\mathbf{x}, t, \mathbf{x}_0, \mathbf{v}_0). \tag{7}$$

The expression of D in (6) was obtained by A. Einstein.

Remark 1. From physics it is known the following result due to Maxwell: Let us suppose that the energy is proportional to the number of particles in a gas and let us denoted $E = \gamma n$, where γ is a constant independent of n. Then,

$$P\{a < v_i^1 < b\} = \frac{\int\limits_a^b \left(1 - \frac{x^2 m}{2\gamma n}\right)^{\frac{3n-3}{2}} dx}{\int\limits_{-\left(\frac{2\gamma n}{m}\right)^{\frac{1}{2}}}^{+\left(\frac{2\gamma n}{m}\right)^{\frac{1}{2}}} \left(1 - \frac{x^2 m}{2\gamma n}\right)^{\frac{3n-3}{2}} dx} \to$$

$$\to \left(\frac{3m}{4\pi\gamma}\right)^{\frac{1}{2}} \int\limits_{a}^{b} e^{-\frac{3mx^2}{4\gamma}}\, dx.$$

Now, for $\gamma = \dfrac{3kT}{2}$ the following Maxwell's result is found

$$\lim_{n\to\infty} P\{a < v_i^1 < b\} = \left(\frac{m}{2\pi kT}\right)^{\frac{1}{2}} \int\limits_{a}^{b} e^{-\frac{mx^2}{2kT}}\, dx.$$

T is called the "absolute temperature", while k is the "Boltzmann's constant".

[For details and proofs see Itô and McKean Jr.[4], Schuss[14], Stroock[15], Orman[12]].

3   The extended Markov property

In some previous papers we have dicussed on Markov processes in a vision of Kiyosi Itô. In this section we shall continue this discussion by considering the extended Markov property. More details and other aspects can be found in Itô and McKean Jr.[4], Itô[5], Bharucha-Reid[1].

As it is known, the intuitive meaning of the Markov process (for example $X(t)$) is the fact that such a process "forget" the past, provided that t_{n-1} is regarded as the present.

Now, the intuitive meaning of the Markov property is that under the condition that the path is known up to time t, the future motion would be as if it started at the point $X_t(\omega) \in S$.

Let S be a *state space* and consider a particle which moves in S. Also, suppose that the particle starting at x at the present moment will move into the set $A \subset S$ with probability $p_t(x, A)$ after t units of time, "irrespectively of its past motion", that is to say, this motion is considered to have a *Markovian character*.

The *transition probabilities* of this motion are $\{p_t(x, A)\}_{t,x,A}$ and we considered that the time parameter $t \in T = [0, +\infty)$.

The state space S is assumed to be a *compact Hausdorff space with a countable open base*, so that it is homeomorphic with a compact separable metric space by the Urysohn's metrization theorem. The σ-field generated by the open space (the topological σ-field on S) is denoted by $K(S)$. Therefore, a *Borel set* is a set in $K(S)$.

The *mean value*

$$m = M(\mu) = \int_{R} x\, \mu(dx)$$

is used for the center and the scattering degree of an one-dimensional probability measure μ having the second order moment finite, and the *variance* of μ is defined by

$$\sigma^2 = \sigma^2(\mu) = \int_R (x - m)^2 \mu(dx).$$

On the other hand, from the Tchebychev's inequality, for any $t > 0$, we have

$$\mu(m - t\sigma, m + t\sigma) \leq \frac{1}{t^2},$$

so that several properties of 1-dimensional probability measures can be derived.

Note that in the case when the considered probability measure has no finite second order moment, σ becomes useless. In such a case one can introduce the central value and the dispersion that will play similar roles as m and σ for general 1-dimensional probability measures.

Definition 1 *A Markov process is a system of stochastic processes*

$$\{X_t(\omega), t \in T, \omega \in (\Omega, K, P_a)\}_{a \in S},$$

that is for each $a \in S$, $\{X_t\}_{t \in S}$ is a stochastic process defined on the probability space (Ω, K, P_a).

The transition probabilities of a Markov process will be denoted by $\{p(t, a, B)\}$.

Now the *Markov property* is expressed in the theorem below.

Theorem 3 *Let be given $\Gamma \in K$. The following is true*

$$P_a(\theta_t \omega \in \Gamma | K_t) = P_{X_t(\omega)}(\Gamma) \quad a.s.(P_a);$$

that is to say

$$P_a(\theta_t^{-1} \Gamma | K_t) = P_{X_t(\omega)}(\Gamma).$$

Remark 2. The following notation can be used

$$P_{X_t(\omega)}(\Gamma) = P_b(\Gamma)|_{b=X_t(\omega)}.$$

To prove the theorem, it will be suffice to show that

$$P_a(\theta_t^{-1} \Gamma \cap D) = E_a(P_{X_t}(\Gamma), D) \tag{8}$$

for $\Gamma \in K$ and $D \in K_t$.

Corollaire 1

$$E_a(G \circ \theta_t, D) = E_a(E_{X_t}(G), D) \quad for \ G \in \mathbf{B}(K), D \in K_t,$$
$$E_a(F \cdot (G \circ \theta_t)) = Ea(F \cdot E_{X_t}(G)) \quad for \ G \in \mathbf{B}(K), F \in \mathbf{B}(K_t),$$
$$E_a(G \circ \theta_t | K_t) = E_{X_t}(G) \quad (a.s.)(P_a) \ for \ G \in \mathbf{B}(K).$$

It can be obseved that the Markov property can be extended as it is given in the following theorem

Theorem 4 *(The extended Markov property).*

$$P_a(\theta_t\omega \in \Gamma | K_{t+}) = P_{X_t}(\Gamma) \quad a.s. \ (P_a)$$

for $\Gamma \in K$.

The theorem results by considering the equality (8) before and by proving it for $D \in K_{t+}$.

References

1. A. T. Bharucha-Reid. Elements Of The Theory Of Markov Processes And Their Applications. Mineola, New York, 1997, Dover Publications, Inc.
2. S. Ginsburg. Algebraic and Automata-Theoretic Properties of Formal Languages. Amsterdam, 1975. North Holland Pub. Co.
3. I. I. Gihman and A. V. Skorohod. Stochastic Differential Equations. Berlin, 1972. Spriger-Verlag.
4. K. Itô and H. P. McKean Jr. Diffusion Processes and their Sample Paths. Berlin Heidelberg, 1996, Springer-Verlag.
5. K. Itô. Stochastic Processes. Ole E. Barndorff-Nielsen, Ken-iti Sato, editors. Berlin Heidelberg, 2004, Springer-Verlag.
6. B. Øksendal. Stochastic Differential Equations: An Introduction with Applications. Sixth Edition, New York, 2003, Springer, Berlin-Heidelberg.
7. G. V. Orman. Random Phenomena and some Systems Generating Words. *Yugoslav Journal of Operation Research* 6:245-256, 1996.
8. G. V. Orman. Stochastic Methods for Generative Systems Analysis. In A. Rizzi, M. Vichi, and H. H. Bock, editors, *Advances in Data Science and Classification*, pages 205-210, Berlin, 1998, Springer.
9. G. V. Orman. Capitole de matematici aplicate. Cluj-Napoca, 1999, Ed. Albastră.
10. G. V. Orman. Lectures on *Stochastic Approximation Algorithms. Theory and Applications.* Duisburg, 2001, Preprint, Univ. "Gerhard Mercator".
11. G. V. Orman. Limbaje formale şi acceptori. Cluj-Napoca, 2002, Ed. Albastră.
12. G. V. Orman. Handbook Of Limit Theorems And Sochastic Approximation. Brasov, 2003, Transilvania University Press.
13. G. V. Orman. On Markov Processes: A Survey Of The Transition Probabilities And Markov Property. In C. H. Skiadas and I. Dimotikalis, editors, *Chaotic Systems: Theory and Applications*, pages 224-232, 2010, World Scientific Publishing Co Pte Ltd.
14. Z. Schuss. Theory and Application of Stochastic Differential Equations. New York, 1980, John Wiley & Sons.
15. D. W. Stroock. Markov Processes from K. Itô Perspective. Princeton, 2003, Princeton Univ. Press.

Construction of Chaotic Generator Using Active Devices

Alpana Pandey, Rahul Deshmukh, Anurag Soni

Department of Electronics and Communication Engineering , Maulana Azad National Institute of Technology, Bhopal (Madhya Pradesh), INDIA

alpanasubodh@gmail.com ; manitanurag@gmail.com ;

Abstract: A chaotic generator based on two operational amplifiers, three capacitors and four resistors is described. The circuit is simulated using PSpice and the hardware implementation is done. The circuit can be implemented easily by using simple available electronic devices in electronics lab. Basically the circuit is an oscillator which behaves chaotically for some values of R. This circuit has low power spectral density thus it can be used as a chaotic generator in many indoor and mobile applications

Index terms- Chaotic, PSpice, Oscillator.

1. Introduction

Today, with a view to developing designed techniques for chaos generator, there is a definite need to characterize the complex behaviour exhibited by oscillators for some combinations of the circuit parameters. From this perspective, it should be noted that by moving the control parameters away from the oscillation condition many different kinds of complex behaviour may arise like chaos. Over the last three decades, many analog chaotic circuits have been proposed. Chua's circuit was the simplest electronic network which exhibits a verity of bifurcation phenomenon and attractors [1]. The circuit consists of two capacitors, inductors, a linear resisters and a nonlinear resistor. PSpice simulation produces quick visual results that satisfy certain learning criteria. Paul Tobin describes the Chua's circuit on PSpice [2]. K. Murli proposed a non-autonomous chaotic circuit based on a transistor, two capacitors and two resistors [3]. Jessica R. Piper proposed a simple autonomous chaotic circuit using op amp and passive components [4]. Analysis of chaotic generators has been subject of great interest because they can be implemented with simple electronic components. In our circuit chaotic signal is generated by simple electronic circuit designed with two AD741 ICs, four resisters and three capacitors. The circuits have extremely low power spectral density. Circuit is beneficial for indoor and mobile applications where high data rates are not required and where low bit error rate are achieved by acknowledgement protocols. Some applications of the circuits are networking devices of embedded systems and personal or body area networks.

2. Practical realization of the circuit

The circuit diagram for chaotic generator is shown in figure 1[4]. The circuit is realized with standard electronic components. The circuit is made on the bread board and the output voltages are measured at node 1 and 2. A practical version of this chaotic generator circuit is built with IC AD741, R_1=47K, R_2=47K, C_1=1nF, C_2=10nF, C_3=20nF, R=47K, R_C =1MΩ. V_1 and V_2 are the voltages taken at node 1 and 2 in the circuit. The plot between V_1 and V_2 is observed on CRO as shown in figure 2.
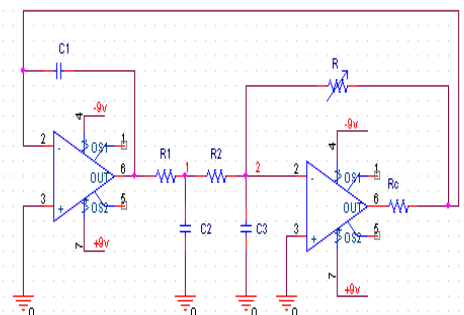
Figure.1 Circuit diagram for chaotic generator.
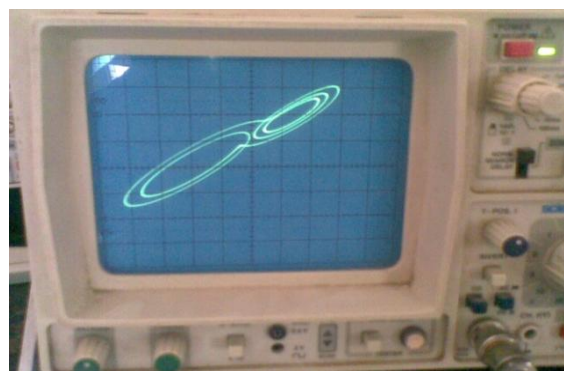
Figure 2. V_1 versus V_2 simulated plot for R=40K

3. Analysis of the circuit

The nonlinearity in this electronic circuit is produced by the operational amplifier. Two operational amplifiers with positive feedback form the chaotic oscillator. The dynamics of the circuit is described by system equation.

$$S^3 + AS^2 + BS + C = 0 \qquad (1)$$

Where the parameters A, B, C are described by

$$A = \frac{R+R2}{RR2C3} + \frac{R1+R2}{R1R2C2} + \frac{1}{R1C1} \qquad (2)$$

$$B = \frac{R+R1+R2}{RR1R2C2C3} + \frac{[R+R2]C2 + RC3}{RR1R2C1C2C3} \qquad (3)$$

$$C = \frac{1}{RR1R2C1C2C3} \qquad (4)$$

By simulation on PSpice, the plots of V_1 Versus time and V_2 Versus time are plotted as shown in figure 3 (a) and (b). Because of the positive feedback the circuit oscillates and the primary observed frequency will be 333Hz. Circuit produce sustained oscillations for the value of R lie between 10K<R<25K . And the circuit generates chaotic attractors for R>25.Figure 4 (a) & (b) shows plots for V_1 versus V_2 for practically implemented and PSpice simulated for R=45K.
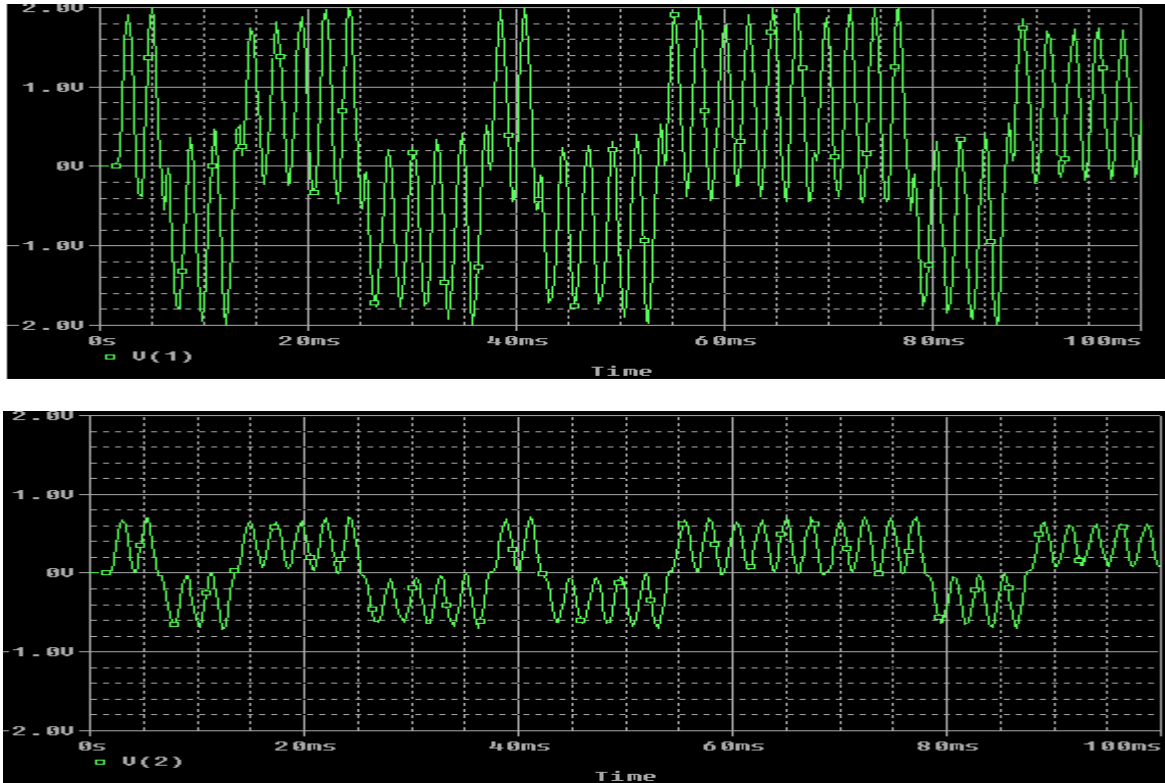
Figure.3. (a) plot for the voltage V_1 versus time (b) plot of the voltage V_2 versus time.
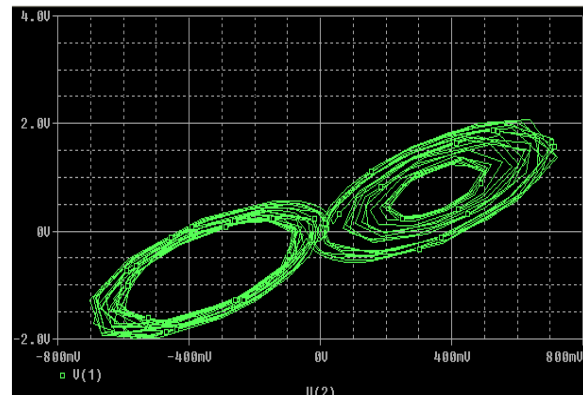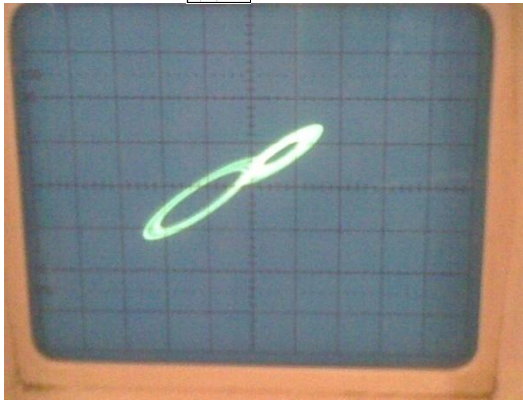
Figure 4. Plot of V_1 versus V_2 (a) oscilloscope photo   (b) simulated PSpice circuit

4. Conclusion

The circuit described in this brief have several advantages. The circuit is easy to fabricate with simple electronic components and it is very compact. The present circuit is general and robust. This circuit behaves chaotically for varying values of R. This chaotic generator is used in chaotic communication systems as encryption key at transmitter end and as a decryption key at the receivers end.

References

[1] Michael Peter Kennedy, "Robust op amp realization of Chua's circuit, "department of electronics and electrical engineering, university college Dublin, vol.46, no.3-4, March April 1992.

[2] Paul Tobin, "PSpice and project based learning at ordinary degree level" Dublin institute of technology, department of electronics and communications engineering, university college Dublin.

[3] E. Lindberg, K. Murali, and A. Tamasevicius, "The smallest transistor based non-autonomous chaotic circuit," *IEEE Trans. Circuits Syst. II, Exp. Briefs*, vol. 52, no. 10, pp. 661–664, Oct. 2005.

[4] Jessica R. Piper and J.C.Sprott," Simple Autonomous Chaotic Circuits" *IEEE Trans. Circuits Syst. II, Exp.Briefs*, vol. 57, no. 9, September 2010.

[5] K. Murali, M. Lakshmanan, and L. O. Chua, "The simplest dissipative nonautonomous chaotic circuit," *IEEE Trans. Circuits Syst. I, Fundam. Theory Appl.*, vol. 41, no. 6, pp. 462–463, Jun. 1994.

[6] A. Elwakil and M. P. Kennedy, "Construction of classes of circuit independent chaotic oscillators using passive-only nonlinear devices," *IEEE Trans. Circuits Syst. I, Fundam. Theory Appl.*, vol. 48, no. 3, pp. 289–307, Mar. 2001.

[7] T. Matsumoto, "A chaotic attractor from Chua's circuit," *IEEE Trans. Circuits Syst.*, vol. CAS-31, no. 12, pp. 1055–1058,Dec. 1984.

[8] M. P. Kennedy, "Chaos in the Colpitts oscillator," *IEEE Trans. Circuits Syst. I*, vol. 41, pp. 771–774, 1994.

[9] Anthony J Lawrance department of Statistics University of Karwich "Recent Theory and New applications in chaos communication".

Chaotic Communication: An overview

Subodh Pandey,Alpana Pandey

Head,SPFU, Bhopal,Madhya Pradesh,INDIA

Subodhpandey88@gmail.com

Abstract-Chaotic communication is a way to utilize the potential of chaos in communication. In this approach, message signal is mapped on to a chaotic signal and at the receiver same key is to be generated to get the actual information. Chaotic signals are easily generated and are aperiodic, impossible to predict, wide band signals having low power spectral density thus they have all advantages of spread spectrum signals. One major advantage of chaotic signals is that they are more secured because only intended receiver can received the signal. This paper provides an overview of chaotic communication, chaos generators and chaotic modulation schemes.

Index terms-Chaotic Communication, Spread Spectrum.

1.Introduction

Once the characteristics of chaotic signals are observed then engineers are thinking to utilize chaos signals as a candidate for spread spectrum signal. Chaotic signals are non periodic thus possess a continuous spectrum having significant strength over a wide range of frequencies. Chaotic signals have complex structure and are of very irregular nature. Chaos generator can produce totally different trajectories if its initial condition is changed and are uncorrelated. Chaotic signal looks like a noise in time domain thus have less risk of interception and are hard to detect by unintended receiver. Chaotic signal are generated first time by chua's diode [1].Recently VLSI chaotic generators are designed. To discuss chaotic communication this paper is organized as follows: In sec II chaotic generators are discussed. In section III chaotic modulation techniques are discussed. Finally sec IV contains some concluding remarks.

2. Chaotic Generators

Many chaotic Generators have been used in chaotic communication. The most common ones are:

- Basic Chua's circuits
- Single stage Collpitt's oscillator
- Using PWM/PPM signals
- Integrated CMOS chaos generator

Fig 1 shows the basic Chua's circuit in which nonlinearity is found in Chua's resistor to generate chaotic signal.
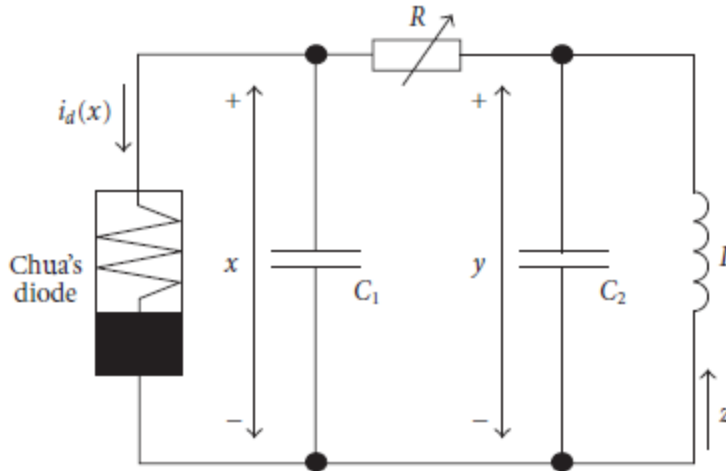
Figure1. Basic Chua's circuit.

Chua's circuit dynamical equation is given by

$$\frac{dx}{dt} = f_1(x, y, z) = \left(\frac{y-x}{RC1}\right) - \frac{id(x)}{C1},$$

$$\frac{dy}{dt} = f_2(x, y, z) = \left(\frac{x-y}{RC2}\right) + \frac{z}{C2},$$

$$\frac{dz}{dt} = f_3(x, y, z) = -\frac{y}{L} - z\left(\frac{rL}{L}\right),$$

$$i_{d\,(x)} = m_0 x + \frac{1}{2}(m_1 - m_0)\{|x + Bp| - |x - Bp|\}$$

Where R, C_1, C_2, and L are passive linear elements, r_L is the inductor's resistance, i_d is the current through Chua's diode with m_0, m_1 and B_p as parameter[1].

The circuit diagram of collpitt's oscillator is shown in Fig 2.The circuit is described by three state equations as [2]
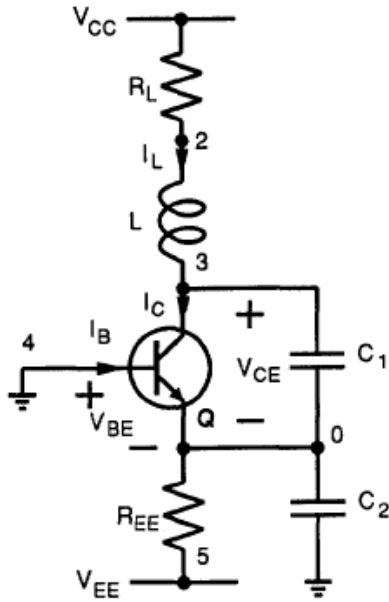
Fig. 2   collpitt's oscillator

$$\dot{x}_1 = \frac{1}{C_1} x_3 - \frac{I_C}{C_1}$$

$$\dot{x}_2 = -\frac{1}{C_2} x_2 - \frac{1}{C_2} x_3 - \frac{1}{C_2} \left\{ \frac{V_{EE}}{R_{EE}} + \beta I_C \right\}$$

$$\dot{x}_3 = -\frac{1}{L} x_1 + \frac{1}{L} x_2 - \frac{R_L}{L} x_3 + \frac{V_{cc}}{L}$$

Codes have been written in MATLAB for three equations. After programming in MATLAB, simulated results have been analysed. The 3D view of chaotic attractor is shown in fig. 3 and output voltage (For R_L = 33 Ω) with respect to time is shown in fig 4.
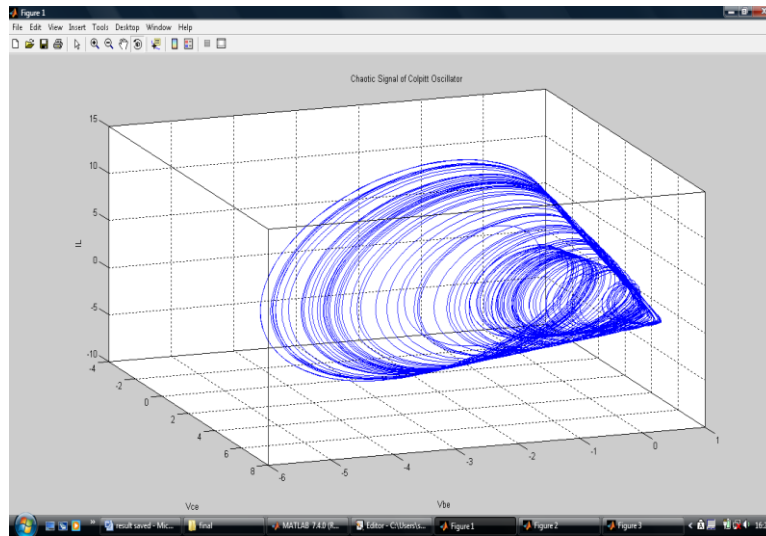
Fig. 3   3D view of chaotic attractor
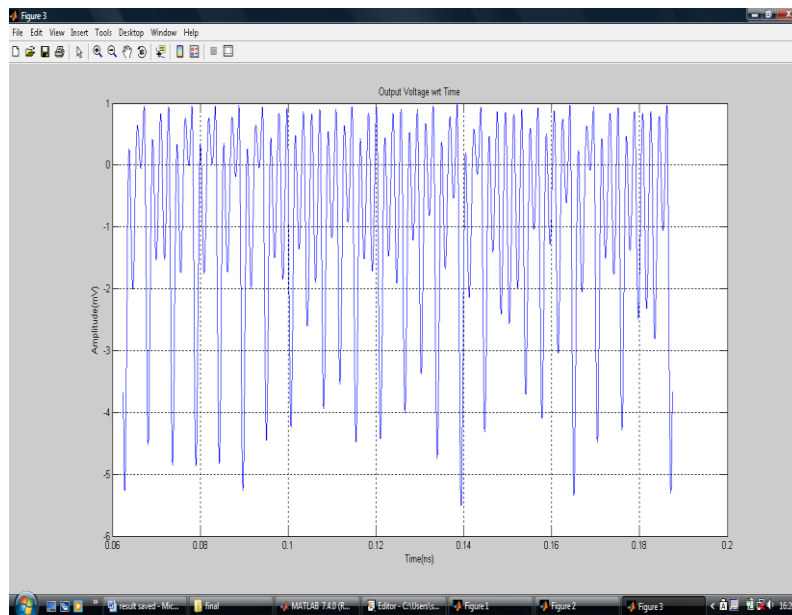
Fig 4 output voltage w.r.t. time of collpitt's oscillator.

3. Chaotic Modulation Techniques

Number of modulation techniques is used in chaotic communication. The most common ones are:

• Chaotic masking

• Chaos shift keying (CSK)

• Chaos on off keying (COOK)

• Differential Chaos shift keying (DCSK)

One of the very first proposals to use chaos in communication is chaotic masking [3] which is applicable to analog and digital messages. The chaotic signal x is added to message signal m, forming the transmitted signal y.
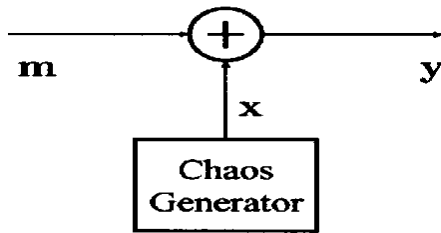
Fig. 5(a)   Chaotic Masking   Fig. 5(b)   Chaos shift keying
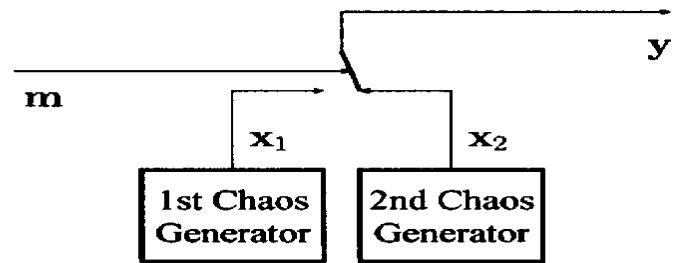
Fig 5 (a) shows the masking describe by $Y(t) = x(t) + m(t)$. CSK is a digital method, depending upon the N ary message symbol, the signal $x_i(t)$ (i = 1,2,3---N) from one of N chaos generators with different characteristics are transmitted. Fig 5(b) shows CSK and output signal is describe by

$$y(t) = \begin{cases} x_1(t) & \text{if } m(t) = m_1 \\ x_2(t) & \text{if } m(t) = m_2 \\ X_N(t) & \text{if } m(t) = m_N \end{cases}$$
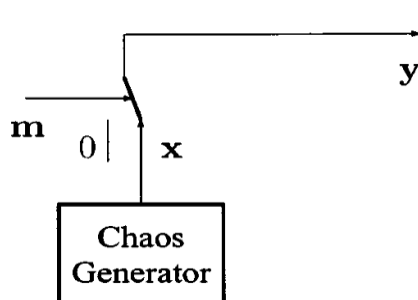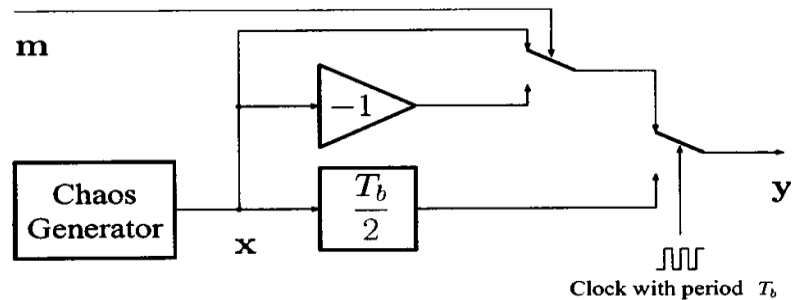
Fig. 5(c)   COOK   Fig. 5(d)   DCSK

A special case of CSK is the chaotic on-off keying (COOK). It uses one chaos generator, which is switched on or off according to a binary message symbol to be transmitted as shown in Fig 5(c) .

In DCSK, two channels are formed by time division, for every message symbol, first the reference signal is transmitted, followed by the modulated reference carrying the message symbol of duration T_b, the transmitted signal becomes

$$x(t) \ , \qquad \text{if } KT_b \leq t \leq \frac{2k+1}{2} \ T_b$$

$$y(t) = x \left(t - \frac{Tb}{2} \right), \qquad \text{if } \frac{2k+1}{2} \ T_b \ \leq t < (k+1) \ T_b \ \text{ and } m(t) = m_1$$

$$\ldots\ldots$$

$$-x \left(t - \frac{Tb}{2} \right), \qquad \text{if } \frac{2k+1}{2} \ T_b \ \leq t < (k+1) \ T_b \ \text{ and } m(t) = m_2$$

For reception of a message, references can be generated at receiver which is synchronized to the generator at transmitter or the reference has to be transmitted in addition to the actual message carrying signal.

4. Conclusion

This paper, gives an overview of chaos generators and chaotic modulation schemes found in literature. A few chaotic generators and Chaotic modulating schemes are described. The Chaotic signal is generated by collpitt's oscillator and waveforms are observed. The performance and the rate of information generation in a chaos generator are remains to be studied. Chaotic communication has many advantages over traditional communication and It is useful where the security is the first priority.

References

[1] R. M. Rubinger, A.W. M. Nascimento, L. F. Mello, C. P. L. Rubinger," **Inductor less Chua's Circuit: Experimental Time Series Analysis"** Mathematical Problems in Engineering, Hindawi Publishing Corporation Volume 2007

[2]. Z. G. Shi, K. S. Chen and L. X. Ran, "*Simulation And Experimental Study Of Chaos Generation In Microwave Band Using Collpitts Circuit,"* Vol.23 No.3 Journal of electronics (China) May 2006.

[3]. ANDREAS ABEL and WOLFGANG SCHWARZ, **"Chaos Communication –Principles , Schemes, And System Analysis"** in Proc.of the IEEE,VOL.90,NO.5,MAY 2002.

[4]. An jam Riaz and Maaruf Ali " **Chaotic communication, there Applications and Advantages over Traditional Methods of Communication"** Proc.of the CSNDSP 08

Chaotic Dynamics of Coupled Nonlinear Circuits in Ring Connection

Maria S. Papadopoulou, Ioannis M. Kyprianidis, Ioannis N. Stouboulos

Physics Department, Aristotle University of Thessaloniki, Greece
E-mails: mpapa@physics.auth.gr, imkypr@auth.gr, stouboulos@physics.auth.gr

Abstract: It is generally difficult to synchronize a ring network that features chaotic behaviour, especially if the system's order is too large. In this paper, we consider a ring network of three identical nonlinear and non-autonomous circuits of fourth order, which are bidirectionally coupled through three coupling linear resistances R_C. We present simulation and experimental results for synchronization of such a network in low frequency area, and derive a sufficient condition for chaotic synchronization of this type of network.
Keywords: Ring connection, Nonlinear circuit, Low frequency area, Chaotic synchronization.

1. Introduction

Synchronization is an important property of chaotic dynamical systems. In the past decades the synchronization in large scale complex networks has attracted lots of attention in various fields of science and engineering [2, 3, 5, 14, 15, 16]. In general, a complex network is a large set of interconnected nodes, where a node is a fundamental unit-joint with detailed contents, which lines intersect or branch.

The nonlinear electric circuits are veritable tools to study the fundamental mechanisms underlying the onset of chaos. A variety of autonomous [7, 8, 12] and non-autonomous [6, 10] circuits have been reported in the literature in recent times. A plethora of bifurcation and chaos phenomena, such as period doubling routes to chaos, intermittency, quasi periodicity, chaotic synchronization and so on, have been studied extensively.

In this paper, theoretical and experimental results of chaos synchronization of three identical non-autonomous circuits, bidirectionally coupled in ring connection network are presented. The system's evolution from non synchronized oscillations to synchronized ones, when its individual circuit exhibits chaotic behaviour, is studied.

2. The Nonlinear, Non-Autonomous Circuit

Chaotic performance of the fundamental non-autonomous circuit has been investigated in the past [4]. It is based on a third order autonomous piecewise linear circuit, which introduced by Chua and Lin [1], and is capable of realizing every member of Chua's circuit family. A second inductor L_2 has been added in the branch of the voltage source $v_s(t)$, in order to enrich circuit's dynamics. The circuit also consists of two active elements, a nonlinear resistor R_N, which has a v-i characteristic of N-type with $G_a=-0.35mS$, $G_b=5.0mS$ and $B_p=0.8V$, and a

negative conductance G_n=-0.50mS. In recent papers, circuit's dynamics in low frequency area has been studied extensively [10, 11, 13]. The circuit's parameters are considered unchangeable during our study. More particularly: L_1=L_2=100mH, C_1=33nF, C_2=75nF and R_1=1KΩ. We use sinusoidal input signal $v_s(t)$ with amplitude V_o equal to 0.60V or 0.75V, while the frequency f ranges from 30Hz to 50Hz. Using the above parameters circuit exhibits chaotic behaviour. In Figures 1a) and b) theoretical and experimental phase portraits v_{C2} vs. v_{C1} for V_o=0.75V and f=35Hz are presented, respectively. The maximum Lyapunov exponent for the above parameters is positive (LE_{max}=0.0156), which indicates that the system exhibits chaotic behaviour.

| a) theoretical | b) experimental |
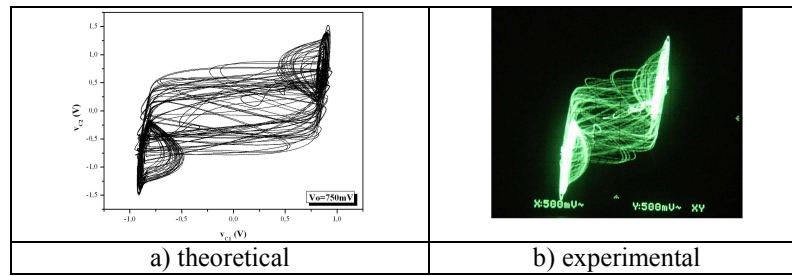
Fig.1. Phase portrait v_{C2} vs. v_{C1} for V_o=0.75V and f=35Hz

3. Dynamics of Ring Connection Topology

In recent paper [9] we have seen that chaotic synchronization of two identical non-autonomous, unidirectionally coupled, nonlinear, fourth order circuits is possible. In this work, chaotic synchronization of three bidirectionally coupled circuits in ring connection, as seen in Figure 2, is studied.
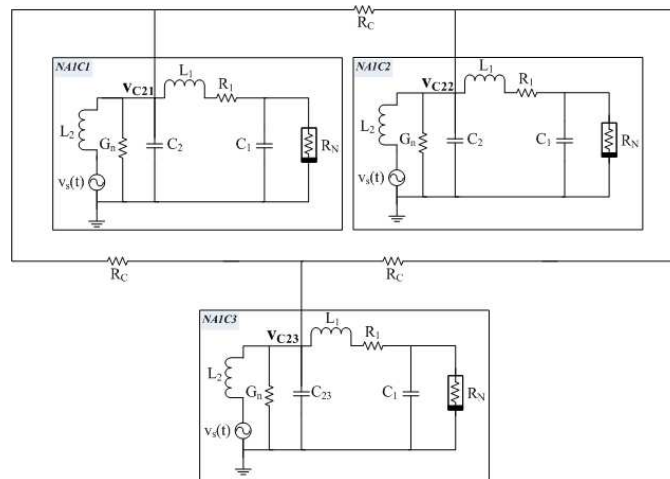
Fig. 2. Three non-autonomous, nonlinear fourth order circuits in ring connection

The resulting set of system's differential equations is derived using Kirchhoff's circuit laws.

$$\frac{dv_{C11}}{dt} = \frac{1}{C_1}\left(i_{L11} - i_{RN1}\right)$$

$$\frac{dv_{C21}}{dt} = -\frac{1}{C_2}\left(G_n \cdot v_{C21} + i_{L11} + i_{L21} - \frac{v_{C23} - v_{C21}}{R_C} + \frac{v_{C21} - v_{C22}}{R_C}\right)$$

$$\frac{di_{L11}}{dt} = \frac{1}{L_1}\left(v_{C21} - v_{C11} - R_1 \cdot i_{L11}\right)$$

$$\frac{di_{L21}}{dt} = \frac{1}{L_2}\left[v_{C21} - R_2 \cdot i_{L21} - v_s(t)\right]$$

$$\frac{dv_{C12}}{dt} = \frac{1}{C_1}\left(i_{L12} - i_{RN2}\right)$$

$$\frac{dv_{C22}}{dt} = -\frac{1}{C_2}\left(G_n \cdot v_{C22} + i_{L12} + i_{L22} - \frac{v_{C21} - v_{C22}}{R_C} + \frac{v_{C22} - v_{C23}}{R_C}\right)$$

$$\frac{di_{L12}}{dt} = \frac{1}{L_1}\left(v_{C22} - v_{C12} - R_1 \cdot i_{L12}\right)$$

$$\frac{di_{L22}}{dt} = \frac{1}{L_2}\left[v_{C22} - R_2 \cdot i_{L22} - v_s(t)\right]$$

$$\frac{dv_{C13}}{dt} = \frac{1}{C_1}\left(i_{L13} - i_{RN3}\right)$$

$$\frac{dv_{C23}}{dt} = -\frac{1}{C_2}\left(G_n \cdot v_{C23} + i_{L13} + i_{L23} - \frac{v_{C22} - v_{C23}}{R_C} + \frac{v_{C23} - v_{C21}}{R_C}\right)$$

$$\frac{di_{L13}}{dt} = \frac{1}{L_1}\left(v_{C23} - v_{C13} - R_1 \cdot i_{L13}\right)$$

$$\frac{di_{L23}}{dt} = \frac{1}{L_2}\left[v_{C23} - R_2 \cdot i_{L23} - v_s(t)\right]$$

Where the current i_{RNi} through the nonlinear element i, with i=1, 2, 3 for circuit 1, 2 and 3 respectively, and input signal $v_s(t)$ are given by equations

$$i_{RNi} = G_b v_{C1i} + 0.5\left(G_a - G_b\right)\left(\left|v_{C1i} + B_p\right| - \left|v_{C1i} - B_p\right|\right)$$

$$v_s(t) = V_o \cos(2\pi f t)$$

In figures 3a) and b) bifurcation diagrams $v_{C21}(t)$-$v_{C22}(t)$ vs. e_C and $v_{C22}(t)$-$v_{C23}(t)$ vs. e_C are presented, where e_C is the coupling parameter and is given by equation

$$e_C = R_1 / R_C$$

Where R_C is the coupling resistance.
We can see that chaotic synchronization of the three identical circuits in ring connection is observed for coupling parameter $e_C > 0.568$, or for coupling resistance $R_C < 1.8k\Omega$.

| a) $v_{C21}(t)$-$v_{C22}(t)$ vs. e_C | b) $v_{C22}(t)$-$v_{C23}(t)$ vs. e_C |
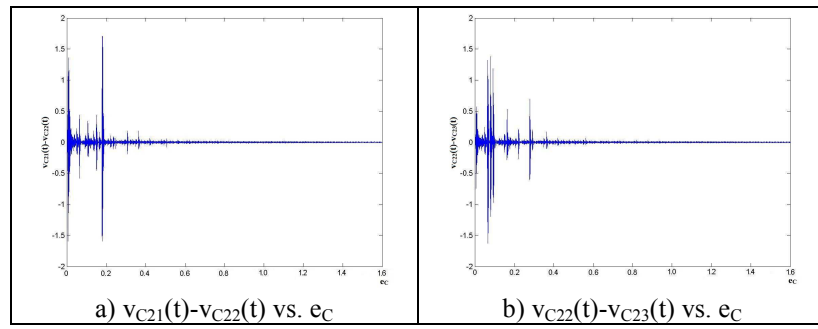
Fig. 3. Bifurcation diagrams for V_o=0.75V and f=35Hz

In figure 4 simulation and experimental results of waveforms $v_{C21}(t)$-$v_{C22}(t)$ for various values of coupling resistance R_C are presented. More particularly, in figures 4a), b) and c) simulation $v_{C21}(t)$-$v_{C22}(t)$ for R_C=1.0MΩ ($e_C \rightarrow 0$), R_C=10.0kΩ (e_C=0.1) and R_C=1.8kΩ (e_C=0.568) are shown, while in figures 4d), e) and f) experimental $v_{C21}(t)$-$v_{C22}(t)$ for the same parameters are illustrated.

| a) R_C=1.0MΩ | b) R_C=10.0kΩ | c) R_C=1.8kΩ |
| d) R_C=1.0MΩ | e) R_C=10.0kΩ | f) R_C=1.8kΩ |
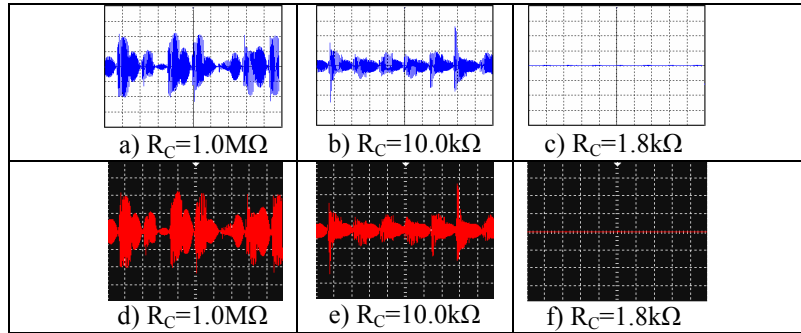
Fig. 4. a), b), c) Simulation and d), e), f) Experimental waveforms $v_{C21}(t)$-$v_{C22}(t)$
(x: 1ms/ div, y: 1V/ div)

In figures 4c) and f) we can see that chaotic synchronization occurs for coupling resistance R_C=1.8kΩ (e_C=0.568). This threshold synchronization value of R_C is lower than in the case of chaotic synchronization of two bidirectionally coupled identical circuits, with the same circuit's settings, which is R_C=2.28 (e_C=0.479) [9].

In figure 5 a collection of results are displayed. Specifically, we can see the threshold synchronization value of coupling parameter e_C versus frequency f, for amplitude of the input sinusoidal signal V_o=0.60V and V_o=0.75V. We can see that the values of e_C in the case of V_o=0.60V are lower than in the case of V_o=0.75V.
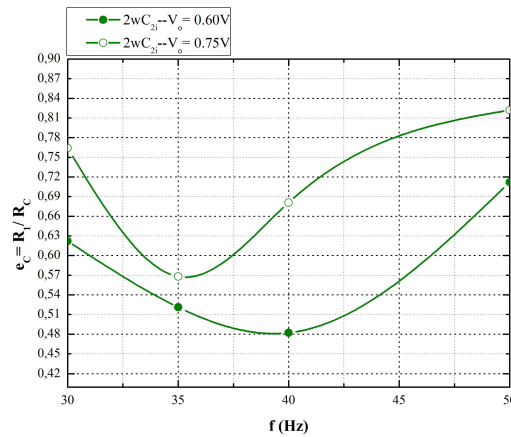
Fig. 5. Threshold synchronization value of coupling parameter e_C vs. f

4. Conclusions

In this paper, we have studied chaos synchronization of three identical non-autonomous circuits, bidirectionally coupled in ring connection network, in low frequency area. Simulation and experimental results of the system's evolution from non synchronized oscillations to synchronized ones, when its individual circuit exhibits chaotic behaviour, were presented. Both, theoretical calculations and experimental results appear to be in complete agreement. We have seen that the values of threshold synchronization coupling parameter e_C in the case of V_o=0.60V are lower than in the case of V_o=0.75V, for various values of input frequency f, but higher than in the case of two bidirectionally coupled identical circuits with the same setup.

References

1. L.O. Chua and G.N. Lin. Canonical Realization of Chua's Circuit Family, *IEEE Trans. on Circuits and Systems*, vol. 37, no. 7, 885–902, 1990.

2. O. Gaci and S. Balev. A General Model for Amino Acid Interaction Networks, *World Academy of Science Engineering and Technology* 44: 401–405, 2008.

3. H. Jeong, B. Tombor, R. Albert, Z.N. Oltvai and A.-L. Barabási. The Large-Scale Organization of Metabolic Networks, *Nature* 407: 651–654, 2000.

4. I.M. Kyprianidis and I. N. Stouboulos. Chaotic and Hyperchaotic Synchronization of Two Nonautonomous and Nonlinear Electric Circuits, *IEEE 8th Int. Conf. on Electronics, Circuits and Systems* 3: 1351–1354, 2001.

5. I.M. Kyprianidis and I.N. Stouboulos. Chaotic Synchronization of Three Coupled Oscillators with Ring Connection, *Chaos Solitons and Fractals*, vol. 17, no. 2-3, 327–336, 2003.

6. E. Lindberg, L. Member, K. Murali and A. Tamasevicius. The Smallest Transistor-Based Nonautonomous Chaotic Circuit, *IEEE Trans. on Circuits and Systems—II: Express Briefs*, vol. 52, no. 10, 661–664, 2005.

7. E. Lindberg, E. Tamaseviciute, G. Mykolaitis, S. Bumeliene, T. Pyragiene, A. Tamasevicius and R. Kirvaitis. Autonomous Third−Order Duffing−Holmes Type Chaotic Oscillator, *European Conference on Circuit Theory and Design*, 663–666, 2009.

8. H. Nakano and T. Saito. Basic Dynamics from a Pulse-Coupled Network of Autonomous Integrate-and-Fire Chaotic Circuits, *IEEE Trans. on Neural Networks*, vol. 13, no. 1, 92–100, 2002.

9. M.S. Papadopoulou, I.M. Kyprianidis and I.N. Stouboulos. Chaos Synchronization and its Application to Secure Communication, *Journal of Concrete and Applicable Mathematics*, vol. 9, no. 3, 205–212, 2011.

10. M.S. Papadopoulou, I.M. Kyprianidis and I.N. Stouboulos. Complex Chaotic Dynamics of the Double-Bell Attractor, *WSEAS Trans. on Circuits and Systems*, vol. 7, no. 1, 12–21, 2008.

11. M.S. Papadopoulou, I.N. Stouboulos and I.M. Kyprianidis. Study of the Behaviour of a Fourth Order Non-Autonomous Circuit in Low Frequency Area, *Nonlinear Phenomena in Complex Systems*, vol. 11, no. 2, 193–197, 2008.

12. I.N. Stouboulos, I.M. Kyprianidis and M.S. Papadopoulou, Antimonotonicity and Bubbles in a 4th Order Non Driven Circuit, *Proc. of the 5th WSEAS Int. Conf. on Non-Linear Analysis Non-Linear Systems and Chaos*, 81–86, 2006.

13. I.N. Stouboulos, I.M. Kyprianidis and M.S. Papadopoulou. Genesis and Catastrophe of the Chaotic Double-Bell Attractor, *Proc. of the 7th WSEAS Int. Conference on Systems Theory and Scientific Computation*, 139–144, 2007.

14. S.H. Strogatz. Exploring Complex Networks, *Nature* 410: 268–276, 2001.

15. X. Wang and G. Chen. Synchronization in Small-World Dynamical Networks, *Int. J. Bifur. Chaos*, vol. 12, no. 1, 187–192, 2002.

16. W. Yu, J. Cao, G. Chen, J. Lü, J. Han and W. Wei. Local Synchronization of a Complex Network Model, *IEEE Trans. on Systems Man and Cybernetics*, vol. 39, no. 1, 230–241, 2009.

Mode-competition in flow-oscillations investigated by means of symbolic-dynamics

Luc R. Pastur[1,2], François Lusseyran[2], and Christophe Letellier[3]

[1] University Paris Sud 11, F-91405 Orsay Cedex, France
    (E-mail: luc.pastur@limsi.fr)
[2] LIMSI-CNRS, BP 133, F-91403 Orsay Cedex, France
[3] CORIA UMR 6614 — Université de Rouen, BP 12, F-76801 Saint-Etienne du
    Rouvray cedex, France

Abstract. The dynamical mode-switching phenomenon, between two dominant frequencies of oscillation in a self-sustained oscillating cavity-flow, is investigated by the means of dynamical system analysis and symbolic dynamics. Two symbols are attributed, according to a partition of the angular first-return map to a Poincaré section. As a result, each symbol is mainly associated with a given mode of oscillation.
Keywords: Fluid mechanics, self-sustained oscillating flows, Poincaré section, angular first-return map, symbolic dynamics.

1 Introduction

Impinging flows have been long studied for their astonishing features and practical applications, ranging from woodwind to structure damage or noise generation. Eddies generated in the unstable shear-layer grow up to saturation while being advected downstream, where they impinge on the downstream cavity-corner. At impingement, a feedback though pressure triggers new perturbations at the leading corner, closing the feedback-loop [8,12,13]. The flow-regime is characterised by self-sustained oscillations and power-spectra organize around a few narrow-banded peaks. Among other features, amplitude modulations [2,7] or mode-competition [6,9,11] may be encountered.

In this contribution, the two-modes competing-regime is investigated using some tools borrowed to the nonlinear dynamical system theory. The competition-process is characterised by means of phase portraits, Poincaré sections and return-maps to the Poincaré section, from which is pursued a symbolic-dynamics-based approach.

2 The cavity-flow

The cavity-scheme is shown in Figure 1(a). It is an open rectangular cavity of length $L = 10$ cm, height $H = 5$ cm and span $W = 30$ cm, defining two aspect-ratios $L/H = 2$ and $W/H = 6$. The inlet-flow generates a
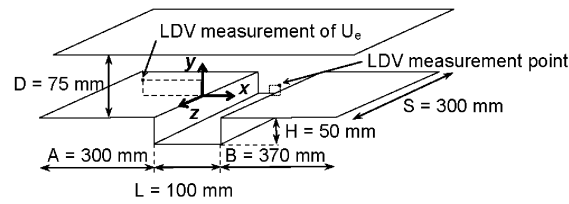
(a) Cavity scheme
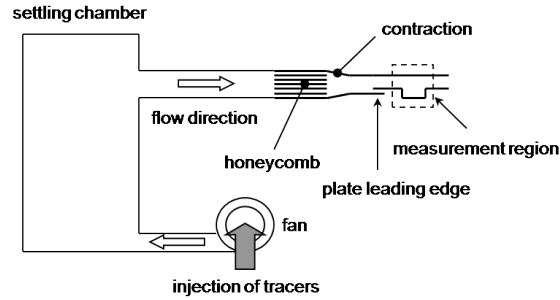
(b) Skecth of the wind-tunnel
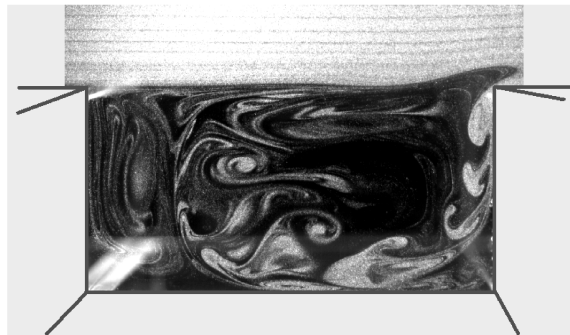
Fig. 1. Experimental setup.

Fig. 2. Side-view smoke-visualisation of the cavity-flow.

shear-layer at the cavity top-plane, which exhibit self-sustained oscillations at some well-defined frequencies in power-spectra. A side-view of the flow is shown in Figure 2. In addition to the shear-layer oscillations, the inlet-flow also initiates a fluid-recirculation inside the cavity, visible in Figure 2. A coordinate-system origin is set mid-span at the upstream edge of the cavity, see Figure 1(a). The x-axis is streamwise, y-axis is normal to the upstream wall along the boundary layer and z-axis is along the cavity span. The cavity is inserted into a vein of span $W = 30$ cm and total height 12.5 cm. Air-flow

is produced by a centrifugal fan located at the entry of the settling chamber, see Figure 1(b). The incoming boundary layer is laminar and stationary. The external velocity U_e is measured upstream of the cavity trailing corner, at $x_e/L = -1$, $y_e/H = 0.5$, using a Laser Doppler Velocimeter (LDV). The air-flow leaves the wind-tunnel directly in the atmosphere. The reference velocity for this study is $U_e = 2.09$ m.s^{-1}, defining a Reynolds number, based on L, $Re_L = U_e L/\nu \simeq 14\,000$. The flow characterisation is based on a LDV measurement of the velocity x-component, downstream of the cavity, at $x/L = 1.15$, $y/H = 0.33$ and $z = 0$. The resulting time-series are resampled, using a linear interpolation, at a sampling-rate of $f_s = 1\,530$ Hz. Acquisition time is about 9 min giving time-series length of about $840\,000$ data points.
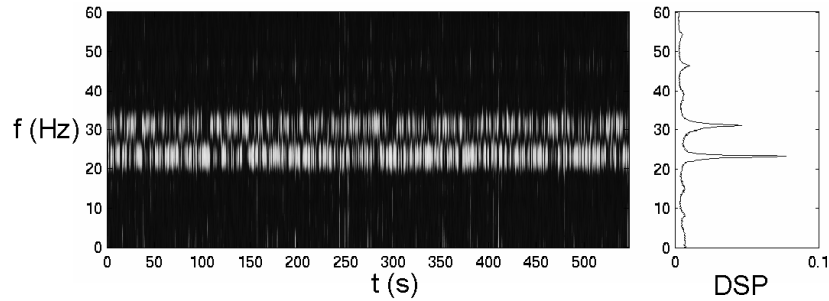
Fig. 3. Frequency analysis of the x-component of the velocity measured with a LDV technique. A power spectral density (to the right) reveals two main frequencies — $f_1 = 23.2$ Hz and $f_2 = 31.0$ Hz. A spectrogram (to the left) — corresponding to the power spectral density plotted as color levels (from dark to bright for increasing amplitudes) — shows that roughly, a single mode dominates at a given time.

For the control-parameters $(L/H, Re_L)$ of the study, two main frequency-components are observed, at $f_1 = 23.2$ Hz and $f_2 = 31.0$ Hz, in the power spectral density (PSD) of Figure 3 (plot on the right). Other peaks are mainly linear combinations of these two frequencies. PSD does not provide any information about the temporal behaviour of the frequency components, since it only evaluates their averaged energetic contribution on the overall time of observation. Instead, the spectrogram of Figure 3 (left plot) clearly exhibits a switching phenomenon between the two dominant modes: when one frequency is powerful in the spectrogram, the other one tends to be weak.

3   Symbolic dynamics analysis

As a first step we reconstruct a phase-portrait of the dynamics from the time-series. Different coordinate-sets can be used, delay or derivative coordinates, as mentioned in earlier works [10,14], or principal-components based

on the singular-value decomposition of a delayed data matrix [1,11]. All these coordinate-sets are equivalent [3]. Here, the reconstructed space is based on principal-components (the X_i's in what follows). The dimensionality of the phase-portrait is estimated using a Grassberger-Proccacia algorithm [5]. The correlation-dimension is found to be about 4.2, meaning that a 10-dimensional-space should be enough to obtain a diffeomorphism between the original phase-space and the reconstructed space, according to Takens' criterion. This is a far too large dimension: as a first step, a projection of the reconstructed space, spanned by the first two principal-components, is used to get some insights about the dynamics.

(a)   (b)
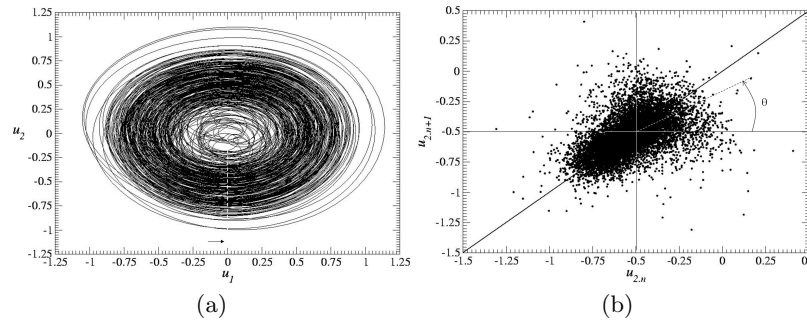
Fig. 4. (a) Phase-portrait spanned by the first two principal-components reconstructed from the measurements of the horizontal component of the velocity. (b) First-return map to a Poincaré section of the phase portrait spanned by the first two principal components reconstructed from the measurements of the x-component of the velocity. The Poincaré section is defined by $X_1 = 0$ and $\dot{X}_1 > 0$ (white dashed-line in (a)).

The phase-portrait of Figure 4(a) exhibits a toroidal structure, the orbit is therefore mainly organized around a torus. The first-return map to a Poincaré section exhibits a cloud of points, see Figure 4(b), meaning that the toroidal structure is filled by the trajectory. From the return-map it is quite difficult to distinguish a deterministic dynamics from a stochastic process. It was shown in the dynamical analysis of a water-jet that a toroidal structure can be conveniently investigated using an angular first-return map [4]. Such a map is built on the angle θ_n associated with the nth iterate of the first-return map as follows. At each point of the first-return map, in Figure 4(b), the angle between the segment joining that point to the barycenter of the first-return map, and the right-hand half-line from the barycenter, is defined as θ_n. In Figure 5 (top), θ_{n+1} is plotted versus θ_n, together with a probability density function $P(\theta_n)$, see Figure 5 (bottom). It clearly appears that the dynamics is mainly organized around two main neighborhoods in the Poincaré section, corresponding to the two peaks of the
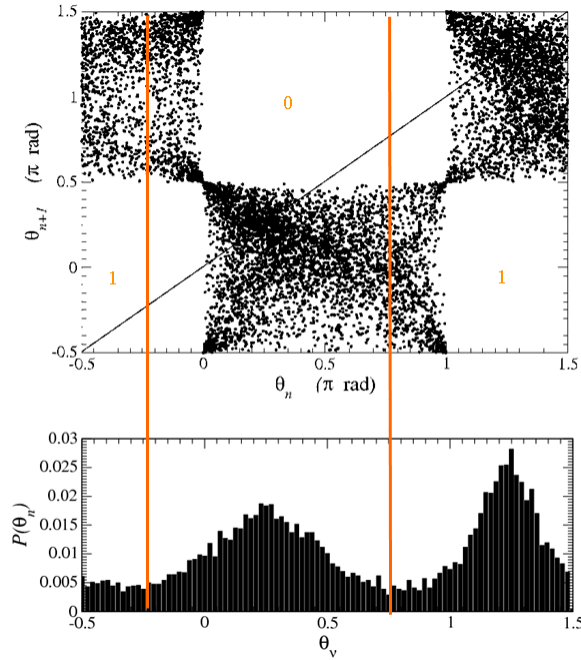
Fig. 5. Angular map built on the first-return map. Two neighborhoods of the first bisecting line are more visited than the other parts. Each neighborhood corresponds to one the two modes identified within the dynamics from a Fourier spectrum.

probability-density function $P(\theta_n)$. These two neighborhoods are located along the bisecting line, *i.e.* $\theta_{n+1} \approx \theta_n$. Since period-1 orbits are involved, it is possible to associate with them a characteristic frequency of oscillation. Consequently, points located in the center of each cloud on the first bisecting-line should correspond to a realization of one of the modes identified with the spectral analysis. Other points — far from the bisecting line — are expected to be associated with transitions from one mode to the other. Therefore, only points in the bisecting line will be taken into account to estimate the mean-time duration of oscillations associated with each of the two orbits.

To begin with, two different symbols, 0 and 1, are introduced, depending on whether two successive crossings of the Poincaré section lies in the angular sector $\theta_n \in [-\pi/4, 3\pi/4]$ (symbol 0) or in the angular sector $\theta_n \in [-\pi/2; -\pi/4] \cup]3\pi/4; 3\pi/2]$ (symbol 1). With this representation, subsequences of identical symbols ...0000.. or ...1111... occur when the dynamics is locked on a given period-1 orbit. Subsequences like ...001011.. evidences transitions between the two orbits.

Probability distributions of symbolic sequences with 8 characters are shown in Figure 6(a). Sequences Σ_i are indexed according to the natural order of the integer associated with the binary number, 0000 0000 being indexed
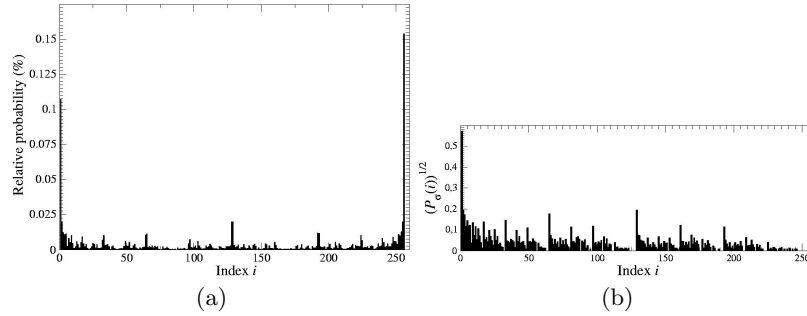
Fig. 6. (a) Probability density functions of the symbolic sequences. Sequences corresponding to repeated symbols ($i = 0$ and $i = 255$) are obviously the most probable. (b) Probability density function of the different symbolic sequences built on the "transitional" symbolic dynamics. The number of points considered in the Poincaré section is $N = 15\,000$.

as $i = 0$. Sequence $0000\,0100$ is for instance associated with index $i = 4$. The histogram of the symbolic sequences realized by the dynamics is not flat. This means that the underlying dynamics does not correspond to a white noise [4]. Obviously two main sequences are observed, Σ_0 and $\Sigma_{255} = 1111\,1111$. Sequence Σ_{255} is slightly more often realized, in agreement with the time durations during which symbols 0 (48%) or 1 (52%) are observed. Isolated from the "background" (probability greater than 0.017), most probable sequences are $\Sigma_{127} = 0111\,1111$, $\Sigma_{128} = 1000\,0000$, $\Sigma_{192} = 1011\,1111$, $\Sigma_{63} = 0100\,0000$, $\Sigma_{252} = 1111\,1100$, $\Sigma_3 = 0000\,0011$, $\Sigma_{254} = 1111\,1110$, $\Sigma_1 = 0000\,0001$, with probabilities of realisation $P_{127} = 0.022$, $P_{128} = 0.023$, $P_{192} = 0.018$, $P_{63} = 0.019$, $P_{252} = 0.018$, $P_3 = 0.017$, $P_{254} = 0.022$, $P_1 = 0.023$, respectively. These most often realized sequences can be paired as follows. Let $\overline{0} = 1$ and $\overline{1} = 0$, that is, the complementary function $\overline{\Sigma}_i$ maps each of its symbols to the other ($0 \mapsto 1$ and $1 \mapsto 0$), then the complementary sequence $\overline{\Sigma}$ corresponds to the sequence of complementary symbols $\{\overline{\sigma}_n\}$. Therefore, $\overline{\Sigma}_{127} = \Sigma_{128}$, $\overline{\Sigma}_{192} = \Sigma_{63}$, $\overline{\Sigma}_{252} = \Sigma_3$, and $\overline{\Sigma}_{254} = \Sigma_1$. Thus, it is found that sequence $\Sigma_j = \overline{\Sigma}_i$ is realized with a probability P_j nearly equal to P_i. There is therefore a symmetry between symbols 0 and 1.

In the same spirit, a "transitional" symbolic-dynamics can be introduced, defining ξ_i such that $\xi_n = R$ if $\sigma_n\sigma_{n+1} = 00$ or $\sigma_n\sigma_{n+1} = 11$ and $\xi_n = T$ if $\sigma_n\sigma_{n+1} = 10$ or $\sigma_n\sigma_{n+1} = 01$. The probability density function of 8-characters words, Ξ_i, based on ξ_n, is shown in Figure 6(b). The main peak is observed for $\Xi_0 = $RRRR RRRR, that is, a sustained mode. The next most often realized sequences are $\Xi_{128} = $ TRRR RRRR, $\Xi_{64} = $ RTRR RRRR, $\Xi_{32} = $ RRTR RRRR, $\Xi_{16} = $ RRRT RRRR, $\Xi_8 = $ RRRR TRRR, $\Xi_4 = $ RRRR RTRR, $\Xi_2 = $ RRRR RRTR, $\Xi_1 = $ RRRR RRRT, ..., which are cyclic permutations of an isolated transition. This is a signature of se-

quences corresponding to more than 8 repeated symbols. Are also found Ξ_{192} = TTRR RRRR, Ξ_{160} = TRTR RRRR, Ξ_{96} = RTTR RRRR, Ξ_{80} = RTRT RRRR, Ξ_{48} = RRTT RRRR. The relative preponderance of these sequences reveals that once the dynamics realizes a symbol, if a transition to the other symbol occurs, it most usually quickly returns to the previous symbol. In other words, once a mode is locked, it tends to exclude the other.
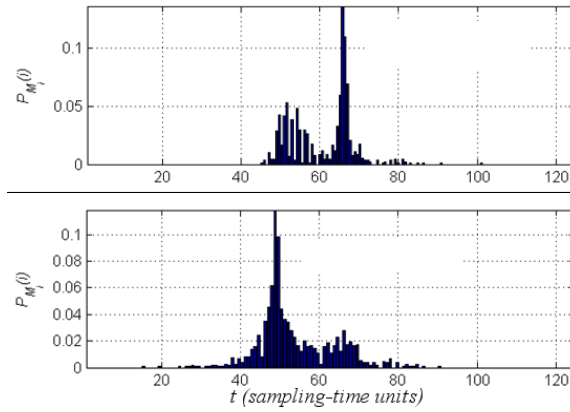
4 Discussion and conclusion

Fig. 7. Distributions of the time-duration between two crossings of the Poincaré section for events associated with symbol 0 (top) or 1 (bottom).

Now the very question is: can we fully associate each symbol with a cycle of oscillation at either f_1 or f_2? Distributions of the time-duration between two successive crossings of the Poincaré section, associated with each symbol 0 or 1, are shown in Figure 7. The mean-time duration of crossings associated with symbol 0 is 0.0319 s, corresponding to a frequency of about 31.3 Hz, rather close to $f_2 = 31.0$ Hz. The mean-time duration of crossings associated with symbol 1 is 0.0430 s, corresponding to a frequency of about 23.2 Hz, similar to $f_1 = 23.2$ Hz. Henceforth, it is reasonable to consider that the events at frequency f_1 essentially contribute to the first partition, while events associated with the second partition are essentially due to frequency f_2. Although fairly good, the relation between symbols and frequencies is not perfect, since it can be seen in Figure 7 that some events with time-durations $\simeq 1/f_1$ are present in the histogram associated with symbol 0, while events occurring with time-durations $\simeq 1/f_2$ are present in the histogram associated with symbol 1.

Symbolic dynamics allows to scan the dynamics of the system at timescales of the order of one basic oscillation, something hardly achievable with Fourier techniques due to the reciprocal relation between time and frequency. As a consequence, while transitions from one cycle of oscillation to the other cannot be detected at the scale of an elementary oscillation with usual techniques, symbolic dynamics has such an ability. One limitation is that the relation between symbol and frequency of oscillation is not perfectly bijective. Nevertheless, with some care, it is possible to detect transitions from one oscillating mode to another at time-scales non-accessible otherwise, making symbolic dynamics a powerful tool for investigating such kind of switching-mode phenomena.

References

1. D. S. Broomhead & G. P. King, Extracting qualitative dynamics from experimental data, *Physica D*, **20**, 217-236, 1986.
2. N. Delprat, Rossiter formula: a simple spectral model for a complex amplitude modulation process?, *Physics of Fluids* **18** (7) (2006).
3. J. F. Gibson, J. D. Farmer, M. Casdagli & S. Eubank, An analytic approach to practical state space reconstruction, *Physica D*, **57**, 1-30, 1992.
4. J. Godelle & C. Letellier, Symbolic sequence statistical analysis for free liquid jets, *Physical Review E*, **62** (6), 7973-7981, 2000.
5. P. Grassberger & I. Proccacia, Measuring the strangeness of strange attractors, *Physica D*, **9**, 189-208, 1983.
6. M. Kegerise, E. Spina, S. Garg & L. Cattafesta, Mode-switching and nonlinear effects in compressible flow over a cavity, *Physics of Fluids*, **16**, 678–687, 2004.
7. C. Knisely, D. Rockwell, Self-sustained low-frequency components in an impinging shear layer, *Journal of Fluid Mechanics* **116**, 157 (1982).
8. J.C. Lin, D. Rockwell, Organized oscillations of initially turbulent flow past a cavity, *AIAA Journal*, **39**, 1139-1151 (2001).
9. F. Lusseyran, L.R. Pastur, C. Letellier, Dynamical analysis of an intermittency in an open cavity flow, *Physics of Fluids* **20**, 114101 (2008).
10. N. H. Packard, J. P. Crutchfield, J. D. Farmer & R. S. Shaw, Geometry from a time series, *Physical Review Letters,* **45** (9), 712-716, 1980.
11. L.R. Pastur, F. Lusseyran, T.M. Faure, Y. Fraigneau, R. Pethieu, P. Debesse, Quantifying the nonlinear mode competition in the flow over an open cavity at medium Reynolds number, *Experiments in Fluids* **44**, 597 (2008).
12. D. Rockwell and C. Knisely, The organized nature of flow impingement upon a corner, *Journal of Fluid Mechanics* **93**, 413 (1979).
13. D. Rockwell & E. Naudascher, Self-sustained oscillations of impinging free shear layers, *Annual Review of Fluid Mechanics*, **11**, 67–94, 1979.
14. F. Takens, Detecting strange attractors in turbulence, *Lecture Notes in Mathematics*, **898**, 366-381, 1981.

Construction of Dynamical Systems from Output Regular and Chaotic Signals

Evgeniy D. Pechuk [1]
Tatyana S. Krasnopolskaya [2]

[1] Institute of Hydromechanics NASU, Kyiv, Ukraine
  (E-mail: uzuzun@i.ua)
[2] Institute of Hydromechanics NASU, Kyiv, Ukraine
  (E-mail: t.krasnopolskaya@tue.nl)

Abstract: The problem of construction of the deterministic dynamical system from output signals (reconstruction) is very important. Two reconstruction methods have been used and compared. First one is the method of successive differentiation and the second is based on delay coordinates. It was firstly suggested to choose time delay parameter from the stable region of a divergence of the reconstructed system. Results show that both methods can capture regular and chaotic signals from reconstructed systems of the third order with nonlinear terms up to sixth order. Types of signals were examined with spectral methods, construction of phase portraits and Lyapunov exponents.
Keywords: Reconstruction, Dynamical system, Chaotic regime, Successive differentiation, Delay time.

1   Introduction

The problem of reconstruction of deterministic dynamical system from output signals is of great importance in studying of properties of experimental signals such as acoustic signals, ECG, EEG and so on. Reconstructed dynamical system may add a significant qualitative information to chaotic data analysis. Stability conditions, bifurcation curves, all types of steady – state regimes could be studied for solutions of a reconstructed system. Two reconstruction methods have been developed by Crutchfield and McNamara [1] and used for variety of signals later [2-4]. The first method is based on suggestion that the signal can be presented by a function that has at least three derivatives, so this is method of successive differentiation. Applying this method the dynamical system has a following form [1-4]:

$$\dot{x}_1 = x_2$$
$$\dot{x}_2 = x_3$$
$$\dot{x}_3 = F_3(x_1, x_2, x_3)$$

where $F_3(x_1, x_2, x_3)$ is a nonlinear function. The second method of reconstruction is based on delay coordinates. We need to reconstruct the dynamical system from the time series of some state variable $x(t)$ with the

fixed sampling step dt. We have series of $s_k = x(kdt)$, $k=0,1,2,...,N$, using value of time delay $\tau = ndt$ (which is chosen to yield optimal reconstruction [1]) we construct the dynamical system in the form [1-4]:

$$\dot{x}_1 = F_1(x_1, x_2, x_3)$$
$$\dot{x}_2 = F_2(x_1, x_2, x_3)$$
$$\dot{x}_3 = F_3(x_1, x_2, x_3)$$

where $x_1(t) = x(t)$; $x_2(t) = x(t+\tau)$; $x_3(t) = x(t+2\tau)$, $F_i(x_1, x_2, x_3)$ are nonlinear functions.

2 Construction of Dynamical Systems from Output Signals of Pendulum System

Reconstruction methods are applied to the signals of a deterministic dynamical system of pendulum oscillations which may have regular and chaotic regimes [5]:

$$\dot{y}_1 = -0.1y_1 - y_2 y_3 - \frac{1}{8}(y_1^2 y_2 + y_2^3)$$

$$\dot{y}_2 = -0.1y_2 + y_1 y_3 - \frac{1}{8}(y_2^2 y_1 + y_1^3) + 1$$

$$\dot{y}_3 = -0.5y_2 - 0.61y_3 + F$$

Nonlinear functions $F_i(x_1, x_2, x_3)$ in the first and second systems have the following form:

$$F(x_1, x_2, x_3) = a + \sum_{i=1}^{3} a_i x_i + \sum_{i,j=1}^{3} a_{ji} x_j x_i + ... + \sum_{o,m,n,k,j,i=1}^{3} a_{omnkji} x_o x_m x_n x_k x_j x_i$$

with nonlinear terms up to third order for the regular signals and up to the six order for the chaotic.

The traditional way to obtain time delay parameter $\tau = ndt$ for the second method of reconstruction is to use time interval when the autocorrelation function is equal to zero [2-4]. For such chosen τ the divergence of a reconstructed system may not be negative. So that we introduce other way to choose τ. Real system is nonconservative and, the divergence of systems should be negative too. For example, for the original pendulum system div is

equal to -0.81. In Figure 1 the dependence of reconstructed systems divergence on n in the steady – state regimes is shown. We choose n for time delay τ from the stable region of div.

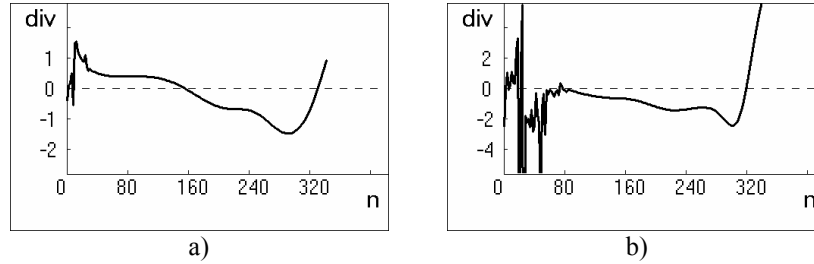a)   b)

Fig. 1. The dependence of reconstructed systems divergence on n for regular initial signal $F = 0.257$ (case a) and chaotic $F = 0.114$ (case b).

For every value of the bifurcation parameter F from the interval $0.1 \leq F \leq 0.3$ the reconstructed systems were built and the output signals were determined. And then the largest Lyapunov exponents [6] were calculated. For that purpose we use the fifth – order Runge – Kuttas method with the precision of $O(10^{-7})$. Initial conditions were selected in the vicinity of the original signal, and for the steady – state regime signals we choose $N = 2^{18}$, $dt = 0.004$.

The dependence of the largest Lyapunov exponent of the pendulum system on values of the bifurcation parameter F is shown in Figure 2.a. The dependences of the largest Lyapunov exponent on F for the first and the second reconstructed dynamical systems are shown in Figure 2.b – c correspondingly.

a)   b)   c)
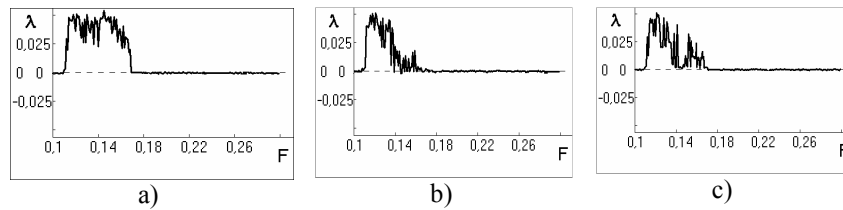
Fig. 2. The largest Lyapunov exponent of the pendulum system (case a) and of the reconstructed systems (cases b and c).

We may see similarity of both graphs to the dependence for the original system in Figure 2.a with the exception of the region $0.15 \leq F \leq 0.18$ where the transition to chaos occurs.

2 Construction Systems from Regular Output Signal

As was shown in the book [5] the solution of the pendulum system would be regular if bifurcation parameter is F=0.257. We used this value and solved the system in order to get the output signal. Then we reconstruct the system using the two methods.

For the second method we reconstruct the system using small initial value for the delay parameter and build the dependence of the divergence on value n and choose n from the stable interval of the delay parameter (Figure 1.a, n=240). As the result the system get the form with nonlinear terms only to the third order of nonlinearity.
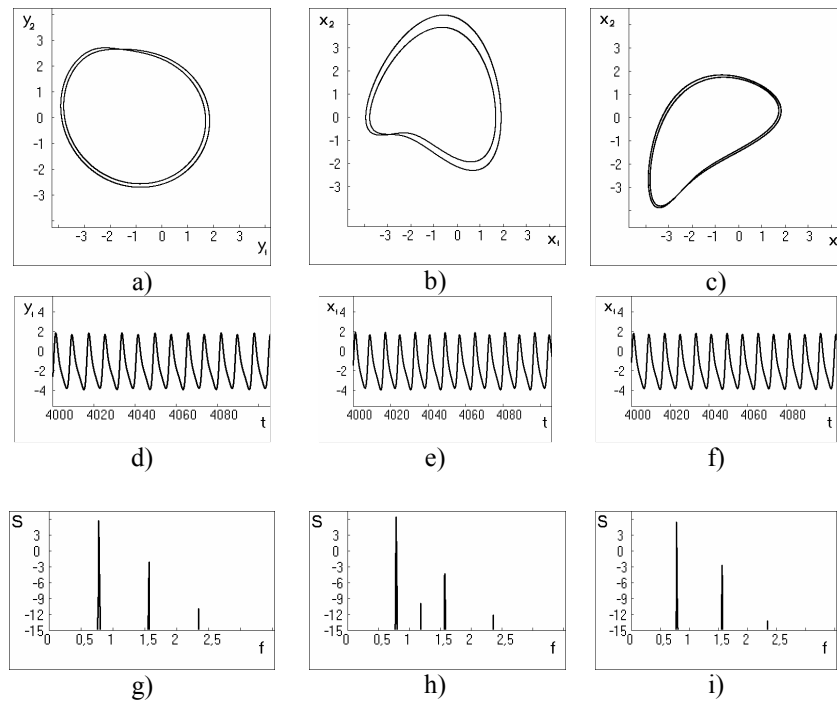
Fig. 3. The portrait of initial pendulum system (F=0.257), case a , the portraits of the reconstructed systems, cases b–c, their time realizations, cases d–f, and power spectrums, cases g–i.

Projections of the limit cycle with two loops on the plane are shown in Figure 3. a–c for the solution of the original system (Figure 3.a) and the reconstructed first and second dynamical systems (Figure 3.b–c). Since for reconstruction we use only the first variable signal phase portrait projections on the plane with the

second variable only qualitatively are look like the original limit cycle with two loops. Time realizations of the first variable and their power spectrums are presented in Figure 3.d–i. Figure 3.d and Figure 3.g describes the solution of the original system, and Figure 3.e–f and Figure 3.h– i gives the information about solutions of the reconstructed dynamical systems.

Since power spectrum indicates the power contained at each frequency, the peak heights corresponds to the squared wave amplitudes (i.e. the wave energy) at the corresponding frequencies. The first method of reconstruction gives the solution which the power spectrum for the regular signals coincides with the output signal power spectrum up to 96% for the first three peaks. The second method gives the precision up to 98%. Also the second method determines the maximum Lyapunov exponent more precisely for chaotic regimes (with a precision to $O(10^{-3})$) than the first method.

3. Construction Systems from Chaotic Output Signal

Now we use such parameter F for the pendulum original system when this system has the chaotic solution, namely F=0.114. Then we reconstruct the system using the two methods of reconstruction with nonlinear function $F_i(x_1, x_2, x_3)$ with nonlinear terms up to the sixth order. For the second method we reconstruct the system using small initial value for the delay parameter and build the dependence of the divergence on value n and choose n from the stable interval of the delay parameter (Figure 1.b, n=240).

Projections of the chaotic attractor of the initial system and of the reconstructed systems are shown in Figure 4.a–c. As could be seen from Figure 4 the both methods qualitatively good approximate chaotic attractor of the original system. Time realizations of the chaotic attractors after finished transient regimes are also similar and given in Figure 4.d–f. Power spectrums for the original signal and for the signals from the reconstructed systems are shown in Figure 4.g– i and may be approximated by the same decay function $S = -6.75 - 8.5 f$.
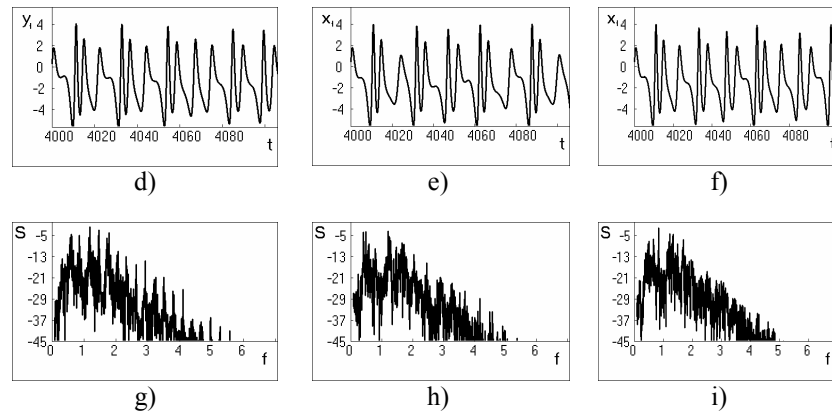

a)   b)   c)

d)   e)   f)

g)   h)   i)
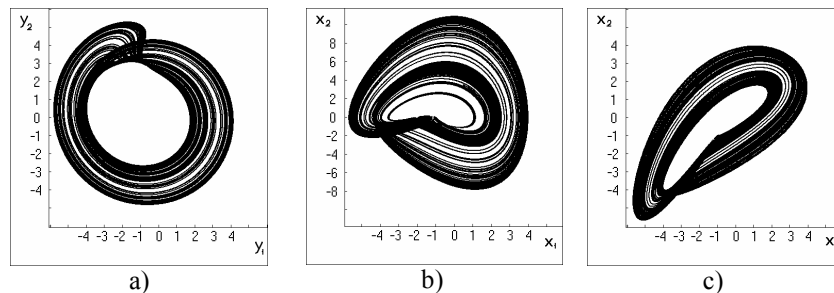
Fig. 4. The portrait of initial system (case a) (F=0.114), the portraits of the reconstructed systems (cases b –c), their time realizations (d –f) and power spectrums (g–i).

3   Construction System from Synthetic ECG Signal

As practical application of the considered methods the signal of a dynamical model for generating synthetic electrocardiogram signals [9] was used. This signal is regular and outwardly looks like the electrocardiogram of healthy man. Using the method of delay the system of eighth order was built. In Figure 5 temporal realization is represented by synthetic electrocardiogram. In Figure 6 temporal realization of the first coordinate of the solution of the reconstructed system is represented. As is obvious from graphs both signals are regular and have an identical period of oscillations.
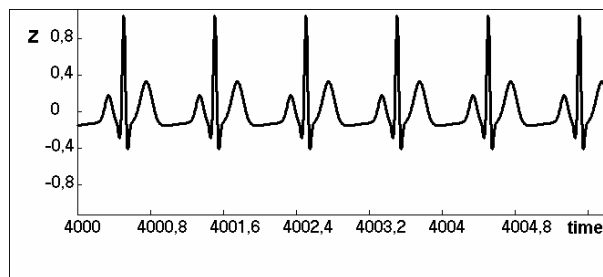
Fig. 5. Synthetic electrocardiogram signal.
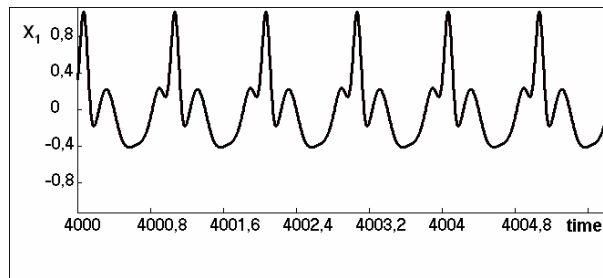
Fig. 6. Signal generated by reconstructed system.

4   Conclusions

Results show that both methods can capture regular and chaotic signals from reconstructed systems of the third order with nonlinear terms up to sixth order. Types of signals were examined with spectral methods, construction of phase portraits and Lyapunov exponents. The first method gives the solution which the power spectrum for the regular signals coincides with the output signal spectrum up to 96 % for the first three peaks. The second method gives a mistake around 2 %. And the second method determines the maximum Lyapunov exponent more precisely for chaotic regimes (with a precision to $O(10^{-3})$) than the first method.

Real systems are nonconservative and, a divergence of systems should be negative. It was suggested for the first time that the delay parameter for the second reconstruction method must be chosen from the stable region of the divergence behaviour of the reconstructed system.

The both methods qualitatively good approximate the phase portrait of chaotic attractor of the original system. Moreover, time realizations of the chaotic attractors after finished transient regimes are quiet similar. And what is more important, power spectrums for the original signal and for the signals from the reconstructed systems may be approximated by the same decay function $S = -6.75 - 8.5f$. Calculations also show that more precisely the value of bifurcation parameter for chaotic regimes gives the second method of reconstruction.

References

1. J. P. Crutchfield, B. S. McNamara. Equations of Motion from a Data Series, *Complex Systems*, vol. 1, 417-452, 1987.

2. N. B. Janson, A. N. Pavlov, T. Kapitaniak, V. S. Anishshenko. Reconstruction of the dynamical systems from the short signals, *Letters into JTP*, vol. 25, no. 11, 7-13, 1999.

3. V. S. Anishshenko. *Acquaintance with nonlinear dynamic,*. Institute of Computer Science, Moscow-Izhevsk, 2002.

4. S. P. Kouznetsov. *Dynamic chaos*, Physmatlit, Moscow, 2001.

5. T. S. Krasnopolskaya, A. Yu. Shvets. *Regular and chaotic dynamics of the systems with limited excitation,*. Institute of Computer Science, Moscow-Izhevsk, 2008.

6. G. Benettin, L. Galgani, J. M. Strelcyn. Kolmogorov entropy and numerical experiments, *Phys. Rev.*, vol. 14, 2338-2345, 1976.

7. M. B. Kennel, R. Brown and H. D. I. Abarbanel. Determining embedding dimension for phase-space reconstruction using a geometrical construction *Phys. Rev. A.,* vol. 45, no. 6, 3403-3408, 1992.

8. V. S. Anishshenko, A. P. Pavlov. Global reconstruction in application to multichannel communication *Phys. Rev. E.*, vol. 57, no. 2, 2455-2458, 1998.

9. P. E. McSharry, G. D. Clifford, L. Tarassenko, L. A. Smith. A dynamical model for generating synthetic electrocardiogram signals, *IEEE Transactions on biomedical engineering*, vol. 50, no. 3, 289-294, 2003.

Analysis and Circuit Realization of
A New 3D Chaotic System

İhsan Pehlivan, Yılmaz Uyaroğlu, Mehmet Ali Yalçın, Abdullah Ferikoğlu

Sakarya University, Serdivan, Sakarya, Turkey
E-mail: ipehlivan@sakarya.edu.tr

Abstract: This paper introduces a new three-dimensional quadratic continuous autonomous chaotic system with golden proportion equilibria, which can generate single folded attractor. Some basic dynamical behaviors, and the dynamical structure of the new chaotic system are investigated either analytically or numerically. Finally, the chaos generator of the new chaotic system are experimentally confirmed via a novel electronic circuit design. It is convenient to use the new system to purposefully generate chaos in chaos applications. A good qualitative agreement is illustrated between the simulations and the experimental results.
Keywords: Chaotic attractor, chaotic system, golden proportion, golden equilibria, chaotic circuit, chaotic oscillator

1. Introduction
As the first chaotic model, the Lorenz system has become a paradigm of chaos research[1]. Chen constructed another chaotic system[2], which nevertheless is not topologically equivalent to the Lorenz's[2, 3]. This system is the dual to the Lorenz system and similarly has a simple structure[3]. Lü and Chen found the critical new chaotic system [4], which represents the transition between the Lorenz and Chen attractors. For the investigation on generic 3D smooth quadratic autonomous systems, Sprott [5-7] found by exhaustive computer searching about 19 simple chaotic systems with no more than three equilibria. It is very important to note that some 3D autonomous chaotic systems have three particular fixed points: one saddle and two unstable saddle-foci (for example, Lorenz system [1], Chen system [2], Lu system [4]). The other 3D chaotic systems, such as the original Rossler system [8], DLS [9] and Burke-Show system [10], have two unstable saddle-foci. Yang and Chen found another 3D chaotic system with three fixed points: one saddle and two stable fixed points [11]. Recently, Yang et al. [12] and Pehlivan et al. [13] introduced and analyzed the new 3D chaotic systems with six terms including only two quadratic terms in a form very similar to the Lorenz, Chen, Lu and Yang–Chen systems, but they have two very different fixed points: two stable node-foci. Therefore, They are very interesting to further find out the new dynamics of the system.

This article introduces another novel three-dimensional quadratic autonomous system with golden equilibria, which can generate single folded attractor.

2. A New 3D Chaotic System and its Analyses

Following nonlinear autonomous ordinary differential equations are the new chaotic system.

$$\dot{x} = y - x - a \cdot z$$
$$\dot{y} = x \cdot z - x$$
$$\dot{z} = -xy - y + b$$

The new system have eight terms, three quadratic nonlinearities and two parameters 'a' and 'b'. Typical parameters are a=2, b=1. Let us consider a volume in a certain domain of the state space. For the system, one has

$$\Delta V = \frac{\partial \dot{x}}{\partial x} + \frac{\partial \dot{y}}{\partial y} + \frac{\partial \dot{z}}{\partial z} = -1 = r$$

with $r = -1$, where r is a negative value. Dynamical system is one dissipative system, and an exponential contraction rate of the system is

$$\frac{dV}{dt} = e^r = e^{-1}$$

In the dynamical system, a volume element V_0 is apparently contracted by the flow into a volume element $V_0 e^{rt} = V_0 e^{-t}$ in time t. It means that each volume containing the trajectory of this dynamical system shrinks to zero as t→∞ at an exponential rate r. So, all this dynamical system orbits are eventually confined to a specific subset that have zero volume, the asymptotic motion settles onto an attractor of the system.

The new system equations has three equilibrum points as

$$E_1(\frac{-a-1+\sqrt{a^2-2a+1+4b}}{2}, \ \frac{a-1+\sqrt{a^2-2a+1+4b}}{2}, \ 1)$$

$$E_2(\frac{-a-1-\sqrt{a^2-2a+1+4b}}{2}, \ \frac{a-1-\sqrt{a^2-2a+1+4b}}{2}, \ 1)$$

$$E_3(0, \ b, \ \frac{b}{a})$$

As the variables x, y, z $\in \Re$, this implies that fixed point to exist, $a \neq 0$ and $a^2 - 2a + 1 + 4b > 0$. So, $(a-1)^2 + 4b > 0$, and $a \in \Re$. When a=0, the system has unbounded solutions.

The equilibrium points of the new system are

$$E_1(\frac{-3+\sqrt{5}}{2}, \ \frac{1+\sqrt{5}}{2}, \ 1), \ E_2(\frac{-3-\sqrt{5}}{2}, \ \frac{1-\sqrt{5}}{2}, \ 1), \ E_3(0, \ 1, \ \frac{1}{2})$$

for a=2 and b=1 values. More interestingly the equilibrium points have Golden Proportion values as

$$E_1(-\tau^{-2}, \ \tau, \ \tau^0), \ E_2(-\tau^2, \ -\tau^{-1}, \ \tau^0), \ E_3(0, \ \tau^0, \ \frac{\tau^0}{2})$$

The famous Golden Proportion $\tau = \frac{1+\sqrt{5}}{2}$, found often in nature. Many objects alive in the natural world that possess pentagonal symmetry, such as marine stars, inflorescences of many flowers, and phyllotaxis objects have a numerical description given by the Fibonacci numbers which are themselves based on the Golden Proportion. In the last few years, the Golden Proportion has played an increasing role in modern physical research[14-21].

For the $E_1(\frac{-3+\sqrt{5}}{2}, \ \frac{1+\sqrt{5}}{2}, \ 1)$, the eigenvalues are found as follows;

$$\lambda_1 = 1.565818, \quad \lambda_2 = -2.331903, \quad \lambda_3 = -0.233915$$

For the $E_2(\frac{-3-\sqrt{5}}{2}, \ \frac{1-\sqrt{5}}{2}, \ 1)$, the eigenvalues are found as follows;

$$\lambda_1 = -1.0579, \ \lambda_2 = 0.0289 + 2.3521 \cdot i, \ \lambda_3 = 0.0290 - 2.3521 \cdot i$$

For the $E_3(0, \ 1, \ \frac{1}{2})$, the eigenvalues are found as follows;

$$\lambda_1 = 0.5 - 0.5 \cdot i, \quad \lambda_2 = -2, \quad \lambda_3 = 0.5 + 0.5 \cdot i$$

For the equilibrum points, according to the Routh-Hurwitz criterion, the case that the real parts of all the roots are negative does not exist. Therefore, the fixed

points are not stable and this implies chaos. So, the system orbits around the unstable equilibrium points.

Phase portraits of the new chaotic system were achieved as performing the numerical simulation for initial conditions $x_0=0$, $y_0=0$, $z_0=0$ and parameters a=2, b=1, and shown in Figure 1- 3.
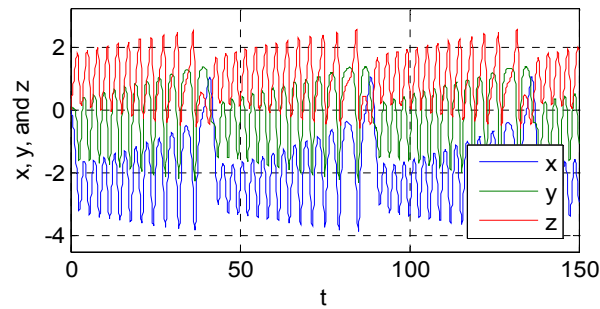

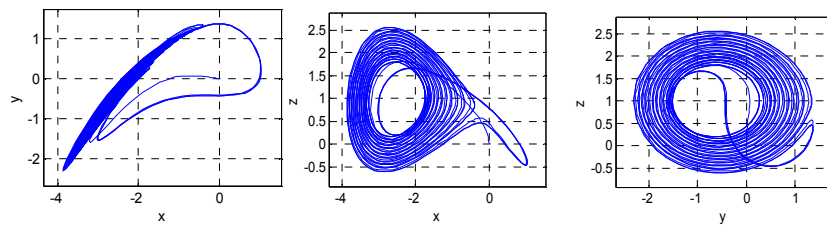Fig. 1. x, y, z chaotic signals of the new chaotic system against to time

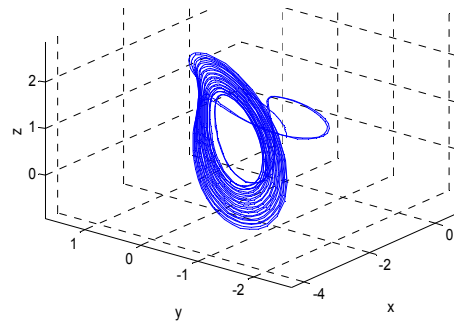Fig. 2. Phase portraits of the new chaotic system

Fig. 3. 3D phase portrait of the new chaotic system

Largest Lyapunov Exponent spectrum of the new chaotic system was achieved as performing the numerical simulation and shown in Figure 4.
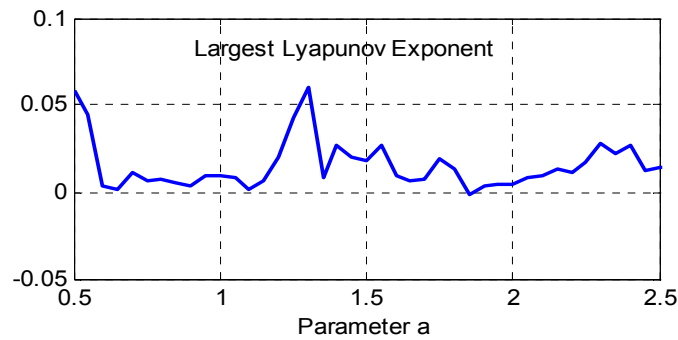
Fig. 4. Largest Lyapunov Exponent Spectrum of the new chaotic system

3. Circuit Realization of the 3D Chaotic System

The electronic circuit schematic and the experimental realization results of the new system for parameters a=2 and b=1, are seen in Fig. 5 and Fig. 6 respectively.
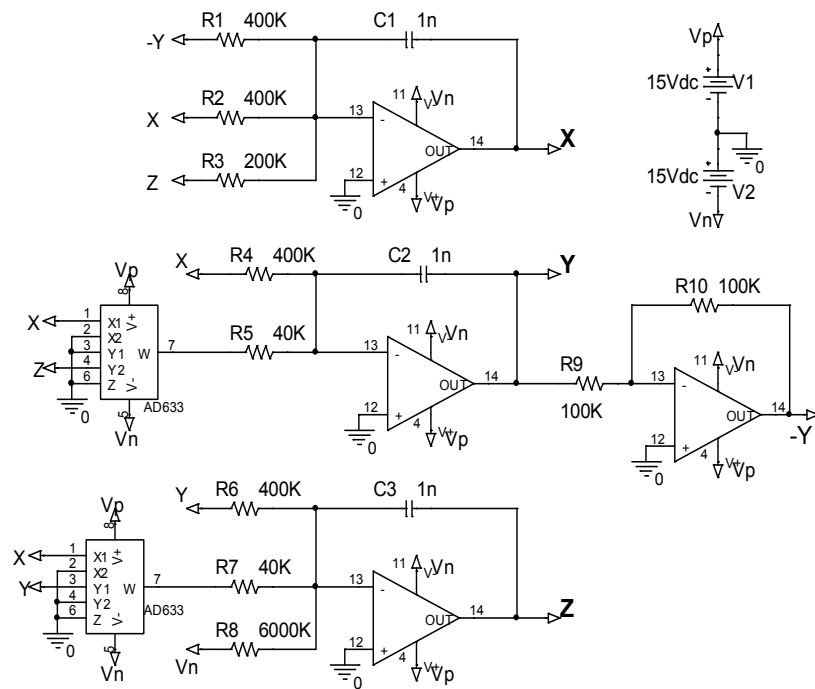

Fig. 5. The electronic circuit schematic of the new chaotic system

Because of the fact that origin(0,0,0) point is not equilibria for the new system, it's not require the initial condition voltages for executing the circuit.

Consequently realization of the new circuit is very easy. Chaotic differential equations of the new circuit are given below.

$$\dot{x} = \frac{1}{R_1\,C_1}\,y \;-\; \frac{1}{R_2\,C_1}\,x \;-\; \frac{1}{R_3\,C_1}\,z$$

$$\dot{y} = \frac{1}{R_5\,C_2}\,x \cdot z \;-\; \frac{1}{R_4\,C_2}\,x$$

$$\dot{z} = -\,\frac{1}{R_7\,C_3}\,x \cdot y \;-\; \frac{1}{R_6\,C_3}\,y \;-\; \frac{V_n}{R_8\,C_3}$$
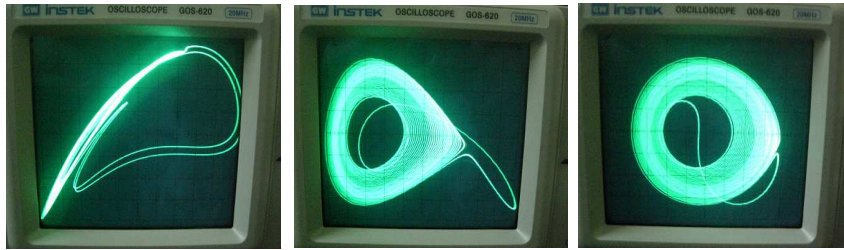

Fig. 6. Phase portraits of the real electronic experimental circuit
of the new chaotic system

4. Conclusions

This article introduces one three-dimensional autonomous interesting new chaotic system with golden proportion equilibria, which can generate single folded attractor. The famous Golden Proportion $\tau = \dfrac{1+\sqrt{5}}{2}$, found often in nature. Many objects alive in the natural world that possess pentagonal symmetry, such as marine stars, inflorescences of many flowers, and phyllotaxis objects have a numerical description given by the Fibonacci numbers which are themselves based on the Golden Proportion. In the last few years, the Golden Proportion has played an increasing role in modern physical research. The chaos generator of the new chaotic system are confirmed via a novel electronic circuit design. Electronic circuitry of the new chaotic system is simple. It is convenient to use the new system to purposefully generate chaos in chaos applications. We believe that the unknown dynamical behaviors of this chaotic attractor deserve further investigation and are desirable for engineering applications in the near future.

Acknowledgements

References

1. E. N. Lorenz, Deterministic nonperiodic flow*; J. Atmos. Sci.*, 20:130–141, 1963.

2. G. Chen and T. Ueta, Yet another chaotic attractor, *Int. J. Bifurcation and Chaos*, Vol. 9,1465-1466, 1999.

3. T. Ueta and G.Chen, Bifurcation analysis of Chen's attractor, *Int. J. Bifurcation and Chaos*, Vol 10(8), pp. 1917-1931, 2000.

4. J. Lü and G. Chen, A new chaotic attractor coined, *Int. J. Bifurcation and Chaos*, Vol. 12(3), 659-661, 2002.

5. J. C. Sprott, Some simple chaotic flows, *Phys. Rev. E* 50, 647–650, 1994.

6. J. C. Sprott, A new class of chaotic circuit, *Phys. Lett. A* 266, 19–23, 2000.

7. J. C. Sprott, Simplest dissipative chaotic flow, *Phys. Lett. A* 228, 271–274, 1997.

8. O. E. Rossler, An equation for continuous chaos, *Phys. Lett. A* 57, 397–398, 1976.

9. G. van der Schrier, L. R. M. Maas, The diffusionless Lorenz equations;Silnikov bifurcations and reduction to an explicit map, *Physica D* 141, 19–36, 2000.

10. R. Shaw, Strange attractor, chaotic behaviour and information flow, *Z. Naturforsch. A* 36, 80–112, 1981.

11. Q. G. Yang, G. R. Chen, A chaotic system with one saddle and two stable node-foci, *Int. J. Bifurcat. Chaos* 18, 1393–1414, 2008.

12. Q. G. Yang, Z. C. Wei, G. R. Chen, A unusual 3D autonomous quadratic chaotic system with two stable node-foci, Int. J. Bifur. Chaos, 2010, doi:10.1142/S0218127410026320.

13. I. Pehlivan, Y. Uyaroglu, A New Chaotic attractor from General Lorenz System Family and its Electronic Experimental Implementation, *Turkish Journal of Electrical Eng. Comput. Sci.* 18(2), 171-184, 2010.

14. M. S. El Naschie, On dimensions of Cantor set related systems, *Chaos, Solitons & Fractals* 3,675–685, 1993.

15. M. S. El Nashie, Quantum mechanics and the possibility of a Cantorian space–time, *Chaos, Solitons & Fractals*, 1,485–487, 1992.

16. M. S. El Nashie, Is quantum space a random cantor set with a golden mean dimension at the core?, *Chaos, Solitons & Fractals*, 4(2), 177–179, 1994.

17. M. S. El Naschie, Complex vacuum fluctuation an a chaotic ''limit'' set of any Kleinian group transformation and the mass spectrum of high energy particle physics via spontaneous self-organization, *Chaos, Solitons & Fractals*, 17, 631–638, 2003.

18. M. S. El Nashie, Experimental and theoretical arguments for the number and mass of the Higgs particles, *Chaos, Solitons & Fractals*, 23,1091–1098, 2005.

19. Y. S. Vladimirov, Quark Icosahedron, charged and Vainberg's angle, *In. Proceedings of the international conference ''Problems of harmony, symmetry and the golden section in nature, science and art''*, Vinnitsa, 15, 69–79, 2003. [in Russian]

438

20. V. V. Petrunenko, To the question on physical essence of the phenomenon decalogarifmic periodicity, *In. Proceedings of the international conference ''Problems of harmony, symmetry and the golden section in nature, science and art''*, Vinnitsa, 15, 80–86, 2003. [in Russian]

21. A. O. Maiboroda, Finding the Golden Section in fundamental relations of physical magnitudes, *In. Proceedings of the international conference "Problems of harmony, symmetry and the golden section in nature, science and art"*, Vinnitsa, 15, 87–94, 2003. [in Russian]

Four-Scroll Stellate New Chaotic System

İhsan Pehlivan, Yılmaz Uyaroğlu, Mehmet Ali Yalçın, Abdullah Ferikoğlu

Sakarya University, Serdivan, Sakarya, Turkey
E-mail: ipehlivan@sakarya.edu.tr

Abstract: This paper introduces a new chaotic system of three-dimensional autonomous ordinary differential equations, which can display strange four-scroll stellate chaotic attractors simultaneously. Some basic dynamical behaviors of the new system investigated via theoretical analysis by means of equilibria and Lyapunov exponent spectrum. Finally, the chaos generator of the new chaotic system is experimentally confirmed via a novel analogue circuit design. It is convenient to use the system to purposefully generate chaos in chaos applications. A good qualitative agreement is illustrated between the simulation results.
Keywords: Chaos, chaotic system, chaotic attractor, chaotic circuit, four-scroll, chaos generator

1. Introduction

As the first chaotic model, the Lorenz system has become a paradigm of chaos research[1]. Chen constructed another chaotic system[2], which nevertheless is not topologically equivalent to the Lorenz's[2, 3]. This system is the dual to the Lorenz system and similarly has a simple structure[3]. Lü and Chen found the critical new chaotic system [4], which represents the transition between the Lorenz and Chen attractors. For the investigation on generic 3D smooth quadratic autonomous systems, Sprott [5-7] found by exhaustive computer searching about 19 simple chaotic systems with no more than three equilibria. It is very important to note that some 3D autonomous chaotic systems have three particular fixed points: one saddle and two unstable saddle-foci (for example, Lorenz system [1], Chen system [2], Lu system [4]). The other 3D chaotic systems, such as the original Rossler system [8], DLS [9] and Burke-Show system [10], have two unstable saddle-foci. Yang and Chen found another 3D chaotic system with three fixed points: one saddle and two stable fixed points [11]. Recently, Yang et al. [12] and Pehlivan et al. [13] introduced and analyzed the new 3D chaotic systems with six terms including only two quadratic terms in a form very similar to the Lorenz, Chen, Lu and Yang–Chen systems, but they have two very different fixed points: two stable node-foci. Therefore, They are very interesting to further find out the new dynamics of the system.

This paper introduces one more interesting complex three-dimensional quadratic autonomous four-scroll stellate chaotic system, which can depict complex 4-scroll chaotic attractors simultaneously.

2. A New Four-Scroll Stellate Chaotic System and its Analyses

Following nonlinear autonomous ordinary differential equations are the new chaotic system.

$$\dot{x} = -a \cdot x + y + y \cdot z$$
$$\dot{y} = x - a \cdot y + b \cdot x \cdot z$$
$$\dot{z} = c \cdot z - b \cdot x \cdot y$$

where $a, b, c \in R$ are parameters of the system. Typical parameters are a=4, b=0.5, c=0.6 . Let us consider a volume in a certain domain of the state space. For the system, one has

$$\Delta V = \frac{\partial \dot{x}}{\partial x} + \frac{\partial \dot{y}}{\partial y} + \frac{\partial \dot{z}}{\partial z} = -a - a + c = -2a + c < 0$$

As the divergence of vector field is negative, it can be concluded that the system is dissipative. It should be noticed that the system will always be dissipative if and only if $c < 2a$ with an exponential rate

$$\frac{dV}{dt} = e^{-2a+c}$$

In the dynamical system, a volume element V_0 is apparently contracted by the flow into a volume element $V_0 \, e^{(-2a+c)\,t}$ in time t. It means that each volume containing the trajectory of this dynamical system shrinks to zero as t→∞ at an exponential rate (-2a+c). So, all this dynamical system orbits are eventually confined to a specific subset that have zero volume, the asymptotic motion settles onto an attractor of the system. This suggests that the dynamics may tend to an attractor as t→∞.

Phase portraits of the new chaotic system were achieved as performing the numerical simulation for initial conditions x_0=0.6, y_0=0, z_0=0 and parameters a=4, b=0.5, c=0.6, and shown in Figure 1.

As can be seen in the Figure 2., the lyapunov exponents of the new system are

$$\lambda_1 = 0.2439, \ \lambda_2 = 0, \ \lambda_3 = -7.6254$$

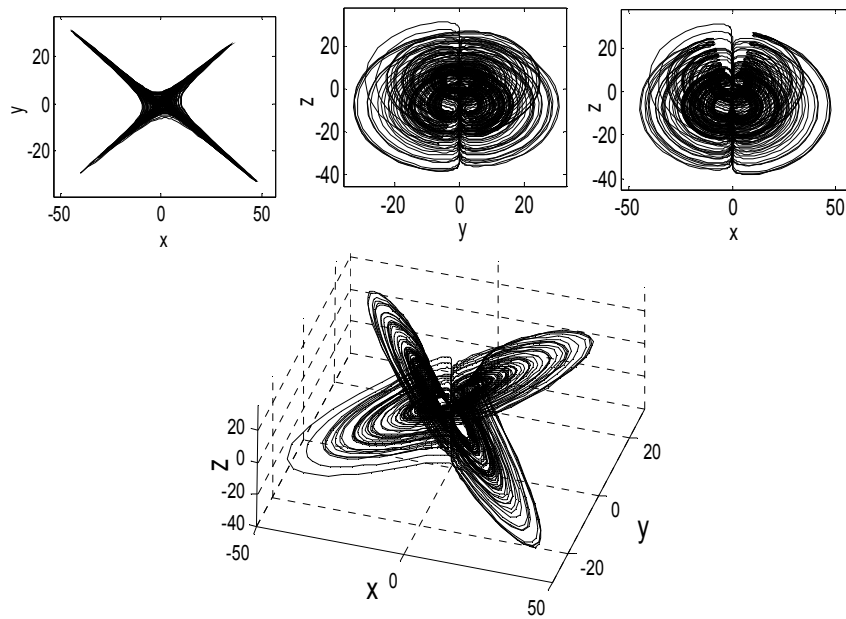for initial conditions x_0=0.6, y_0=0, z_0=0 and parameters a=4, b=0.5, c=0.6,

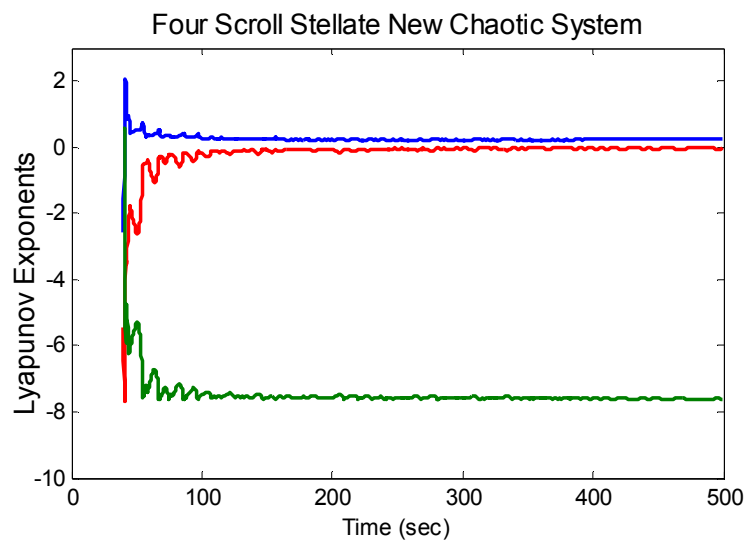Fig. 1. 2D and 3D Phase portraits of the four-scroll stellate new chaotic system

Fig. 2. Lyapunov Exponents of the new chaotic system for initial conditions
$x_0=0.6$, $y_0=0$, $z_0=0$ and parameters a=4, b=0.5, c=0.6

The new system equations have five equilibrum points as

$(0,0,0)$, $(\pm 3.648, \ \mp 2.361, \ -7.179)$, $(\pm 2.548, \ \pm 1.968, 4.179)$

for a=4, b=0.5, c=0.6 .

For the fixed point $E_1(x^*, y^*, z^*) = (\ 0 \ , \ 0 \ , \ 0 \ )$ the Jacobian matrix of the system is given as follows:

$$ J(E_1) = \begin{pmatrix} -4 & 1 & 0 \\ 1 & -4 & 0 \\ 0 & 0 & 0.6 \end{pmatrix} $$

Obviously, the characteristic equation about the equilibria E_1 is :

$\det(\lambda I - J(E_1)) = \lambda^3 + 7.4 \cdot \lambda^2 + 10.2 \cdot \lambda - 9 = 0$, by solving the characteristic equation, the eigenvalues are found as

$$ \lambda_1 = -5, \quad \lambda_2 = -3, \quad \lambda_3 = 0.6 \ . $$

For the fixed point $E_2(x^*, y^*, z^*) = (\ 3.648, \ -2.361, \ -7.179)$ the Jacobian matrix of the system is given as follows:

$$ J(E_2) = \begin{pmatrix} -4 & -6.179 & -2.361 \\ -2.590 & -4 & 1.824 \\ 1.181 & -1.824 & 0.6 \end{pmatrix} $$

Obviously, the characteristic equation about the equilibria E_2 is :

$\det(\lambda I - J(E_2)) = \lambda^3 + 7.4 \cdot \lambda^2 + 1.312 \cdot \lambda + 48.928 = 0$, by solving the characteristic equation, the eigenvalues are found as

$$ \lambda_1 = -8, \quad \lambda_2 = 0.3 + 2.455 \cdot \mathbf{i}, \quad \lambda_3 = 0.3 - 2.455 \cdot \mathbf{i} \ . $$

For the fixed point $E_3(x^*, y^*, z^*) = (\ -3.648 \ , \ +2.361 \ , \ -7.179 \ )$ the Jacobian matrix of the system is given as follows:

$$J(E_3) = \begin{pmatrix} -4 & -6.179 & 2.361 \\ -2.590 & -4 & -1.824 \\ -1.181 & 1.824 & 0.6 \end{pmatrix}$$

Obviously, the characteristic equation about the equilibria E_3 is :

$\det(\lambda I - J(E_3)) = \lambda^3 + 7.4 \cdot \lambda^2 + 1.312 \cdot \lambda + 48.928 = 0$, by solving the characteristic equation, the eigenvalues are found as

$$\lambda_1 = -8, \quad \lambda_2 = 0.3 + 2.455 \cdot \mathbf{i}, \quad \lambda_3 = 0.3 - 2.455 \cdot \mathbf{i}$$
.

For the fixed point $E_4(x^*, y^*, z^*) = (\ 2.548,\ 1.968\ ,\ 4.179\ )$ the Jacobian matrix of the system is given as follows:

$$J(E_4) = \begin{pmatrix} -4 & 5.179 & 1.968 \\ 3.090 & -4 & 1.274 \\ -0.984 & -1.274 & 0.6 \end{pmatrix}$$

Obviously, the characteristic equation about the equilibria E_4 is :

$\det(\lambda I - J(E_4)) = \lambda^3 + 7.4 \cdot \lambda^2 - 1.244 \cdot \lambda + 28.48 = 0$, by solving the characteristic equation, the eigenvalues are found as
$$\lambda_1 = -8, \quad \lambda_2 = 0.3 + 1.863 \cdot \mathbf{i}, \quad \lambda_3 = 0.3 - 1.863 \cdot \mathbf{i}\ .$$

For the fixed point $E_5(x^*, y^*, z^*) = (\ -2.548,\ -1.968\ ,\ 4.179\ )$ the Jacobian matrix of the system is given as follows:

$$J(E_5) = \begin{pmatrix} -4 & 5.179 & -1.968 \\ 3.090 & -4 & -1.274 \\ 0.984 & 1.274 & 0.6 \end{pmatrix}$$

Obviously, the characteristic equation about the equilibria E_5 is :

$\det(\lambda I - J(E_5)) = \lambda^3 + 7.4 \cdot \lambda^2 - 1.244 \cdot \lambda + 28.48 = 0$, by solving the characteristic equation, the eigenvalues are found as

$$\lambda_1 = -8, \quad \lambda_2 = 0.3 + 1.863 \cdot \mathbf{i}, \quad \lambda_3 = 0.3 - 1.863 \cdot \mathbf{i}\ .$$

The equilibria and eigenvalues for certain systems are tabulated in Table I.

Table I. Equilibria and eigenvalues for certain chaotic systems

System	Parameters	Equilibria	Eigenvalues
Lorenz system	a=10, b=8/3, c=28	(0,0,0)	-22.8277, -2.6667, 11.8277
		$(\pm 6\sqrt{2}, \pm 6\sqrt{2}, 27)$	-13.8546, 0.0940 ± 0.1945·i
Chen system	a=35, b=3, c=28	(0,0,0)	-30.8359, -3, 23.8359
		$(\pm 3\sqrt{7}, \pm 3\sqrt{7}, 21)$	-18.4288, 4.2140 ±14.8846·i
Lü system	a=36, b=3, c=20	(0,0,0)	-36, -3, 20
		$(\pm 2\sqrt{15}, \pm 2\sqrt{15}, 20)$	-22.6516, 1.8258 ±13.6887·i
The new system(1)	a=4, b=0.5, c=0.6		-5, -3, 0.6
		(0, 0, 0)	-8, 0.3 ± 2.455·i
		$(\pm 3.648, \mp 2.361, -7.179)$	-8, 0.3±2.455·i
		$(\pm 2.548, \pm 1.968, 4.179)$	-8, 0.3±1.863·i
			-8, 0.3±1.863·i

Figure 3. shows the Lyapunov Exponents Spectrum of the new system for varying parameter c, and constant parameters a=4, b=0.5. As can be seen from the Lyapunov exponents spectrum, the new system is chaotic when a positive Lyapunov exponent.
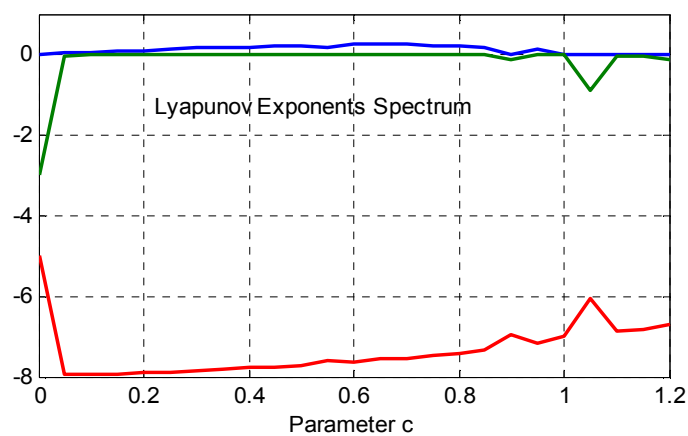
(a)
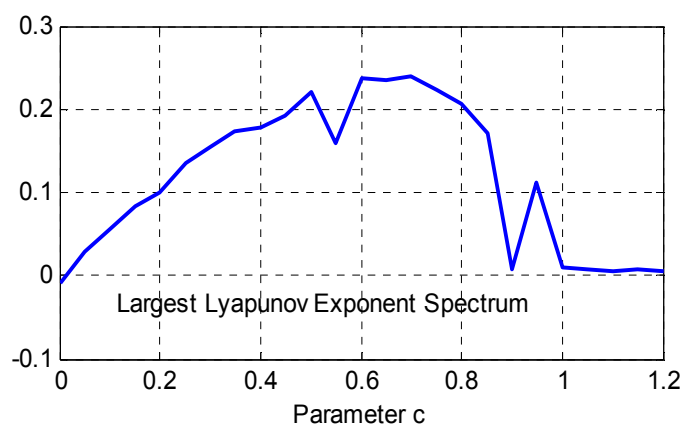
(b)

Fig. 3. (a) Lyapunov Exponent Spectrum of the new system for varying parameter c, and constant parameters a=4, b=0.5. (b) Largest Lyapunov Exponent Spectrum of the new system for varying parameter c, and constant parameters a=4, b=0.5.

3. Circuit Realization of the Four-Scroll Chaotic System

The designed electronic circuit schematic and the Orcad-PSpice simulation results of the new chaotic circuit for parameters a=4, b=0.5, c=0.6, are seen in Fig. 4 and Fig. 5-6 respectively.

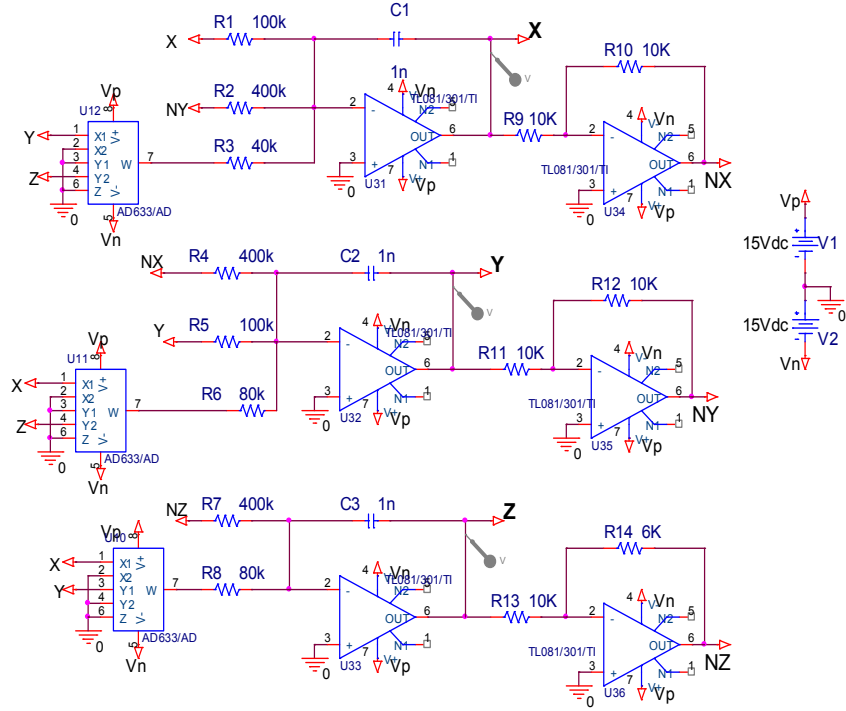Fig. 4. The electronic circuit schematic of the new chaotic system

Chaotic differential equations of the new circuit are given below.

$$\dot{x} = \frac{1}{R_1 \, C_1} x - \frac{1}{R_2 \, C_1} y - \frac{1}{R_3 \, C_1} y \cdot z$$

$$\dot{y} = \frac{1}{R_4 \, C_2} x - \frac{1}{R_5 \, C_2} y + \frac{1}{R_6 \, C_2} x \cdot z$$

$$\dot{z} = \frac{1}{R_7 \, C_3} z - \frac{1}{R_8 \, C_3} x \cdot y$$
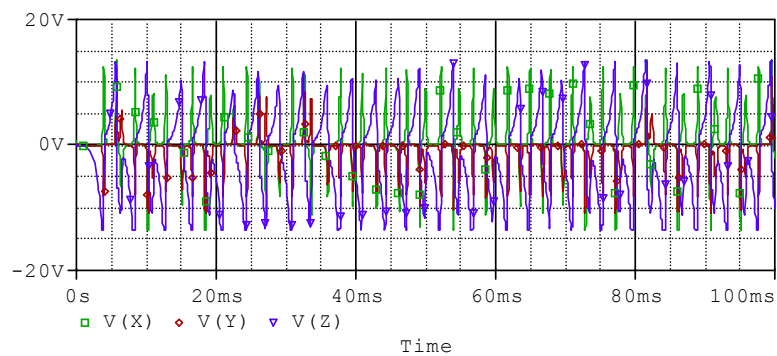
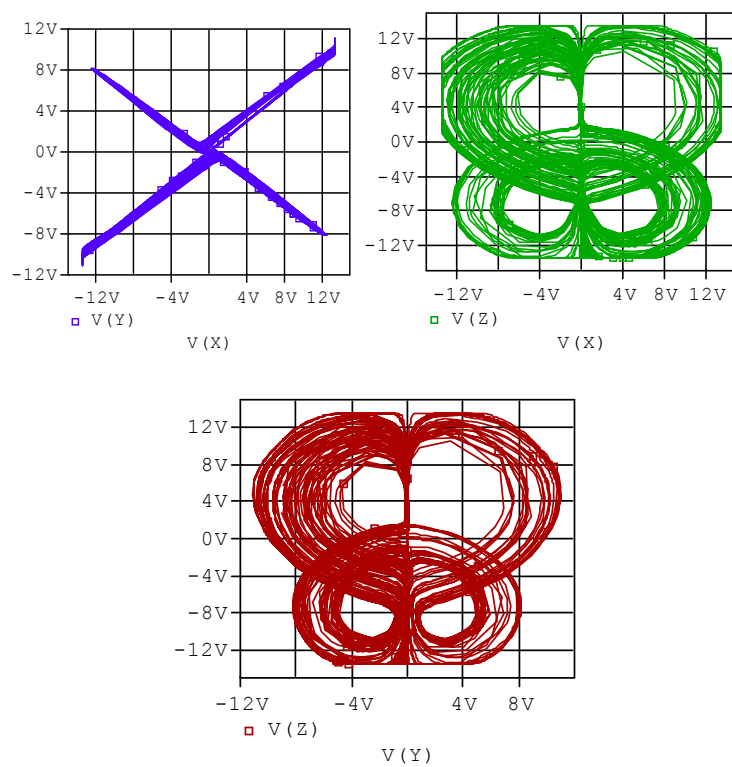Fig. 5. x, y, z chaotic signals of the new chaotic system against to time

Fig. 6. Phase portraits of the new chaotic system

4. Conclusions

This article introduces one three-dimensional autonomous interesting new chaotic system which can display strange four-scroll stellate chaotic attractors simultaneously. Our investigation was completed using a combination of theoretical analysis and simulations.The chaos generator of the new chaotic system are confirmed via a novel electronic circuit design. Electronic circuitry of the new chaotic system is simple. It is convenient to use the new system to purposefully generate chaos in chaos applications. We believe that the unknown dynamical behaviors of this chaotic attractor deserve further investigation and are desirable for engineering applications in the near future.

Acknowledgements

References

1. E. N. Lorenz, Deterministic nonperiodic flow; *J. Atmos. Sci.*, 20:130–141, 1963.

2. G. Chen and T. Ueta, Yet another chaotic attractor, *Int. J. Bifurcation and Chaos*, Vol. 9,1465-1466, 1999.

3. T. Ueta and G.Chen, Bifurcation analysis of Chen's attractor, *Int. J. Bifurcation and Chaos*, Vol 10(8), pp. 1917-1931, 2000.

4. J. Lü and G. Chen, A new chaotic attractor coined, *Int. J. Bifurcation and Chaos*, Vol. 12(3), 659-661, 2002.

5. J. C. Sprott, Some simple chaotic flows, *Phys. Rev. E* 50, 647–650, 1994.

6. J. C. Sprott, A new class of chaotic circuit, *Phys. Lett. A* 266, 19–23, 2000.

7. J. C. Sprott, Simplest dissipative chaotic flow, *Phys. Lett. A* 228, 271–274, 1997.

8. O. E. Rossler, An equation for continuous chaos, *Phys. Lett. A* 57, 397–398, 1976.

9. G. van der Schrier, L. R. M. Maas, The diffusionless Lorenz equations;Silnikov bifurcations and reduction to an explicit map, *Physica D* 141, 19–36, 2000.

10. R. Shaw, Strange attractor, chaotic behaviour and information flow, *Z. Naturforsch.* A 36, 80–112, 1981.

11. Q. G. Yang, G. R. Chen, A chaotic system with one saddle and two stable node-foci, *Int. J. Bifurcat. Chaos* 18, 1393–1414, 2008.

12. Q. G. Yang, Z. C. Wei, G. R. Chen, A unusual 3D autonomous quadratic chaotic system with two stable node-foci, Int. J. Bifur. Chaos, 2010, doi:10.1142/S0218127410026320.

13. I. Pehlivan, Y. Uyaroglu, A New Chaotic attractor from General Lorenz System Family and its Electronic Experimental Implementation, *Turkish Journal of Electrical Eng. Comput. Sci.* 18(2), 171-184, 2010.

Lindenmeyer Systems and the Harmony of Fractals

Pedro Pestana

CEAUL — Centro de Estatística e Aplicações da Universidade de Lisboa
Portuguese Catholic University – School of the Arts, CITAR, Porto, and Lusíada
University, Lisboa, Portugal
(E-mail: pedro.duarte.pestana@gmail.com)

Abstract. An interactive musical application is developed for realtime improvisation with a machine based on Lindenmeyer-systems. This has been used on an installation whose goal is to draw the attention of unexperienced users to the wealth of realtime applications in computer music. Issues on human computer interaction and improvisation grammars had to be dealt with, as well as probabilistic strategies for musical variation. The choice of L-systems as a basis for machine composition is a consequence of their ability to create results that easily have aesthetic appeal, both in the realms of sound and image.

Keywords: human-computer interaction, L-systems, fractals in algorithmic music composition, interactive composition, improvisation, computer music.

1 Introduction

Musical variation, and composition rules defined by Schönberg, exploit to a certain extent the self-similarity of fractals, and Lindenmeyer (cf. Rozenberg[11]) created algorithms (in biological research) that can be exploited fully using iteration in algorithmic music composition. But can fractals create harmony of sound and *cantabile* music as well as they create beauty for the eyes in graphical arts?

We present examples of an interactive algorithmic music composition system exploiting Lindenmeyer's technique, generating some forms of minimalist music based on user input, and further developments using the interaction of probability models, fractals and chaos.

Lindenmayer systems, or L-systems, are parallel formal grammars introduced in 1968 by the botanist Aristid Lindenmayer[3] as "a theoretical framework for studying the development of simple multicellular organisms" (Prusinkiewicz and Lindenmayer[10]). As such, in essence an L-system is a rule-based generative system that, drawing from a finite set of symbols, applies substitution schemes starting with an initial subset, called in Prusinkiewicz[9] an axiom. In Chomsky grammars, substitutions are made in series, with each pass focusing exclusively on a sole symbol, while L-systems are parallel, in the sense that all symbols are replaced within each iteration.

Extending the initial application of L-systems, developments were made in order to generate realistic computer images of plants and trees (Smith[15]), fractal curves (Prusinkiewicz[8]), and musical scores (Prusinkiewicz[9]).

Given words with a fair amount of complexity, an L-system will exhibit a noticeable degree of self-similarity over iterations, which makes its results memorable and pleasing when interpreted as musical height or visual branching, in the sense that there is an equilibrium of expected and unexpected developments. In other words, as Schröder[12], p. 109, boldly presents the key ideas of Birkhoff's *theory of aesthetic value*, the results are pleasing and interesting since they are neither too regular and predictable like a boring brown noise with a frequency dependence f^{-2}, nor a pack of too many surprises like an unpredictable white noise with a frequency dependence f^{-0}.

The remainder of this paper is organized as follows. In Section 2 we describe implementations of L-systems for the automatic generation of music. In Section 3 the focus is on the analysis of musical parameters from user input, such as pitch velocity and duration, and their mapping to L-systems. Section 4 deals with possible extensions of this work to polyphonic input and output, and Section 5 deals with the specific implementation of this project. Finally, in Section 6, we briefly discuss further issues and possible developments.

2   Construction of an L-system

L-systems come in several categories: context-free (OL-systems) or context-sensitive (IL-systems); deterministic or non-deterministic; propagative or non-propagative, and so on. The interested reader is referred to Manousakis[4] and to Rozenberg[11] for an extensive review of different types of L-systems. The present work uses non-deterministic OL-systems, as described below.

Let $\mathcal{A}$ denote an alphabet of letters ℓ, $\mathcal{V}$ the vocabulary, i.e. the set of words $w = \ell_1 \ell_2 \cdots \ell_n$ (strings of letters from this alphabet); $\emptyset$, the empty set, is considered a word.

A production $P : \mathcal{A} \longrightarrow \mathcal{V}$ is described by random variables associated with each $\ell \in \mathcal{A}$, i.e.

$$\ell \quad \overset{P}{\mapsto} \quad P(\ell) = X_\ell = \begin{cases} w_k \\ \\ p_k = \mathrm{P}[X_\ell = w_k] \end{cases},$$

and *j-letter* $\mathcal{L}_j : \mathcal{V} \longrightarrow \mathcal{A}$ selects the j-letter of any given word,

$$w = \ell_1 \ell_2 \cdots \ell_k \quad \overset{\mathcal{L}_j}{\mapsto} \quad \mathcal{L}_j(w) = \ell_j.$$

We assume that if $\ell_i \neq \ell_j$, then X_{ℓ_i} and X_{ℓ_j} are independent. If the actual result of $P(\ell)$ is w, we write $\ell \mapsto w$, and say that ℓ is the predecessor of w, or alternatively that w is the successor of ℓ.

If $w = \ell_1 \ell_2 \cdots \ell_k$, $\mathbf{P}(w) = P(\mathcal{L}_1(w))P(\mathcal{L}_2(w)) \cdots P(\mathcal{L}_k(w))$. A *production* of size k with root w_0, $\mathcal{P}_{w_0,k}$ is

$$\mathcal{P}_{w_0,k}(\cdot) = \mathbf{P}(\mathbf{P}(\mathbf{P}(\cdots \mathbf{P}(\cdot) \cdots))),$$

and $\mathcal{P}_{w_0}(\cdot) = \bigcup_{k \in \mathbb{N}} \mathcal{P}_{w_0,k}(\cdot)$.

An OL-system is an ordered triplet $G = \{\mathcal{A}, w_0, P_{w_0}\}$, with $w_0 \in \mathcal{A}$ the starting point for the successive iterations, and P_{w_0} is a production of finite size with root w_0. In an OL-system the predecessor is a one-letter word whereas the successor can be of arbitrary length (it can even be an empty word). In a non-deterministic system, different successor words may occur according to a probabilistic distribution. Hence the production may be described in terms of a branching process, whose many possible trajectories are tied to the possibilities that actually do occur.

A very easy construction of a musical grammar (McCormack[5]) could be built by taking an alphabet $\mathcal{A} = \{C, D, E, F, G, A, B\}$ corresponding to the notes of a C major scale (or an even larger musical scale alphabet), an axiom that would be given by user input and a set of productions that may be arbitrary or may follow rules from common practice of harmony. Alternative constructions have been given by Soddell and Soddell[16], who map branching angles to changes in pitch, Prusinkiewicz[9] where a deterministic OL-system is used to generate a graphical turtle interpretation of the production, and then the resulting curve is traversed and the height of each line segment is interpreted as pitch among others. Most of the studied constructions have seamlessly resulted in pleasing musical results and in our approach we opted for the former, more literal one.

As an example, consider the alphabet $\{C, D, E_b, F, G, A_b, B\}$, the root $w_0 = DE_bCB$ (the celebrated Shostakovich signature, used in many of his mature works), and the stochastic transition matrix — a sparse matrix, so that the equilibrium of expected and unexpected generates aesthetic value — describing the probabilities governing the productions P:

	A_b	A_bE_b	A_bG	B	C	CFD	CFG	DC	E_b	F	G	GA_b	GF
C	0	0	0	0.7	0	0	0	0	0	0	0.2	0	0.1
D	0	0	0.8	0	0	0	0	0	0	0	0.2	0	0
E_b	0	0	0	0.8	0.2	0	0	0	0	0	0	0	0
F	0	0	0	0	0.2	0	0.7	0	0	0	0	0.1	0
G	0	0.2	0	0	0.7	0.1	0	0	0	0	0	0	0
A_b	0	0	0	0	0.2	0	0	0.8	0	0	0	0	0
B	0.2	0	0	0	0	0	0	0	0.7	0.1	0	0	0

Assume we get the sequence

$$
\begin{array}{c|c}
w_0 = DE_bCB & 1 \\
w_1 = A_bGBGE_b & 0.0896 \\
w_2 = DCCFDE_bA_bE_bB & 0.00896 \\
w_3 = A_bGBBCFGA_bGBDCBE_b & 0.078675968 \\
w_4 = DCCE_bE_bBCFGCDCCE_bGBE_bB & 0.004934557
\end{array}
$$

with the probabilities indicated in the right column. So, in this example, with probability 3.11678×10^{-7} we get $\mathcal{P}_{DE_bCB,4} = DCCE_bE_bBCFGCDCCE_bGBE_bB$.

Observe that the rich theory of Markov chains, and concepts such as communicating evens, cyclicity, stationarity, can therefore be imported to analyse productions.

3 Analyzing user input

In the proposed interaction model, a user inputs a musical phrase which serves as the root (axiom), and given a significant pause the system reacts branching into the successive iterations given by the production set. At any point the user could feel inspired by the results and step in with a new musical phrase as a new root, stopping the automatic production, from which the computer draws new material according to the same set of productions or a revised version of it. The focus of this work is on the user-satisfaction with the musical results, and as such it was decided that the interface should not be a tried and tested one such as the music keyboard. This is also helpful in that it allows us to use a very robust MIDI communication, leading to a clear interpretation of pitch, velocity and duration.

The possibility of having the computer analyzing the intention of the musical input and generating different productions would be the first step towards a musical and engaging result. A first approach should consist on scale detection, and Chai and Vercoe's strategy based on hidden Markov models (see Chai and Vercoe[1]) was used in order to extrapolate the global outline of the production set, cf. also Noland and Sandler[6]. The set itself was constructed in strict adherences to classic common practice as described by authors such as Piston[7], as it was deemed that the musical results should be satisfying to a wide non-expert "random" audience.

An additional concern has been how to map user-inputted velocity and duration into the productions of the model. Three approaches have been considered and tested for note duration:

- Having an additional algorithm for tempo detection and building a parallel fixed set of productions for note duration.
- Keeping the duration that was given by user-input across successive generations of productions.
- Cycling through the set of user-inputted durations.

The first approach has been abandoned. Without further constraints forcing the user to adhere to a tempo it would have been unmusical to let the computer-generated productions have a strictly quantized feel as a result of the original input being free from adequate rules. The second approach has also been discarded, since after a few generations a pattern of unnatural repetitiveness would begin to emerge, creating unmusical productions. The

third approach has been, surprisingly, musically rewarding, as it potentiated the natural feel that resulted from the self-similarity of successive iterations. Consequently, it has been our choice to govern this parameter. The last member of the set needs to be automatically generated, as there is no way to infer the duration of the user's last note. For this we simply repeat the previous duration value.

It was also not clear from the start which solution would be better for velocity mapping and again different paths were evaluated:

- Quantizing the velocity to a set value given by the average value of the user input.
- Giving a fixed velocity to each of the words in the vocabulary, again averaging the user-inputted value for that word.
- Keeping the velocity that was given by user-input across successive generations of productions
- Cycling through the set of user-inputted velocities.

In fact, any of those solutions proved to be too mechanical, and we had to create a new rule that would allow for musical variety. We choose to create a set of user-inputted velocities, and to discard at random one value from the set in each iteration. The result is immediately more natural, since now there is a much longer period before any pattern of duration-velocity pairs can repeat.

4   Extending the system towards polyphony

The above discussion on analysis is straightforward for monophonic input and output, but the possibility of using multiple voices poses a string of new issues that are not so easily solvable. On the input side, making the distinction between harmonic movement and melodic movement is fraught with ambiguity and the allocation of each melodic movement to a unique voice is also a tremendous challenge. On the output side, decisions had to be made as to adherence to melodic rules and voice independence. Each problem has to be addressed in turn.

The distinction between harmonic and melodic movement cannot depend on simultaneity, when human input is considered. Users never perform with infinitesimal precision and we must therefore create time windows within which two events can be considered simultaneous. A sensible time window would be in the range of 30-50 ms, according to the Haas principle or precedence effect, that states that the human listener integrates all sound events that occur within that time frame. This is a very bold statement from a musical perspective as musical interpretation and style might at times dictate that events that are technically simultaneous should be performed with enough separation between them to clearly exceed the above-mentioned interval. One well-known and consistent example is the Flamenco's *rasgueado*, where the

harmonic intervals are always performed as a very quick succession. We must therefore agree on an extended interval based not on a Haas-inspired pursuit of simultaneity, but on the opposite idea of what would not be a melodic interval. With this in mind we can safely say that is untypical for a performer to go faster than a eighth-note on a 120 bpm tempo which would point us to a 63 ms window. This is of course ambiguous and might be prone to error on fast ornamentations.

Correctly distributing events between voices in a setting where different voices might have different musical durations and pauses is a subject that has not yet been successfully solved. Indeed, it is not clear whether the rules described in the previous section would work with multiple axioms as a starting point. Due to those yet unsolved questions, for the time being, the input side of polyphony has been dropped and the user would only be allowed to play monophonically.

It was however interesting from a musical standpoint that the output could be done polyphonically with the aid of an automatic accompaniment. A simplification of the model proposed by Schwarz *et al.*[13], based on HMM, has been used in order to extend the system, using a low and sparsely-generated voice.

5 Implementation

The system was implemented in Max/MSP, making use of the in-build Jitter object jit.linden. A first patcher parses the input and does the scale analysis, and feeds the finished list to the patcher responsible for the productions (shown in Fig. 1). The productions are fed to a third patcher that converts them to MIDI and sends them as UDP packages to SuperCollider, where a simple implementation of a quasi-sinusoidal synth that resembles a vibraphone is used as a sound module.

An example we fed the system with Shostakovich's aforementioned signature $DSCH$ (used musically as D, E_b, C, B) played as a pair of quavers followed by a pair of semi-quavers of equal velocity. The input patcher interprets the motif as played in C harmonic minor and constructs the set of productions already presented as a sparse stochastic transition matrix in Section 2, presented below in a more readable condensed form for those not wanting to dive in stochastic processes theory:

$$P = \begin{cases} P_{11} : C \xrightarrow{70\%} B & P_{12} : C \xrightarrow{20\%} G & P_{13} : C \xrightarrow{10\%} GF \\ P_{21} : D \xrightarrow{80\%} G & P_{22} : D \xrightarrow{20\%} A_bG \\ P_{31} : E_b \xrightarrow{80\%} B & P_{32} : E_b \xrightarrow{20\%} C \\ P_{41} : F \xrightarrow{70\%} CFG & P_{42} : F \xrightarrow{20\%} C & P_{43} : F \xrightarrow{10\%} GA_b \\ P_{51} : G \xrightarrow{70\%} C & P_{52} : G \xrightarrow{20\%} A_bE_b & P_{53} : G \xrightarrow{10\%} CFD \\ P_{61} : A_b \xrightarrow{80\%} DC & P_{62} : A_b \xrightarrow{20\%} C \\ P_{71} : B \xrightarrow{70\%} E_b & P_{72} : B \xrightarrow{20\%} A_b & P_{73} : B \xrightarrow{10\%} F \end{cases}.$$

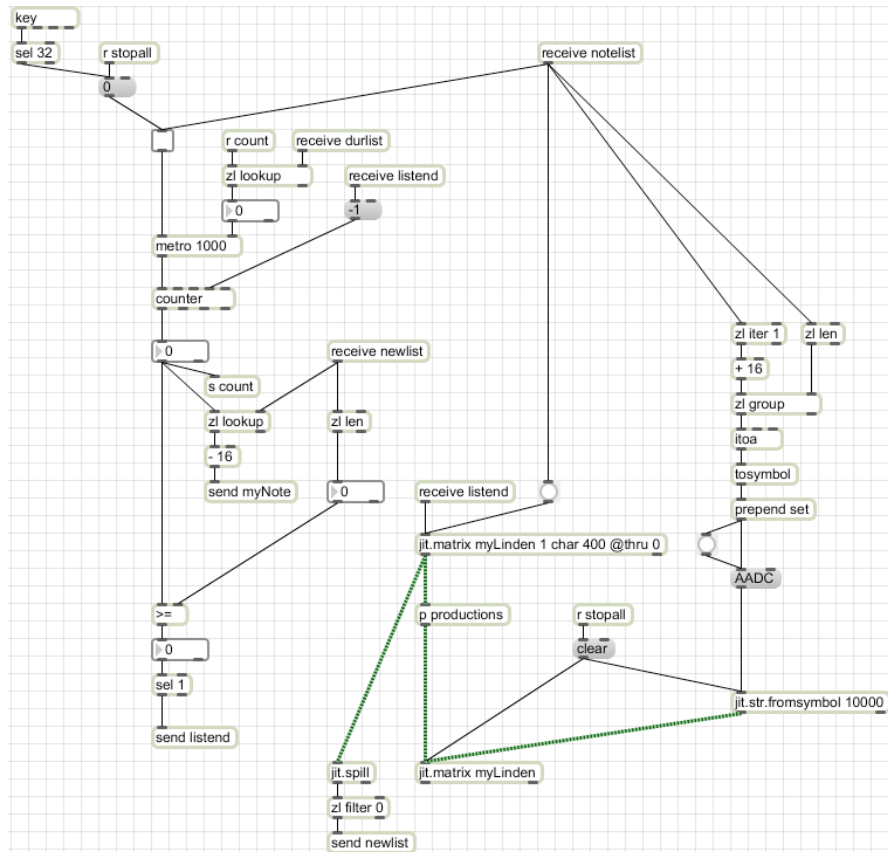The result can be heard at http://www.stereosonic.org/lindenmayer.

Fig. 1. Max/MSP main patcher

6 Concluding remarks

Many alternative ways do exist of music composition tied to fractals, cf. Johnson[2] and Skiadas[14], for instance. OL-systems as used in our examples generate appealing musical productions as far as letters map onto words of small size. Otherwise, the system must be interrupted by the user, since a rather small number of iterations generates a musical output that is too clumsy. The organisation of natural languages, and namely of the mating songs of birds and insects, seems to incorporate a strategy of long range dependence axed on a sequence of modulated shortcut Markov-type memories. Hence, for more elaborated vocabularies and mappings, it would be sensible to use only the r last letters from the $(k\text{-}1)$-th iteration to map onto the k-th iteration, instead of using all the letters as described for OL-systems. This is easily implemented using an *endletters* application $\mathcal{E}_r : \mathcal{V} \longrightarrow \mathcal{A}$ selecting

the r-endletters of any given word,

$$w = \ell_1 \ell_2 \cdots \ell_k \quad \stackrel{\mathcal{E}_r}{\mapsto} \quad \mathcal{E}_r(w) = \ell_{k-r+1} \ell_{k-r+2} \cdots \ell_{k-1} \ell_k,$$

so that the memory of the initial $k - r$ letters is erased and the musical composition will flow more naturally.

References

1. W. Chai and B. Vercoe. Detection of key change in classical piano music. *Proceedings of the 6th International Conference on Music Information Retrieval*, 2006. London.
2. R. S. Johnson. Composing with Fractals. In J. Fauvel, R. Flood and R. Wilson, eds., *Music and Mathematics*, 2006. Oxford University Press.
3. A. Lindenmayer. Mathematical models for cellular interaction in development, *Journal of Theoretical Biology*, 18: 280–315, 1968.
4. S. Manousakis. *Musical L-Systems*. M.Sc. Thesis in Sonology, The Royal Conservatory, 2006. The Hague.
5. J. McCormack. Grammar-Based Music Composition. In Stocker et al., eds. *Complex Systems 96: from Local Interactions to Global Phenomena*, 1996. IOS Press.
6. K. Noland and M. Sandler. Key Estimation Using a Hidden Markov Model. Inn *International Society for Music Information Retrieval*, 121–126, Victoria, 2006. Canada.
7. W. Piston. *Harmony*. New York, 1941. W.W. Norton & Company.
8. P. Prusinkiewicz. Graphical applications of L-systems. *Proceedings of Graphics Interface'86*, 247-253, 1986a.
9. P. Prusinkiewicz. Score Generation with L-Systems. *Proc. Intl. Computer Music Conf '86*, 455-457, 1986b.
10. P. Prusinkiewicz and A. Lindenmayer. *The Algorithmic Beauty of Plants*, 1990. Springer.
11. G. Rozenberg. *Lindenmeyer Systems: Impacts on Theoretical Computer Science, Computer Graphics, and Developmental Biology*, 1992. Springer Verlag.
12. M. Schroeder. *Fractals, Chaos, Power Laws: Minutes from an Infinite Paradise*. New York, 2009. Dover.
13. D. Schwarz, N. Orio and N. Schnell. *Robust Polyphonic MIDI Score Following with Hidden Markov Models*, 2004. ICMC.
14. C.H. Skiadas. Exploring and simulating chaotic advection: A difference equations approach. In C. H. Skiadas, ed., *Recent Advances in Stochastic Modeling and Data Analysis*, pages 287–294, Singapore, 2007. World Scientific.
15. A.R. Smith. Plants, fractals, and formal languages. *Computer Graphics*, 18(3): 1-10, 1984.
16. F. Soddell and J. Soddell. Microbes and Music. In *PRICAI 2000 Topics in Artificial Inteligence*, pages 767–777, 2000. Springer.